



NAVAL POSTGRADUATE SCHOOL

Monterey, California



THESIS

NONTRADITIONAL WINDOWS
IN SPECTRAL ANALYSIS

by

Ramiro Moreira-Paredes

June, 1993

Thesis Advisor:

Ralph Hippenstiel

Approved for public release; distribution is unlimited.



Unclassified

Security Classification of This Page

REPORT DOCUMENTATION PAGE

1a. REPORT SECURITY CLASSIFICATION Unclassified			1b. RESTRICTIVE MARKINGS		
2a. SECURITY CLASSIFICATION AUTHORITY			3. DISTRIBUTION/AVAILABILITY OF REPORT Approved for public release; distribution is unlimited.		
2b. DECLASSIFICATION/DOWNGRADING SCHEDULE			5. MONITORING ORGANIZATION REPORT NUMBER(S)		
4. PERFORMING ORGANIZATION REPORT NUMBER(S)			7a. NAME OF MONITORING ORGANIZATION Naval Postgraduate School		
6a. NAME OF PERFORMING ORGANIZATION Naval Postgraduate School		6b. OFFICE SYMBOL (if applicable) EC	7b. ADDRESS (City, State, and Zip Code) Monterey, CA 93943-5000		
6c. ADDRESS (City, State, and Zip Code) Monterey, CA 93943-5000			9. PROCUREMENT INSTRUMENT IDENTIFICATION NUMBER		
8a. NAME OF FUNDING/SPONSORING ORGANIZATION		8b. OFFICE SYMBOL (if applicable)	10. SOURCE OF FUNDING NUMBERS		
8c. ADDRESS (City, State, and Zip Code) Monterey, CA 93943-5000			Program Element No	Project No	Task No
11. TITLE (Include Security Classification) NONTRADITIONAL WINDOWS IN SPECTRAL ANALYSIS					
12. PERSONAL AUTHOR(S) MOREIRA, Ramiro					
13a. TYPE OF REPORT MASTER'S THESIS		13b. TIME COVERED From To		14. DATE OF REPORT (year, month, day) 1993 JUNE 17	
15. PAGE COUNT 128					
16. SUPPLEMENTARY NOTATION The views expressed in this thesis are those of the author and do not reflect the official policy or position of the Department of Defense or the U S. Government.					
17. COSATI CODES			18. Subject Terms (continue on reverse if necessary and identify by block number)		
FIELD	GROUP	SUBGROUP	SPECTRAL ANALYSIS, FOURIER TRANSFORM, AUTOCORRELATION, BIAS AND VARIANCE, FAST FOURIER TRANSFORM, PERIODOGRAM, CLASSICAL WINDOWS, NONTRADITIONAL WINDOWS, DAMPED SINUSOIDS, FREQUENCY RESOLUTION, RECORD LENGTH.		
19. Abstract (continue on reverse if necessary and identify by block number) This thesis studies a new data weighting function, which consists of a complex valued window known as the linear complex valued FM chirp window. This type of window, when used with the Fourier transform, produces a magnitude spectrum which permits identification of single sinusoids and multiple sinusoids which can be separated in frequency by less than one DFT bin. This allows determination of whether or not one or multiple signals are present. The chirp window seems to have better resolution properties than classical windows. When the chirp window is used with a signal that contains a frequency step (i.e., FSK), the resultant spectrum is markedly different for the upward shift and downward shift cases. The work of this thesis consists of replicating the results of J. Griffiths in his paper "A Novel Window For High Resolution Fourier Transform" to establish the signal to noise ratio dependency of this type of window, and to study its behavior when damped sinusoids are present. Additionally, a review of classical windows and sidelobe behavior is presented. All simulations were performed using MATLAB.					
20. DISTRIBUTION/AVAILABILITY OF ABSTRACT __ UNCLASSIFIED/UNLIMITED <input checked="" type="checkbox"/> SAME AS REPORT __ DTIC USERS			21. ABSTRACT SECURITY CLASSIFICATION Unclassified		
22a. NAME OF RESPONSIBLE INDIVIDUAL RALPH HIPPENSTIEL			22b. TELEPHONE (Include Area Code) 408-656-2633		22c. OFFICE SYMBOL EC/Hi

DD FORM 1473, 84MAR

83 APR edition may be used until exhausted.
All other editions are obsolete.

Security classification of this page

Unclassified.

Approved for public release; distribution is unlimited.

NONTRADITIONAL WINDOWS IN SPECTRAL ANALYSIS

by

Ramiro Moreira-Paredes
Major, Ecuadorian Air Force
B.S., Ecuadorian Army Polytechnic

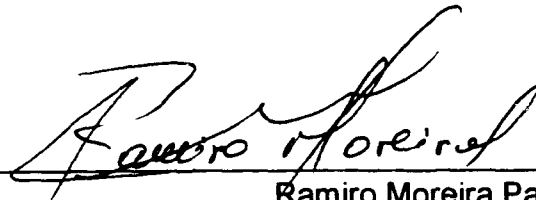
Submitted in partial fulfillment
of the requirements for the degree of

MASTER OF SCIENCE IN ELECTRICAL ENGINEERING

from the

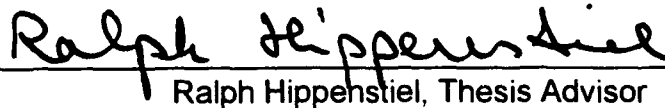
NAVAL POSTGRADUATE SCHOOL
June, 1993

Author:



Ramiro Moreira Paredes

Approved By:



Ralph Hippenstiel, Thesis Advisor



Tri Ha, Second Reader



Michael A. Morgan, Chairman

Department of Electrical and Computer Engineering

ABSTRACT

This thesis studies a new data weighting function, which consists of a complex valued window known as the linear complex valued FM chirp window. This type of window, when used with the Fourier transform, produces a magnitude spectrum which permits identification of single sinusoids and multiple sinusoids which can be separated in frequency by less than one DFT bin. This allows determination of whether or not one or multiple signals are present. The chirp window seems to have better resolution properties than classical windows. When the chirp window is used with a signal that contains a frequency step (i.e., FSK), the resultant spectrum is markedly different for the upward shift and downward shift cases. The work of this thesis consists of replicating the results of J. Griffiths in his paper "A Novel Window For High Resolution Fourier Transform" to establish the signal to noise ratio dependency of this type of window, and to study its behavior when damped sinusoids are present. Additionally, a review of classical windows and sidelobe behavior is presented. All simulations were performed using MATLAB.

[illegible]

CONTENTS

I. INTRODUCTION	1
II. SPECTRAL ESTIMATION	4
A. BACKGROUND	4
B. PERIODOGRAM FOR DETERMINISTIC SIGNALS	6
C. PERIODOGRAM FOR STOCHASTIC PROCESSES	11
1. Bias of the Periodogram	13
2. Variance of the Periodogram	16
D. PERIODOGRAM AVERAGING	17
III. CLASSICAL WINDOWS	21
A. INTRODUCTION	21
B. WINDOWING A DISCRETE SIGNAL	23
C. CLASSICAL WINDOWS	25
D. COMPARISON OF CLASSICAL WINDOWS	30
1. Rectangular Window	30
2. Triangular Window	32
3. Hamming Window	35

4. Blackman Window	37
5. Kaiser-Bessel Window	41
E. HARMONIC ANALYSIS USING CLASSICAL WINDOWS	44
IV. NONTRADITIONAL WINDOWS	55
A. INTRODUCTION	55
B. FM CHIRP WINDOW DEFINITION AND EXPERIMENTAL RESULTS	56
C. SIGNAL TO NOISE RATIO SENSITIVITY OF FM CHIRP WINDOW	62
D. CHIRP WINDOW APPLIED TO DAMPED SINUSOIDS	67
E. NUMERICAL BEHAVIOR OF CHIRP WINDOW	69
V. CONCLUSIONS AND RECOMMENDATIONS	88
APPENDIX A. RELATIONSHIP BETWEEN THE TRANSFORM OF A CONTINUOUS SIGNAL AND A SAMPLED SIGNAL.	93
APPENDIX B. PROCESSING GAIN	96
APPENDIX C. AN ALTERNATIVE NONTRADITIONAL WINDOW	100
APPENDIX D. MATLAB PROGRAMS	105
LIST OF REFERENCES	116

INITIAL DISTRIBUTION LIST	117
---------------------------------	-----

LIST OF FIGURES

FIGURE 2.1. CONDITIONAL PROBABILITY DENSITY FUNCTION FOR GOOD AND BAD ESTIMATORS	8
FIGURE 3.1. RECTANGULAR WINDOW	32
FIGURE 3.2. TRIANGULAR WINDOW	34
FIGURE 3.3. HAMMING WINDOW	36
FIGURE 3.4. BLACKMAN WINDOW	39
FIGURE 3.5. EXACT BLACKMAN WINDOW	40
FIGURE 3.6. KAISER-BESSEL WINDOW FOR $\alpha=2$	42
FIGURE 3.7. KAISER-BESSEL WINDOW FOR $\alpha=3$	43
FIGURE 3.8. RECTANGULAR WINDOW ($f_1 = 10$ BIN, $f_2 = 16$ BIN)	47
FIGURE 3.9. RECTANGULAR WINDOW (TWO SIGNALS: $f_1=10.5$ BIN, $f_2=16$ BIN)	47
FIGURE 3.10. TRIANGULAR WINDOW (TWO SIGNALS: $f_1=10.5$ BIN, $f_2=16$ BIN)	48
FIGURE 3.11. HAMMING WINDOW (TWO SIGNALS: $f_1=10.5$ BIN, $f_2=16$ BIN)	48

FIGURE 3.12. BLACKMAN WINDOW (TWO SIGNALS: $f_1=10.5$ BIN, $f_2=16$ BIN)	49
FIGURE 3.13. EXACT BLACKMAN WINDOW (TWO SIGNALS: $f_1=10.5$ BIN, $f_2=16$ BIN)	49
FIGURE 3.14. KAISER-BESSEL WINDOW FOR $\alpha=2$ (TWO SIGNALS: $f_1=10.5$ BIN, $f_2=16$ BIN)	50
FIGURE 3.15. KAISER-BESSEL WINDOW FOR $\alpha=3$ (TWO SIGNALS: $f_1=10.5$ BIN, $f_2=16$ BIN)	50
FIGURE 3.16. SIDELobe LEVELS OF CLASSICAL WINDOWS	51
FIGURE 3.17. CLASSICAL WINDOWS SIMULATION WITH LOW-LEVEL SIGNAL-TO-NOISE RATIO	53
FIGURE 3.18. CLASSICAL WINDOWS SIMULATION WITH HIGH-LEVEL SIGNAL-TO-NOISE RATIO	54
FIGURE 4.1. NONTRADITIONAL FM CHIRP WINDOW	73
FIGURE 4.2. MAGNITUDE SPECTRUM FOR LINEAR FM CHIRP WINDOW	74
FIGURE 4.3. PHASE SPECTRUM FOR LINEAR FM CHIRP WINDOW	74
FIGURE 4.4. MAGNITUDE SPECTRUM FOR SINGLE SIGNAL	75

FIGURE 4.5. MAGNITUDE SPECTRUM FOR TWO SINUSOIDS	75
FIGURE 4.6. MAGNITUDE SPECTRUM USING CONVENTIONAL WINDOWS	76
FIGURE 4.7. MAGNITUDE SPECTRUM USING A FREQUENCY STEPPED SIGNAL	77
FIGURE 4.8. CHIRP WINDOW WITH VARYING LEVELS OF SIGNAL TO NOISE RATIO (SINGLE SINUSOID)	78
FIGURE 4.9. RECTANGULAR WINDOW WITH VARYING LEVELS OF SIGNAL TO NOISE RATIO (TWO SINUSOIDS ONE BIN APART)	79
FIGURE 4.10. HAMMING WINDOW WITH VARYING LEVELS OF SIGNAL TO NOISE RATIO (TWO SINUSOIDS ONE BIN APART)	80
FIGURE 4.11. COMPLEX FM CHIRP WINDOW WITH VARYING LEVELS OF SIGNAL TO NOISE RATIO (TWO SINUSOIDS ONE BIN APART)	81
FIGURE 4.12. RECTANGULAR WINDOW WITH VARYING LEVELS OF SIGNAL TO NOISE RATIO (TWO SINUSOIDS ONE HALF BIN APART)	82

FIGURE 4.13. HAMMING WINDOW WITH VARYING LEVELS OF SIGNAL TO NOISE RATIO (TWO SINUSOIDS ONE HALF BIN APART)	83
FIGURE 4.14. CHIRP WINDOW WITH VARYING LEVELS OF SIGNAL TO NOISE RATIO (TWO SINUSOIDS ONE HALF BIN APART)	84
FIGURE 4.15. CHIRP WINDOW WITH SINGLE DAMPED SINUSOID (VARYING VALUES OF TIME CONSTANT)	85
FIGURE 4.16. CHIRP WINDOW WITH TWO DAMPED SINUSOIDS (VARYING VALUES OF TIME CONSTANT)	86
FIGURE 4.17. TRANSFORM OF CHIRP WINDOW	87
FIGURE C.1. SQUARE CHIRP WINDOW	103
FIGURE C.2. MAGNITUDE SPECTRUM OF THE SQUARE CHIRP WINDOW	104

I. INTRODUCTION

The general problem of spectral analysis is that of determining the spectral content of a random process based on a finite set of observations from that process. A variety of parametric and non-parametric techniques have been developed. Because of the relative ease with which Fourier spectra can be computed and the fact that the resulting spectral estimate (which is the magnitude squared of the transform) is directly proportional to the power of sinusoidal processes, the Fourier based non-parametric technique is a valued and widely used tool in spectrum analysis. This estimate is called the periodogram.

In many practical cases data consists of sinusoidal signals embedded in white Gaussian noise, and in such cases it may be advantageous to apply a data window to the signal before computing the periodogram. Without data windowing, a lower level signal may be masked by the sidelobes of a higher level signal, provided that the signals are close in frequency. Windows can be used as weighting functions applied to data to reduce the spectral leakage associated with finite observation interval, or in other words, data windowing will reduce the magnitude of the periodogram at frequencies not near the signal frequency. This reduction is made at expense of increasing the bandwidth of the main lobe of the spectral estimates.

Generally, the traditional windows used in spectral analysis (rectangular, Hamming, Blackman, Kaiser, etc.) are positive, real valued, symmetric functions. One draw back of windows is their influence on the ability to detect spectral lines that are separated in frequency by an amount which is small compared to the spectral width of a single spectral component. The main objective of this thesis is to study a new data window in conjunction with the Fourier transform approach. This window possesses "high resolution" capabilities. The window to be studied is the complex linear FM chirp window presented by L. J. Griffiths [Reference 1].

Chapter II is a short review of spectral estimation. The classical method of spectral estimation, the periodogram, is analyzed in detail. Deterministic signals and wide-sense stationary stochastic processes are examined. Due to the random nature of the signal in the last case, the mean and the variance of the periodogram are important issues that need to be addressed.

In Chapter III the main traditional windows, presented by F. J. Harris [Reference 2], will be developed by considering the method used by A. H. Nuttall [Reference 3] in analyzing the sidelobe behavior of windows. The performance of these windows in detecting a weak spectral line in the presence of a strong nearby line will be examined. If additive white Gaussian noise (AWGN) is present, the smaller signal will many times not be detected. A simulation using a signal composed of two equal amplitude sinusoids, not centered at bin frequencies, will be given.

Chapter IV will examine the results obtained by L. Griffiths [Reference 1] using the high resolution window which consists of a complex linear FM chirp. For high signal to noise ratios averaging is not necessary. The Fourier based spectral estimate is used for a single complex valued sinusoid and for two complex valued sinusoids. The results obtained are then compared with those found using a traditional raised-cosine window. Also, an example to illustrate the effect of the frequency chirp window on frequency shift keyed (FSK) signals is presented. Finally, the validity of this window is examined when the data consists of complex valued damped sinusoidal signals, and in addition the signal to noise ratio (SNR) dependency of this window is established.

Chapter V is devoted to conclusions and recommendations concerning the use of nontraditional windows in spectral analysis.

II. SPECTRAL ESTIMATION

A. BACKGROUND

The main objective of spectral estimation is to determine the spectral content of a random process from a finite set of observations. The Power Spectral Density (PSD) of the sampled sequence is defined by:

$$P_s(f) = \sum_{k=-\infty}^{\infty} R_{xx}(k) \exp(-j2\pi f k T_s) \quad (1)$$

where T_s is the interval between successive samples. This requires that the autocorrelation function $R_{xx}(k)$ is known for all values of k . In most practical cases, these values are not available. Instead, only N samples of the random signal $x(t)$ may be available, and from this limited data set the PSD must be estimated. It is necessary to find a method of estimating $\hat{P}_s(f)$ which permits the use of a finite data set. A question that has to be posed is whether or not this estimate is "consistent."

To determine consistency it is necessary to introduce some definitions such as bias, variance and frequency resolution. Given that N data samples are available, $x_n = x(nT_s)$ where $n = 0, 1, \dots, N-1$, and that an estimate of a given quantity Y is desired. Y could be the mean of the signal, its autocorrelation, its

PSD, or some other quantity of interest. The estimate of Y is denoted by the function

$$\hat{Y} = g(x_0, x_1, \dots, x_{N-1}). \quad (2)$$

Because x_0, x_1, \dots, x_{N-1} are random variables, \hat{Y} is also a random quantity with probability density function (PDF) $f(\hat{Y}/Y)$. In order to obtain a consistent estimator, it is necessary to choose $g(x_0, x_1, \dots, x_{N-1})$ such that its PDF is centered on the true value of Y , and has as small a variance as possible. Conversely, a poor estimator will have a probability density with a large variance and/or will not be centered on the true value of Y . These concepts are illustrated in Figure 2.1.

The "bias" b of an estimator is defined by the difference between its true value Y and the conditional average of its estimator \hat{Y} . Therefore,

$$b = Y - E[\hat{Y}/Y] \quad (3)$$

where, from [Ref. 4],

$$E[\hat{Y}/Y] = \int \dots \int_{-\infty}^{\infty} g(x_0, \dots, x_{N-1}) f(x_0, \dots, x_{N-1}/Y) dx_0 \dots dx_{N-1} \quad (4)$$

where $g(x_0, \dots, x_{N-1}) = x_0 x_1 x_2 \dots x_{N-1}$. An "unbiased" estimator is one for which $b = 0$.

The "variance" of estimator \hat{Y} relates to the width of the conditional probability density function $f(\hat{Y}/Y)$ and is defined by

$$\sigma_{\hat{Y}}^2 = E[(\hat{Y}/Y)^2] - (E[\hat{Y}/Y])^2 \quad (5)$$

where $E[(\hat{Y}/Y)]$ is the conditional expectation of \hat{Y} , as defined above, and $E[(\hat{Y}/Y)^2]$ is calculated by

$$E[(\hat{Y}/Y)^2] = \int \cdots \int_{-\infty}^{\infty} [g(x_0, \dots, x_{N-1})]^2 f(x_0, \dots, x_{N-1}/Y) dx_0 \cdots dx_{N-1} \quad (6)$$

An estimator is called "consistent" if both its bias and variance approach zero as the number of samples becomes large. Another concept of interest, "frequency resolution" will be introduced in the next section.

In this thesis, the only kind of estimator that will be considered is the nonparametric spectral estimation tool known as the periodogram.

B. PERIODOGRAM FOR DETERMINISTIC SIGNALS

The periodogram is one of the methods of classical spectral estimation, and is defined as the squared magnitude of the Discrete Fourier Transform (DFT) performed directly on the data set [Ref. 5]. Because the method of computation is relatively easy and fast when using the Fast Fourier Transform (FFT), the periodogram is the most popular estimator.

To develop a general formula to compute the periodogram, consider first the case of a "deterministic" analog signal $x(t)$, that is a continuous function of time. If $x(t)$ is absolutely integrable, then the signal energy ξ is finite and given by

$$\xi = \int_{-\infty}^{\infty} |x(t)|^2 dt < \infty \quad (7)$$

The Fourier transform of $x(t)$ exists, and is given by

$$X(f) = \int_{-\infty}^{\infty} x(t) \exp(-j2\pi f t) dt, \quad (8)$$

while the squared modulus of the Fourier transform is often called the spectrum $S(f)$ of $x(t)$, where

$$S(f) = |X(f)|^2. \quad (9)$$

Parseval's energy theorem relates energy by

$$\int_{-\infty}^{\infty} |x(t)|^2 dt = \int_{-\infty}^{\infty} |X(f)|^2 df = \int_{-\infty}^{\infty} S(f) df, \quad (10)$$

which means that the energy of the time domain signal is equal to the energy of the frequency domain transform. Therefore, $S(f)$ is an Energy Spectral Density (ESD); in other words, it represents the distribution of energy as a function of frequency.

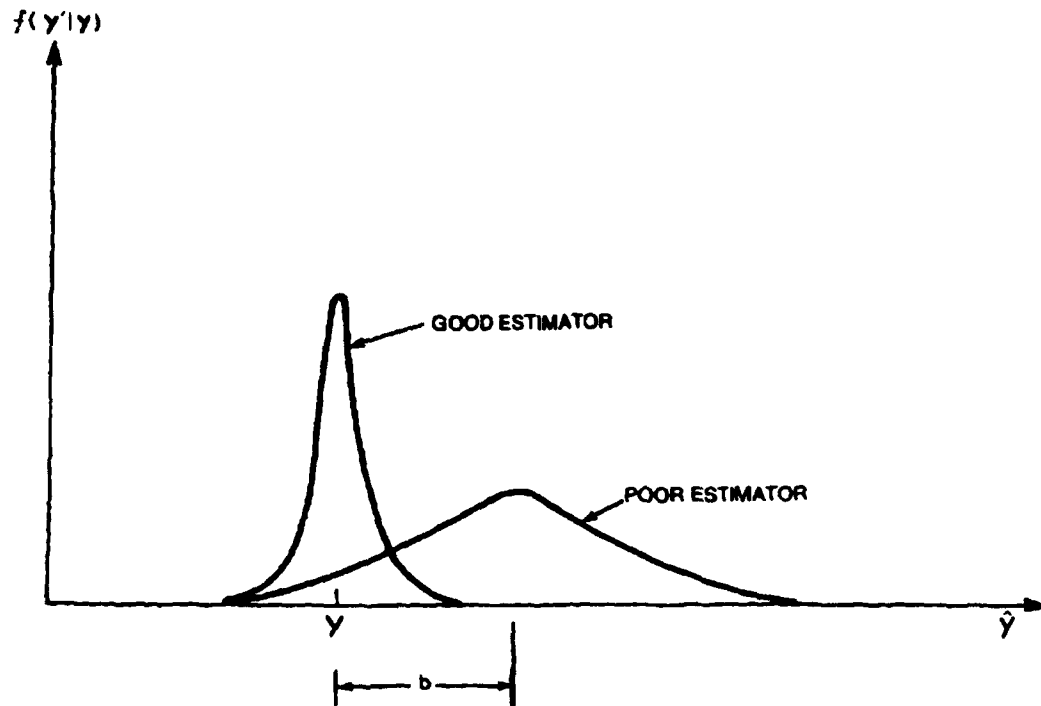


Figure 2.1. Conditional Probability Density Function For Good And Bad Estimator

To obtain a discrete sequence, $x(t)$ has to be sampled at regular intervals T_s , which results in

$$x_n = x(nT_s) \text{ for } -\infty < n < \infty \quad (11)$$

The sampled sequence x_n can be represented as the product of $x(t)$ and an infinite set of equal spaced delta functions, as in

$$x_n = \sum_{n=-\infty}^{\infty} x(t)\delta(t - nT_s). \quad (12)$$

Taking the Fourier transform of x_n leads to

$$X'(f) = \int_{-\infty}^{\infty} \left[\sum_{n=-\infty}^{\infty} x(t)\delta(t - nT_s)T_s \right] \exp(-j2\pi ft)dt, \quad (13)$$

(The factor T_s ensures conservation of integrated area between Equation (8) and Equation (13) [Ref. 5].)

hence

$$X'(f) = T_s \sum_{n=-\infty}^{\infty} x_n \exp(-j2\pi fnT_s). \quad (14)$$

$X'(f)$ and $X(f)$ will be identical in value over the interval $-\frac{1}{2T_s} < f < \frac{1}{2T_s}$ as long as $x(t)$ is band limited. Thus, the ESD is

$$S'(f) = |X'(f)|^2 = S(f). \quad (15)$$

In order to define a Discrete Fourier Transform (DFT), it is necessary to consider the following conditions:

- The data sequence is available from a finite time "window" that is $n = 0$ to $n = N-1$;
- The transform is discretized for N values by taking samples at frequencies $f = m\Delta f$ where $\Delta f = \frac{1}{NT_s}$ and $m = 0, 1, \dots, N-1$. The DFT is defined as

$$X_m = T_s \sum_{n=0}^{N-1} x_n \exp(-j2\pi m \Delta f n T_s) \quad (16)$$

where $\Delta f = \frac{1}{NT_s}$, hence

$$X_m = T_s \sum_{n=0}^{N-1} x_n \exp(-j2\pi mn/N) \quad , \text{ for } m = 0, 1, \dots, N-1. \quad (17)$$

- The inverse DFT is given by

$$x_n = \Delta f \sum_{m=0}^{N-1} X_m \exp(j2\pi mn/N) \quad , \text{ for } n = 0, 1, \dots, N-1, \quad (18)$$

therefore the discrete Energy Spectral Density may be defined as

$$S_m = |X_m|^2 \quad (19)$$

where X_m is the DFT of x_n for $0 < m < N-1$;

- For a deterministic signal $x(t)$, both the discrete S_m , and the continuous $S'(f)$ have been called periodogram spectral estimates.

C. PERIODOGRAM FOR STOCHASTIC PROCESSES

A different point of view must be taken when $x(t)$ is Wide Sense Stationary (WSS) stochastic process rather than deterministic, finite energy signal. In this case the parameter of interest is the power (time average of energy) density as a function of the energy becomes very large, i.e., $\xi \rightarrow \infty$. The autocorrelation function of a stationary random process is given by

$$R_{xx}(\tau) = E[x^*(t + \tau)x(t)] \quad (20)$$

where E is the expectation operator. This expression provides the basis for spectrum analysis, rather than $x(t)$ itself. The PSD of a random process $x(t)$ is defined as the Fourier transform of $R_{xx}(\tau)$

$$P_x(f) = F[R_{xx}(\tau)], \quad (21)$$

or

$$P_x(f) = \int_{-\infty}^{\infty} R_{xx}(\tau) \exp(-j2\pi f\tau) d\tau. \quad (22)$$

Usually, the autocorrelation function $R_{xx}(\tau)$ is unknown, thus the assumption that the random process $x(t)$ is ergodic has to be made in order to permit the substitution of time averages for ensemble averages. Under this assumption $R_{xx}(\tau)$ may be expressed as

$$R_{xx}(\tau) = \lim_{T \rightarrow \infty} \frac{1}{2T} \int_{-T}^T x(t + \tau)x^*(t) dt \quad (23)$$

and it is possible to show that $P_x(f)$ may be expressed as [Ref. 5]

$$P_x(f) = \lim_{T \rightarrow \infty} E \left[\frac{1}{2T} \left| \int_{-T}^T x(t) \exp(-j2\pi ft) dt \right|^2 \right]. \quad (24)$$

In the last expression it is important to note the presence of the expectation operator since, due to the ergodic property of $R_{xx}(\tau)$, the limit $T \rightarrow \infty$ in $P_x(f)$ without the expected value does not converge in any statistical sense.

If $P_x(f)$ is sampled for values $n = 0, 1, \dots, N - 1$, then

$$P_s(f) = \lim_{T \rightarrow \infty} \frac{1}{NT_s} \left| T_s \sum_{n=0}^{N-1} x_n \exp(-j2\pi f n T_s) \right|^2, \text{ for } -\frac{1}{2T_s} \leq f \leq \frac{1}{2T_s}. \quad (25)$$

Note that the expectation factor has been ignored, which can cause statistically inconsistent results (i.e., the variance of spectral estimate does not decrease even if longer sequences are used). The Fast Fourier Transform (FFT) is used to evaluate $P_s(f)$. In fact if $f_m = m\Delta f$ (equally spaced frequencies for $m = 0, 1, \dots, N - 1$) with $\Delta f = \frac{1}{NT_s}$, then

$$P_s(f_m) = \hat{P}_m = \frac{1}{NT_s} \left| T_s \sum_{n=0}^{N-1} x_n \exp\left(\frac{-j2\pi mn}{N}\right) \right|^2. \quad (26)$$

By definition, the DFT (hence FFT) of x_n is given by

$$X_m = T_s \sum_{n=0}^{N-1} x_n \exp\left(\frac{-j2\pi mn}{N}\right), \quad (27)$$

and therefore

$$\hat{P}_m = \hat{P}_{\text{per}(m)} = \frac{1}{NT_s} |X_m|^2. \quad (28)$$

Replacing the value of X_m , the formula for the periodogram is obtained by

$$\hat{P}_{\text{per}(m)} = \frac{T_s}{N} \left| \sum_{n=0}^{N-1} x_n \exp\left(\frac{-j2\pi mn}{N}\right) \right|^2. \quad (29)$$

This last expression may be efficiently computed using the FFT.

It is important to note that the periodogram has some limitations, such as:

- The frequency resolution Δf is limited by the length of the data record to $\Delta f = \frac{1}{NT_s}$;
- Because the DFT can be written as the convolution of the true Fourier transform with the Fourier transform of a rectangular window, there is a limited ability (due to leakage), to detect weak peaks in the presence of strong peaks.
- Random data can produce other difficulties because the periodogram is not a consistent estimator, as is shown in Section 2.3.1 and 2.3.2.

1. Bias of the Periodogram

The bias of the estimator $\hat{P}_{\text{per}(f)}$ can be determined by computing its mean value and then comparing it with the true power spectral density.

If $x(t)$ is a WSS process, then the PSD of the sampled sequence x_n is given by

$$P_s(f) = \sum_{k=-\infty}^{\infty} R_{xx}(k) \exp(-j2\pi k f T_s). \quad (30)$$

The periodogram can be written as

$$\hat{P}_{\text{per}}(f) = \frac{1}{N} \left| \sum_{n=0}^{N-1} x_n \exp(-j2\pi f n T_s) \right|^2 \quad (31)$$

where

$$f = \frac{m}{NT_s} \text{ for } m = 0, 1, \dots, N - 1. \quad (32)$$

The ensemble average of $\hat{P}_{\text{per}}(f)$ using

$$R_{xx}(n - m) = E[x_n x_m]$$

is expressed

$$E[\hat{P}_{\text{per}}(f)] = \frac{1}{N} \sum_{n=0}^{N-1} \sum_{m=0}^{N-1} R_{xx}(n - m) \exp(-j2\pi(n - m)fT_s). \quad (33)$$

For an arbitrary function $g(k)$, it can be shown that

$$\sum_{n=0}^{N-1} \sum_{m=0}^{N-1} g(n - m) = \sum_{k=-(N-1)}^{N-1} (N - |k|)g(k), \quad (34)$$

hence

$$E[\hat{P}_{\text{per}}(f)] = \sum_{k=-(N-1)}^{N-1} \left(1 - \frac{|k|}{N}\right) R_{xx}(k) \exp(-j2\pi k f T_s) \quad (35)$$

If Equation 35 is compared with Equation 30, it is seen, for k not equal to 0, that the results are not equal, and therefore the estimate $\hat{P}_{\text{per}}(f)$ is biased. The bias of this estimator is defined as the difference between the true PSD and the mean value of the estimator (i.e., if both are equal then the estimator is unbiased). The last equation can also be written as

$$E[\hat{P}_{per}(f)] = \sum_{k=-\infty}^{\infty} w(k) R_{xx}(k) \exp(-j2\pi k f T_s) \quad (36)$$

where $w(k)$ is the triangular window given by

$$w(k) = \begin{cases} 1 - \frac{|k|}{N} & \text{for } |k| < N - 1 \\ 0 & \text{elsewhere} \end{cases} \quad (37)$$

The periodogram windows the autocorrelation with a triangular window. This corresponds to the convolution of the Fourier transform of the two functions.

Thus, Equation 36 can be written in terms of $W(f)$, the Fourier transform of $w(k)$ and the Fourier transform of $R_{xx}(k)$ which according to Equation 30 is the true PSD $P_s(f)$. Therefore

$$E[\hat{P}_{per}(f)] = \int_{-\frac{1}{2}}^{\frac{1}{2}} P_s(f') W_N(f - f') df', \quad (38)$$

where

$$W_N(f) = \frac{1}{N} \left(\frac{\sin \pi f N}{\sin \pi f} \right)^2. \quad (39)$$

From Equation 38 it can be seen that the Periodogram average is equivalent to viewing the true spectrum through the spectral window $W_N(f)$. Because $W_N(f)$ becomes more and more sharply peaked about $f = 0$ as $N \rightarrow \infty$, it is evident from Equation 38 that although the periodogram is biased, it is

asymptotically unbiased. In other words, if enough data is available, that is $N \rightarrow \infty$ then

$$\lim_{N \rightarrow \infty} E[\hat{P}_{\text{per}}(f)] \rightarrow P_s(f). \quad (40)$$

Hence, the mean converges to the true PSD. It is also evident from Equation 38 that the resolution of the periodogram is determined by the spectral width of $W_N(f)$ which is approximately $\Delta f = \frac{1}{NT_s}$, where T_s is the interval between successive samples and N is the number of samples.

2. Variance of the Periodogram

The variance of the periodogram is given by

$$\text{Var}(\hat{P}_{\text{per}}(f)) = \text{Cov}(\hat{P}_{\text{per}}(f), \hat{P}_{\text{per}}(f)), \quad (41)$$

where the covariance is defined by

$$\text{Cov}(\hat{P}_{\text{per}}(f_1), \hat{P}_{\text{per}}(f_2)) = E[\hat{P}_{\text{per}}(f_1)\hat{P}_{\text{per}}(f_2)] - E[\hat{P}_{\text{per}}(f_1)]E[\hat{P}_{\text{per}}(f_2)]. \quad (42)$$

Assuming white Gaussian noise of spectral height $P(f)$, the covariance becomes

$$\text{Cov}(\hat{P}_{\text{per}}(f_1), \hat{P}_{\text{per}}(f_2)) = P_s(f_1)P_s(f_2) \left[\left(\frac{\sin N \pi (f_1 + f_2) T_s}{N \sin \pi (f_1 + f_2) T_s} \right)^2 + \left(\frac{\sin N \pi (f_1 - f_2) T_s}{N \sin \pi (f_1 - f_2) T_s} \right)^2 \right]. \quad (43)$$

For $f_1 = f_2 = f$ this becomes

$$\text{Var}(\hat{P}_{\text{per}}(f)) = (P_s(f))^2 \left[1 + \left(\frac{\sin 2 \pi f N T_s}{N \sin 2 \pi f T_s} \right)^2 \right]. \quad (44)$$

If $N \rightarrow \infty$, then

$$\text{Var}(\hat{P}_{\text{per}}(f)) = (P_s(f))^2. \quad (45)$$

It is important to note that the variance is a "constant" independent of N , or as $N \rightarrow \infty$ the variance does not approach to zero. Therefore the periodogram is not a consistent estimator. The standard deviation (square root of the variance) is as large as the mean (the quantity to be estimated).

The fact that the variance of the periodogram does not decrease with increasing data record length may be attributed to the lack of an expectation operator in the definition of $P(f)$. The periodogram can be enhanced to make it a consistent estimator. To reduce the variance, at expense of frequency resolution, a number of periodograms can be averaged.

D. PERIODOGRAM AVERAGING

The data record x_0, x_1, \dots, x_{N-1} can be divided into K segments, each consisting of M samples (i.e., $N = KM$). This means there are K subrecords, given by

- Subrecord 1 x_0, x_1, \dots, x_{M-1}
- Subrecord 2 $x_M, x_{M+1}, \dots, x_{2M-1}$
- Subrecord 3 $x_{2M}, x_{2M+1}, \dots, x_{3M-1}$

- Subrecord K $x_{(K-1)M}, x_{(K-1)M+1}, \dots, x_{N-1}$

For each of these records, the periodogram is computed as

$$\hat{P}_{\text{per}}(f, k) = \frac{1}{M} \left| \sum_{n=kM}^{(k+1)M-1} x_n \exp(-j2\pi n f T_s) \right|^2, \text{ for } k = 0, 1, \dots, K-1. \quad (46)$$

The average of these periodograms is given by

$$\hat{P}_{\text{avper}}(f) = \frac{1}{K} \sum_{k=0}^{K-1} \hat{P}_{\text{per}}(f; k) \quad (47)$$

or

$$\hat{P}_{\text{avper}}(f) = \frac{1}{KM} \sum_{k=0}^{K-1} \left| \sum_{n=kM}^{(k+1)M-1} x_n \exp(-j2\pi n f T_s) \right|^2. \quad (48)$$

It is important to note that because the length of each data record is now M , the frequency resolution has been reduced by a factor of K , from

$$\Delta f = \frac{1}{NT_s} \text{ to } \Delta f = \frac{1}{MT_s} \quad (\text{recall that } N = KM).$$

Therefore, whatever improvement found in the variance is traded off against a loss in resolution.

To determine whether this averaged periodogram is consistent, its bias and variance have to be computed. The mean value of the average periodogram will be the same as the mean value of the periodogram based on any of the individual

data sets. Since the periodogram for each data set is identically distributed and the data are assumed to be statistically independent as well as stationary

$$E[\hat{P}_{\text{avper}}(f)] = \frac{1}{K} \sum_{k=0}^{K-1} E[\hat{P}_{\text{per}}(f; k)] = E[\hat{P}_{\text{per}}(f; 0)] \quad (49)$$

or

$$E[\hat{P}_{\text{avper}}(f)] = E\left[\frac{1}{M} \left| \sum_{n=0}^{M-1} x_n \exp(-j2\pi n f T_s) \right|^2\right]. \quad (50)$$

Using Equation 35 and Equation 38 with N replaced by M

$$E[\hat{P}_{\text{avper}}(f)] = \sum_{k=-(M-1)}^{(M-1)} \left(1 - \frac{|k|}{M}\right) R_{xx}(k) \exp(-j2\pi k f T_s) \quad (51)$$

hence

$$E[\hat{P}_{\text{avper}}(f)] = \int_{-\frac{1}{2}}^{\frac{1}{2}} P(f') W_M(f - f') df' \quad (52)$$

where

$$W_M(f) = \frac{1}{M} \left(\frac{\sin \pi M f T_s}{\sin \pi f T_s} \right)^2. \quad (53)$$

Comparing $E[\hat{P}_{\text{avper}}(f)]$ in Equation 52 with the true PSD in Equation 30, it is clear that this estimator is "biased". Furthermore, because $M \leq N$ the resolution is poorer (i.e.: $\Delta f = \frac{1}{M T_s}$) than the one obtained using all of the data. Although resolution is lost, the advantage using the averaged periodogram is evident when its variance is computed. The variance of the averaged periodogram is

$$\text{Var}(\hat{P}_{\text{avper}}(f)) = \frac{1}{K} \text{Var}(\hat{P}_{\text{per}}(f)) = \frac{1}{K} (P_s(f))^2 \left[1 + \left(\frac{\sin 2\pi M f T_s}{M \sin 2\pi f T_s} \right)^2 \right] \quad (54)$$

or

$$\text{Var}(\hat{P}_{\text{avper}}(f)) \rightarrow \frac{1}{K} (P_s(f))^2. \quad (55)$$

The variance has been reduced by a factor of K below that of the unaveraged periodogram.

Periodogram averaging allows reduction of the variance of the estimate at the expense of frequency resolution. The value of K must be chosen in such a way as to obtain an desirable reduction in variance at an acceptable frequency resolution.

Finally, a technique known as the "Welch Method" will be mentioned. This technique consists of windowing each data segment $(x_0, x_1, \dots, x_{M-1})$ with a non-rectangular window before forming the periodogram (i.e., x_n is replaced by $w_n x_n$, where w_n is the window weighting). The advantages of this technique are the same as discussed in the context of straight periodogram averaging. For instance, if triangular windows with 50% overlap are used, the frequency resolution is poorer by a factor of 1.42 due to the windows, but the variance is improved by a factor of 1.77 [Ref. 4] due to the overlap.

III. CLASSICAL WINDOWS

A. INTRODUCTION

Generally, a signal $x(t)$ can exist in the entire interval $(-\infty, \infty)$, but this signal is often corrupted by noise. From the point of view of spectral analysis, the detection and estimation of the signal necessitates that it be of finite length, in other words, every observed signal that has to be processed must be of finite length. Considerations of spectral analysis include:

- Detectability of tones in the presence of nearby strong spectral components.
- Resolvability of similar strength nearby spectral components.

Spectral analysis data involves two basic operations: sampling and windowing. It is necessary to define the observation interval (NT_s) (sec.), where, N is the number of uniformly spaced samples of the observed signal and T_s is the time interval between samples.

The selection of a finite time interval (NT_s) leads to an interesting peculiarity of spectral analysis: If the record length NT_s is selected in such way that it is not an integer multiple of the period of the signal, a discontinuity will be introduced by truncating the signal. This produces the undesired effect known as "leakage", the non-zero projection of smeared frequency components.

Windows can be defined as weighting functions applied to data in order to reduce the spectral leakage associated with finite observation interval. Essentially, the window function is applied to data to reduce the order of the discontinuity at the boundary of the periodic extension.

The requirements of real-world machine processing also dictate that the data set be of finite extent. As an example, the pair $x(nT_s)$ (the sampled signal) and $X_s(f)$ (the Fourier transform of $x(nT_s)$), is not suited for numerical computation. This is so because the number of samples $x(nT_s)$ of $x(t)$ is not finite, and because $X_s(f)$, or the Fourier transform of the sampled data, is continuous rather than discrete, where

$$X_s(f) = \frac{1}{T_s} \sum_{m=-\infty}^{\infty} X\left(f - \frac{m}{T_s}\right) \quad (56)$$

Appendix A contains the derivation of the above equation.

It is therefore necessary to limit the sequence $x(nT_s)$ to a finite number of samples and sample $X_s(f)$ at some appropriate location, in order to obtain the discrete function

$$X(m) = X_s\left(f = \frac{m}{T_0}\right) \text{ where } m = \text{integer and } T_0 = \text{record length.}$$

The objective is to get the discrete pair $x(nT_s)$ and $X(m)$, for a good approximation to the continuous Fourier transform pair $x(t)$, $X(f)$.

B. WINDOWING A DISCRETE SIGNAL

If $x(nT_s)$ is the sampled version of the signal and $w(nT_s)$ is the sampled window function, then the Fourier transform of the windowed sampled data signal is given by

$$G_s(f) = \sum_{n=0}^{N-1} g(nT_s) \exp(-j2\pi f n T_s) \quad (57)$$

where $g(nT_s)$ is the windowed sampled signal defined as

$$g(nT_s) = x(nT_s) w(nT_s), \text{ then}$$

$$G_s(f) = \sum_{n=0}^{N-1} x(nT_s) w(nT_s) \exp(-j2\pi f n T_s) \quad (58)$$

where

$$w(nT_s) = 0, \text{ for } n \geq N \text{ and } n < 0 \quad (59)$$

and N = number of uniformly spaced samples of the observed signal.

The effects of the window in the spectral estimate are shown by the interpretation of the Equation 58. This equation shows that the transform $G_s(f)$ is the transform of a product, and because multiplication in the time domain

corresponds to the convolution of the two corresponding transforms in the frequency domain, it follows that

$$G_s(f) = \int_{-\infty}^{\infty} X(f')W(f-f')df' \quad (60)$$

or

$$G_s(f) = X(f) * W(f). \quad (61)$$

This last equation is the key to the effects of processing finite length data, since it represents the sum of all of the spectral contributions to each f weighted by the window centered at f' and measured at f [Ref. 5].

The samples of the Fourier transform $G_s(f)$ of the windowed sampled signal, can be related to the discrete Fourier transform if the sampling rate is at $f = \frac{m}{T_0}$. Therefore,

$$G(m) = G_s(f = \frac{m}{T_0}) = \sum_{n=0}^{N-1} g(nT_s) \exp(-j2\pi nmT_s/T_0) \text{ for } m = 0, 1, \dots, N-1. \quad (62)$$

The record length is defined as $T_0 = NT_s$. The discrete Fourier transform pair is obtained as

$$G(m) = \sum_{n=0}^{N-1} g(nT_s) \exp(-j2\pi nm/N), \quad (63)$$

and the inverse discrete Fourier transform is defined by

$$g(n) = \frac{1}{N} \sum_{m=0}^{N-1} G(m) \exp(j2\pi mn/N). \quad (64)$$

At this point is important to emphasize the following points:

- Both $G(m)$ and $g(n)$ are periodic.
- The values of $G(m)$ for $0 \leq m \leq \frac{N}{2}$ correspond to the positive frequencies of $X(f)$.
- If T_s is chosen in accordance with the sampling theorem, and $T_0 = NT_s$ is sufficiently large, (i.e., to improve $\Delta f = \frac{1}{T_0}$) then for $0 \leq m \leq N-1$ the discrete transform $G_s(f)$ is a good approximation to the samples $X(f)$ of the continuous transform.

C. CLASSICAL WINDOWS

Classic windows are weighting functions, generally of the form of a raised cosine, used in spectral analysis to reduce spectral leakage. In past years, several classical windows have been developed [Ref. 2]. In this chapter a reconstruction of these main traditional windows will be made, along with a comparative study of the performance of these windows in the detection of a weak spectral line in the presence of a strong nearby line.

A brief definition of the principal parameters used when comparing windows performance is provided below.

- The **equivalent noise bandwidth** measures the bandwidth of the window.

The objective is to minimize the bandwidth of the window in order to eliminate the noise in the passband region of the signal.

- **Processing Gain** (PG) is defined as the ratio of output signal-to-noise ratio to input signal-to-noise ratio (i.e., $PG = \frac{S_o/N_o}{S_i/N_i}$). A detailed approach to PG is given in Appendix B.

- The **highest side lobe level** is the measure of the highest peak sidelobe relative to the main lobe, and is an indicator of how well a window suppresses the leakage effect. A window should exhibit low sidelobes away from the main lobe to reduce the effects produced by spectral leakage.

- The **scalping loss** is defined as the ratio of coherent gain for a tone located half a bin from a DFT sample point to the coherent gain for a tone located at a DFT sample point, and is related to minimum detectable signal.

Two important concepts are here introduced: *Coherent gain*, defined as the sum of the window term $w(nT_s)$, or the DC signal gain of the window (i.e., coherent gain = $\sum_n w(nT_s)$); and a *bin* that is defined as the fundamental frequency resolution (i.e., bin = $\frac{f_s}{N}$ where f_s is the sampling frequency and N is the number of samples).

- The **worst case processing loss** measures the reduction of the output signal to noise ratio as a result of windowing and of worst case frequency location, and is defined as the sum of maximum scalping loss of a window

and of processing loss due to that window. It is an important parameter since it allows for maximizing the detectability of tones.

- ♦ The **minimum resolution bandwidth** (3.0 dB bandwidth) is related to the minimum separation between two equal strength spectral lines such that their respective main lobes can be resolved. The criterion for this resolution is the 3 dB bandwidth of the window and means that two equal strength main lobes separated in frequency by less than their 3 dB bandwidths will not be resolved easily as two distinct spectral lines.
- ♦ The **6 dB bandwidth** defines the resolution of the windowed DFT. The DFT output points are the linear addition of the spectral components weighted through the window at a given frequency, therefore the sum at the crossover point of the kernels must be smaller than the individual peaks if the two peaks are to be resolved. This means that at the crossover point the gain from each kernel must be less than 0.5 or the crossover point must occur beyond the 6 dB points of the window.

Of all the above mentioned parameters, the most important is the sidelobe level, since it allows for reduction of the bias produced by leakage. Therefore, an analysis of the sidelobe behavior of the windows following the approach presented by H. Nuttall is considered next. The relationships obtained will be used in analyzing the performance of windows [Ref. 3]. The windows of interest are of the form

$$w(t) = \frac{1}{L} \sum_{k=0}^K a_k \cos(2\pi kt/L) \text{ for } |t| \leq \frac{L}{2} \quad (65)$$

where K is an integer, (i.e., $K + 1$ is the number of terms in the window equation), a_k is a real constant, and L is the duration of the window. The Fourier transform of $w(t)$ is given by

$$W(f) = \int_{-L/2}^{L/2} w(t) \exp(-j2\pi ft) dt \quad (66)$$

where the window $w(t)$ is a continuous function of time, and possesses all orders of derivatives for $|t| \leq \frac{L}{2}$. However, discontinuities in $w(t)$ or its derivatives occur at $t = \pm \frac{L}{2}$. These discontinuities dictate the asymptotic behavior of $W(f)$. The window $w(t)$ is normalized according to

$$\sum_{k=0}^K a_k = 1 \quad (67)$$

$$w(0) = \frac{1}{L} \sum_{k=0}^K a_k = \frac{1}{L}. \quad (68)$$

It is also observed that

$$w\left(\pm \frac{L}{2}\right) = \lim_{|t| \rightarrow L/2^-} w(t) = \frac{1}{L} \sum_{k=0}^K (-1)^k a_k. \quad (69)$$

This last equation may or may not be equal to zero. With non-zero values, $w(t)$ is discontinuous at $t = \pm \frac{L}{2}$ and $W(f)$ will decay at $1/f$ (hence, 6 dB roll off per

octave). At a value of zero $w(t)$ is continuous for all t . Also $w'(t)$ is continuous for all t since

$$w'(t) = -\frac{2\pi}{L^2} \sum_{k=0}^K k a_k \sin(2\pi k t/L) \quad (70)$$

and

$$\lim_{|t| \rightarrow L/2} w'(t) = 0. \quad (71)$$

However, $w''(t)$ may not be continuous at $t = \pm L/2$ because

$$w''(t) = -\frac{4\pi^2}{L^3} \sum_{k=0}^K k^2 a_k \cos(2\pi k t/L) \quad (72)$$

and

$$\lim_{|t| \rightarrow \frac{L}{2}} w''(t) = -\frac{4\pi^2}{L^3} \sum_{k=0}^K (-1)^k k^2 a_k. \quad (73)$$

This last equation may or may not be equal to zero. If it is not zero, then $w''(t)$ is discontinuous at $t = \pm L/2$ and $W(f)$ will decay at $1/f^3$ (hence, 18 dB roll off per octave). However if it is zero, then $w''(t)$ is continuous for all t , and it follows that $w'''(t)$ is also continuous for all t , then $W(f)$ decays at least as fast as $1/f^5$ [Ref. 3].

D. COMPARISON OF CLASSICAL WINDOWS

Next the most important classic windows (i.e., rectangular, triangular, Hamming, Blackman and Kaiser windows) will be constructed, and their sidelobe behavior compared. The other significant parameters will be identified following those presented by F. J. Harris [Ref. 2]. The Fourier based spectral estimate of the window was obtained from the magnitude of the Fourier transform by

$$W(m) = \left| \sum_{n=0}^{N-1} w(n) \exp(-j2\pi nm/N) \right|^2. \quad (74)$$

In the simulation the window length is fixed at 51, while the FFT is taken at a size of 1024 (i.e., zero pad to 1024). Also, we will use normalized coordinates, and the resultant sequence will be shifted so that the left end point coincides with the origin. The sample period $T_s = 1$ allows to have a bin with a width of $1/N$.

1. Rectangular Window

This window is unity over the observation interval [Ref. 7]. The window for a DFT is defined as

$$w(n) = 1 \text{ for } n = 0, 1, \dots, N - 1 \quad (75)$$

The spectral window is given by

$$W(\theta) = \exp \left[-j \left(\frac{N}{2} - 1 \right) \theta \right] \frac{\sin(\frac{N}{2}\theta)}{\sin(\frac{1}{2}\theta)} \quad (76)$$

where

$$\theta = 2\pi T \quad \text{and} \quad T_s = 1.$$

As shown in Figure 3.1, the magnitude squared transform of this window is seen to be a sinc function, which has a DFT main lobe of two bins and a first sidelobe level approximately 13 dB down from the main lobe peak (which agrees with Harris [Ref. 2]). Since for this window there is only one coefficient non-zero, the window decays at only 6 dB/octave, which is the expected rate for a function with a discontinuity.

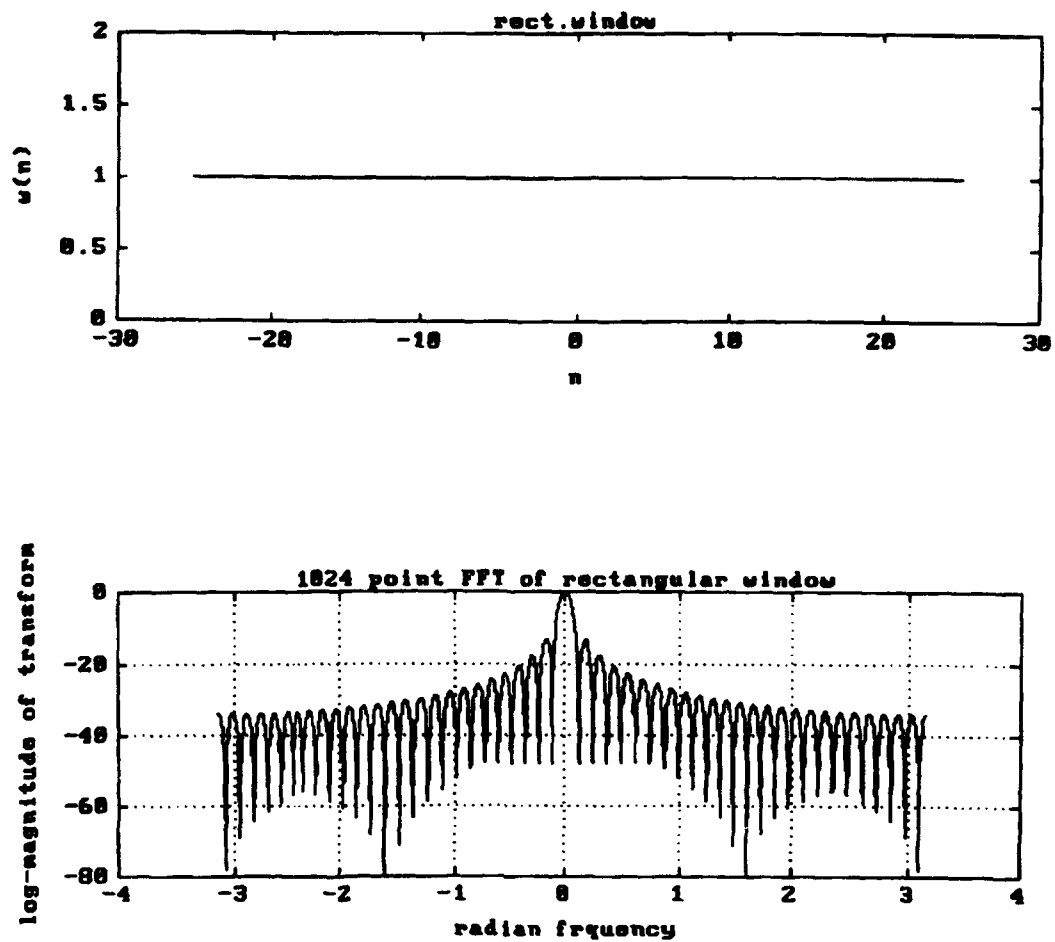


Figure 3.1. Rectangular Window.

2. Triangular Window

This window is defined as

$$w(n) = \frac{n}{N/2} \text{ for } n = 0, 1, \dots, N/2 \quad (77)$$

$$w(n) = w(N - n) \text{ for } n = N/2, \dots, N - 1. [\text{Ref. 8}] \quad (78)$$

The transform of a triangular window is given by

$$W(\theta) = \frac{2}{N} \exp \left[-j \left(\frac{N}{2} - 1 \right) \theta \right] \left[\frac{\sin \frac{N}{4} \theta}{\sin \frac{1}{2} \theta} \right]^2 . \quad (79)$$

This means that the transform of the window is the digital sinc² function.

Figure 3.2 shows the windows and the magnitude squared transform. The main lobe width is twice that of the rectangular window transform, and the sidelobe level (approximately 26 dB down from the main lobe peak) is twice as low as that of a rectangular window transform.

Because this window has a discontinuity in the first derivative, the sidelobes fall off at -12 dB/octave.

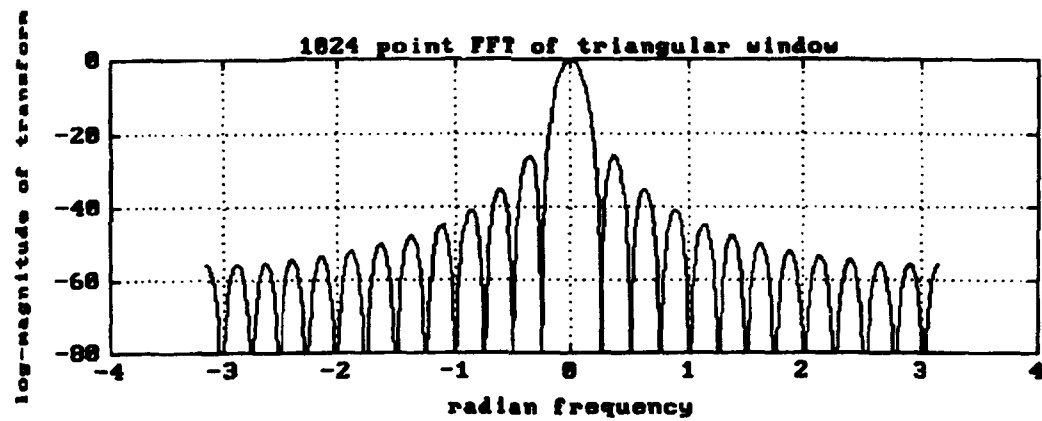
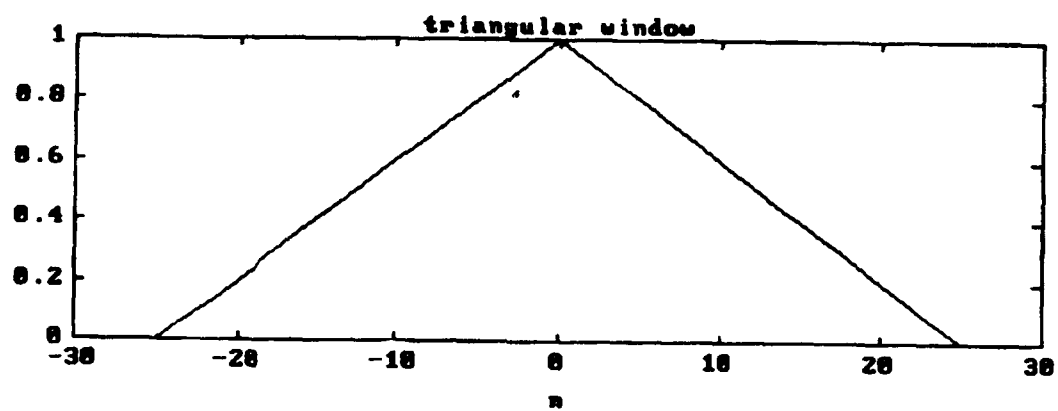


Figure 3.2. Triangular Window.

3. Hamming Window

This window is given by [Ref. 8]

$$w(n) = 0.54 - 0.46 \cos\left(\frac{2\pi}{N}n\right) \text{ for } n = 0, 1, \dots, N - 1 \quad (80)$$

The magnitude squared transform of this window is shown in Figure 3.3, and indicates that a marked improvement in the sidelobe level is realized. For this window the sidelobe level is seen to be approximately 43 dB lower than the main lobe peak. However, a broadening of the width of the main lobe should also be noted.

Because Equation 69 does not equal zero for the coefficients of Hamming window, this window has an asymptotic decay of 6 dB/octave.

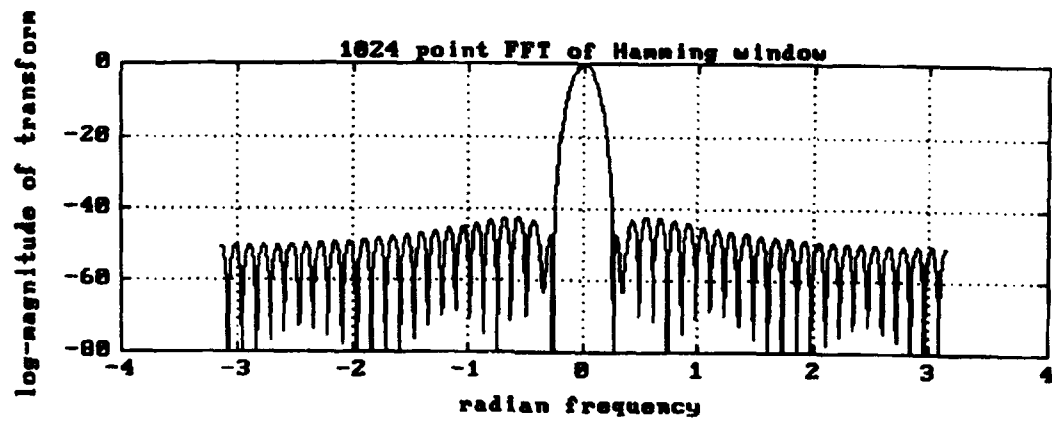
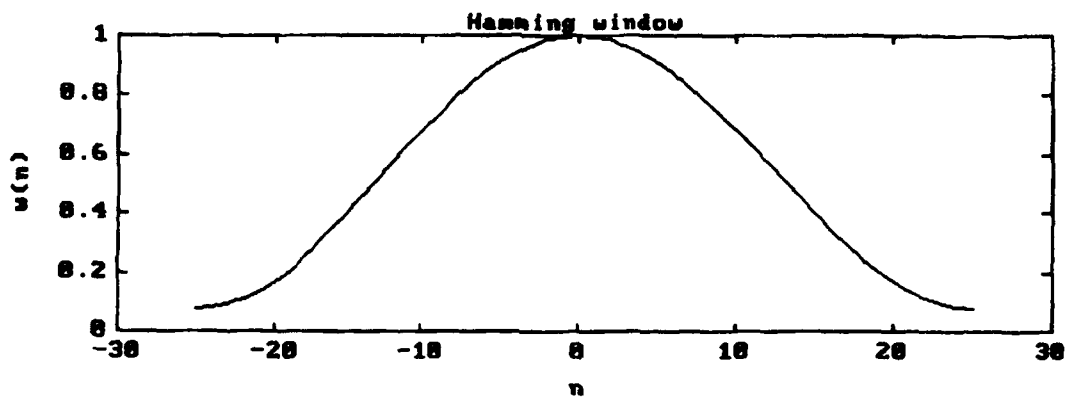


Figure 3.3. Hamming Window.

4. Blackman window

The equation for this window has three non-zero coefficients and was developed to achieve a window with a relatively narrow main lobe and low sidelobes [Ref. 8]. It is given by

$$w(n) = 0.42 - 0.5 \cos\left(\frac{2\pi}{N}n\right) + 0.08 \cos\left(\frac{2\pi}{N}2n\right) \quad (81)$$

for $n = 0, 1, \dots, N - 1$.

The Blackman window is shown in Figure 3.4. Its largest sidelobe is approximately 58 dB down from the main lobe peak. For the coefficients of this window Equation 69 is zero but Equation 73 is not, thus this window has an asymptotic decay of 18 dB/octave.

When referred to as the exact Blackman window, the following (exact) coefficients are included:

$$a_0 = 7938/18608$$

$$a_1 = 9240/18608$$

$$a_2 = 1430/18608.$$

When constructing this window, results differ from those of Harris [Ref. 2]. The exact Blackman window is depicted in Figure 3.5 and shows the largest sidelobe to be approximately 65 dB below the main lobe peak, not 51 dB down as cited in Harris work [Ref. 3]. Experimental results were closer to those presented by Nuttall (68.2 dB lower) [Ref. 3]. The rate of fall off is only 6 dB/octave. (Equation 69 is not equal to zero for the coefficients of this window).

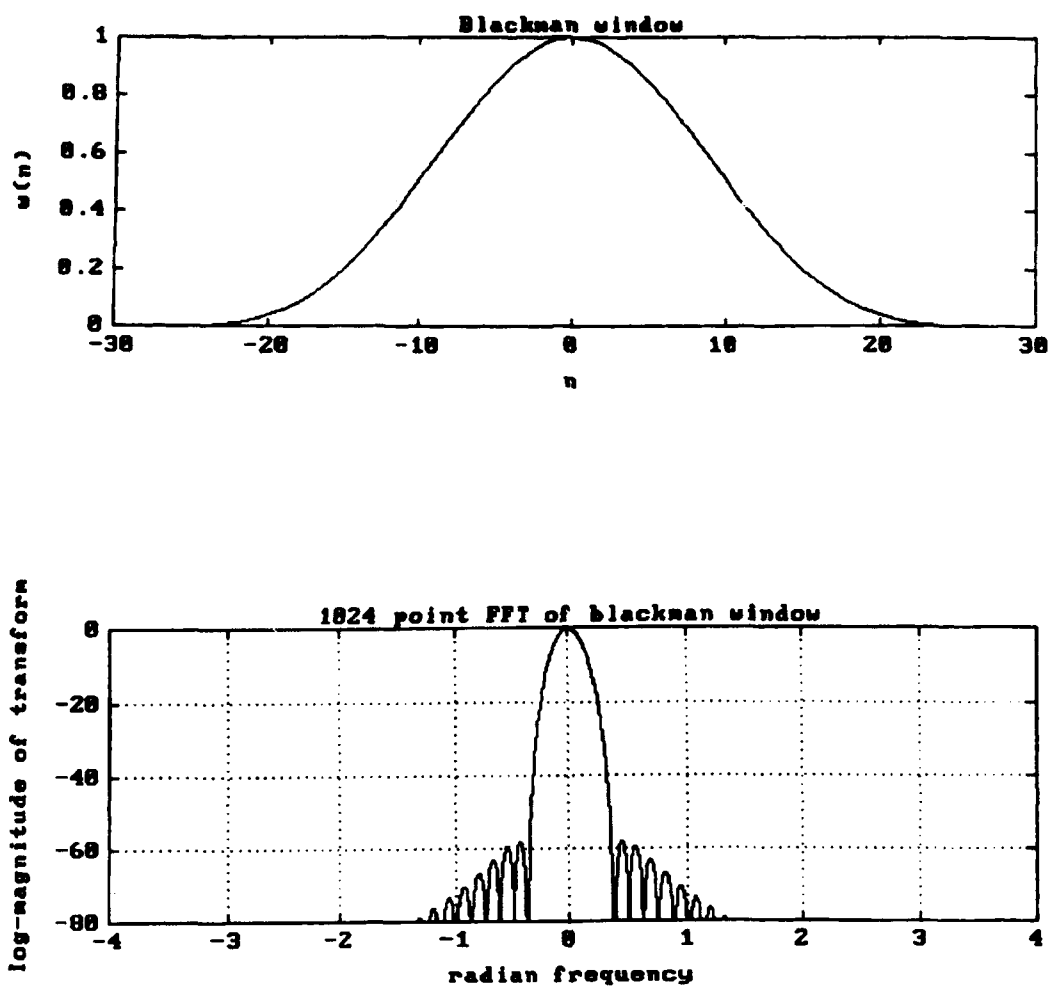


Figure 3.4. Blackman Window.

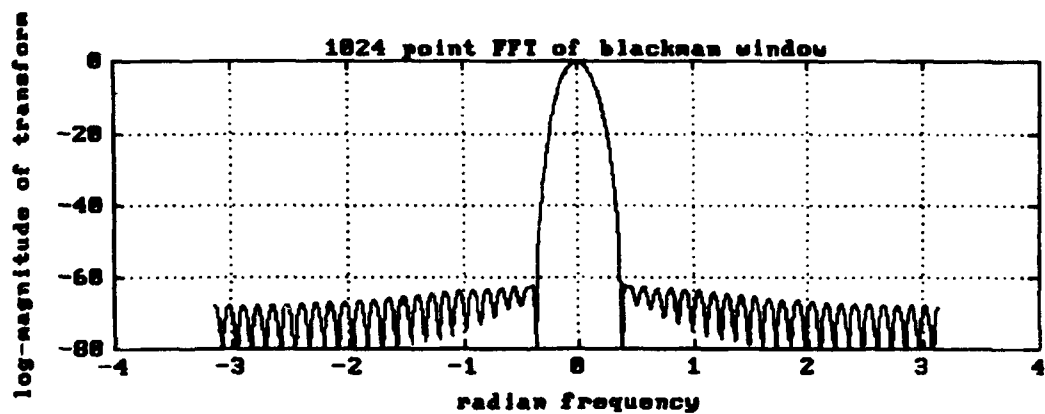
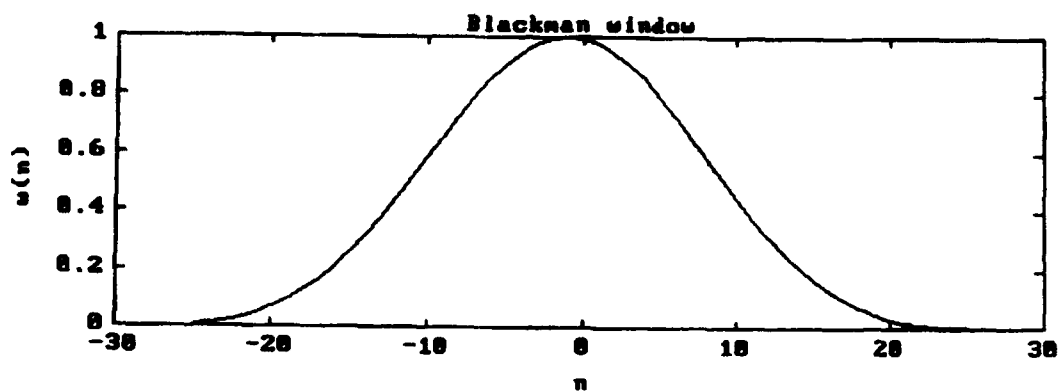


Figure 3.5. Exact Blackman Window.

5. Kaiser-Bessel Window

This window is of the form of the zero-th order modified Bessel function [Ref. 9] and is given by

$$w(n) = \frac{I_0(\pi\alpha \sqrt{1.0 - \frac{n^2}{N^2}})}{I_0(\pi\alpha)} \text{ for } 0 \leq |n| \leq \frac{N}{2}, \text{ where} \quad (82)$$

$$I_0(x) = \sum_{k=0}^{\infty} \left[\frac{\left(\frac{x}{2}\right)^k}{k!} \right]^2. \quad (83)$$

The parameter α can be selected, and its choice is a tradeoff between sidelobe level and mainlobe width. The transform is approximately given by

$$W(\theta) = \frac{N}{I_0(\alpha\pi)} \frac{\sinh\left(\sqrt{\alpha^2\pi^2 - (N\theta/2)^2}\right)}{\sqrt{\alpha^2\pi^2 - (N\theta/2)^2}}. \quad (84)$$

This window is presented in Figure 3.6 and Figure 3.7 for the values $\alpha = 2$ and $\alpha = 3$, respectively.

The figures demonstrate that for value of $\alpha = 2$ the highest sidelobe peak is approximately 50 dB down from the mainlobe peak, whereas for $\alpha = 3$ the sidelobe peak is approximately -70 dB, but a considerable increment in main lobe width should be noted. For both cases a fall off of 18 dB/octave is observed.

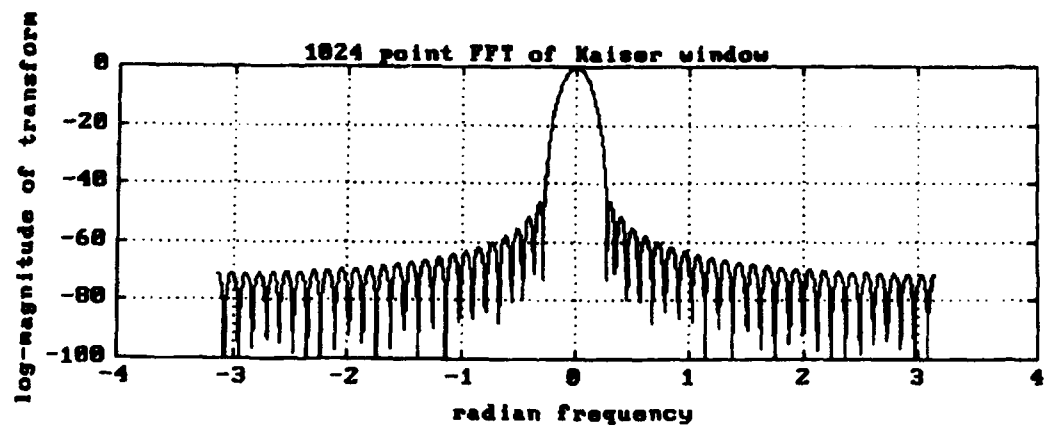
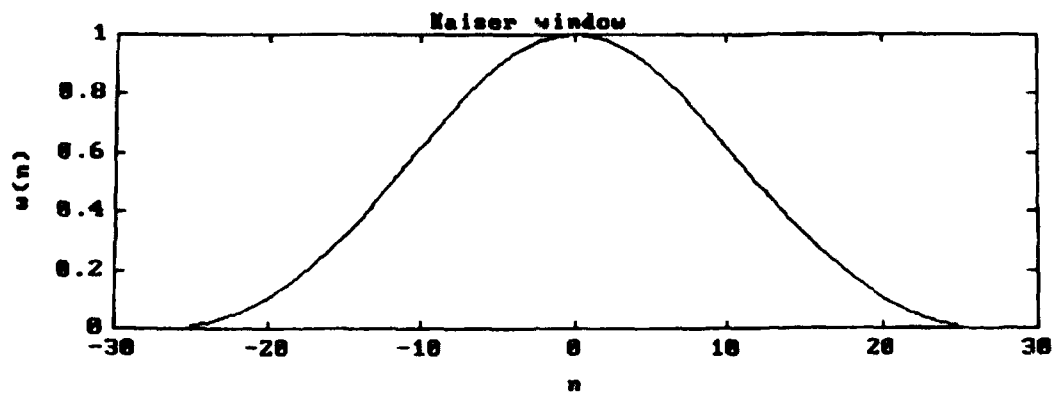


Figure 3.6. Kaiser-Bessel Window For $\alpha = 2$

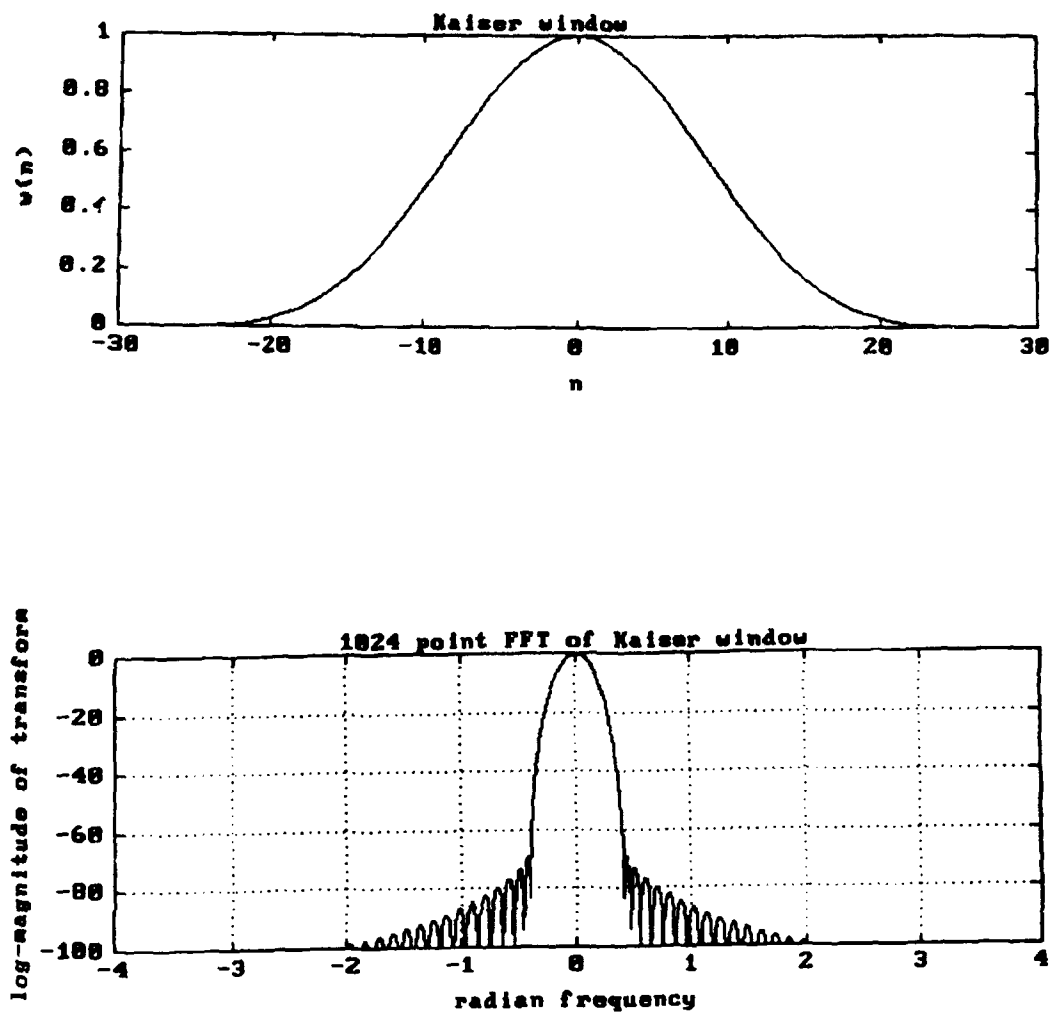


Figure 3.7. Kaiser-Bessel Window For $\alpha = 3$.

E. HARMONIC ANALYSIS USING CLASSICAL WINDOWS

The experiment to be described follows closely that presented by Harris [Ref. 2]. The objective is to demonstrate the influence that classical windows have on the detection of a weak spectral line in the presence of a strong nearby line. A signal composed of two frequencies has been considered, with the following parameters:

- ♦ sampling frequency $f_s = 1$ Hz.,
- ♦ record length $T_0 = 256$,
- ♦ number of samples $N = 256$,
- ♦ signal amplitudes $A_1 = 1$, $A_2 = 0.01$ (40 dB separation),
- ♦ signal frequencies $f_1 = 10.5$ bins $\approx 10.5 f_s / N$ and $f_2 = 16$ bins $= 16 f_s / N$.

It is interesting to observe the behavior of the rectangle window when the two spectral lines are located exactly in DFT bins (i.e. $f_1 = 10$ bin, $f_2 = 16$ bins). This is shown in Figure 3.8, where we can observe that the rectangular window allows identification of each spectral line with no interaction. However, in the present analysis the more difficult problem (i.e. $f_1 = 10.5$ bins) will be presented, that is where the poorer resolution occurs.

The power spectrum for a signal with $f_1 = 10.5$ bins and $f_2 = 16$ bins is shown in Figure 3.9, where the sidelobe of the larger signal has completely hidden the mainlobe of the smaller signal. This is due to the fact that the sidelobe level of the rectangle window 5.5 bins from the center is only at 25 dB down from the

peak (see Figure 3.1). Therefore the smaller signal (5.5 bins away from the largest) could not be detected because its main peak is at more than 25 dB down (i.e., -40 dB).

The case when applying a triangular window is presented in Figure 3.10, where the side lobes have fallen by a factor of two over the rectangle window's sidelobes (i.e., the -30 dB level has fallen to -60 dB). Also, the sidelobes of the largest signal have fallen to approximately -43 dB at the smaller signal so it is barely detectable (its mean peak level is at -40 dB). The artifacts at the base of the side lobe structure are probably due to the coherent addition of the kernels of the two signals.

The results of applying the Hamming window are presented in Figure 3.11. Here the weak signal can be detected, since its peak appears approximately at 35 dB down or approximately at 3 dB over the side lobe of the largest signal. Note that the sidelobe structure of the larger signal extends over the entire spectral range.

We next apply the Blackman window, and the results are depicted in Figure 3.12. The presence of the smaller signal can clearly be seen, since there is a deep null between the two lobes of approximately 17 dB. The artifact at the base of the large signal lobe is the sidelobe structure of that signal. The rapid rate of fall-off of the side lobes should be noted.

In Figure 3.13 the results of applying the exact Blackman window are presented. As in the Blackman window, the smaller signal is detected, since an approximately 20 dB null between the lobes of the two signals is observed. Note that now the sidelobe structure of the larger signal extends over the spectral range. However, this leakage is not too severe, since it is about 60 dB lower than the main lobe peak.

The last window to be demonstrated is the Kaiser-Bessel window, and the results are presented in Figures 3.14 and 3.15 for the values $\alpha = 2$ and $\alpha = 3$, respectively. Here too, an obvious detection of the weak signal can be made. It is important to note the effect of choosing the parameter ' α ', since a trade off between sidelobe level and main lobe width must be considered. For instance, with $\alpha = 2$, a null of approximately 20 dB is between the two main lobes, and the side lobe structure of the larger signal is about 60 dB below the main lobe, as illustrated in Figure 3.14. However, an improvement in the sidelobe level should be noted when $\alpha = 3$, but at expenses of an increment in the main lobe width, shown in Figure 3.15.

Figure 3.16 illustrates sidelobe levels for some of the windows discussed above [Ref. 10].

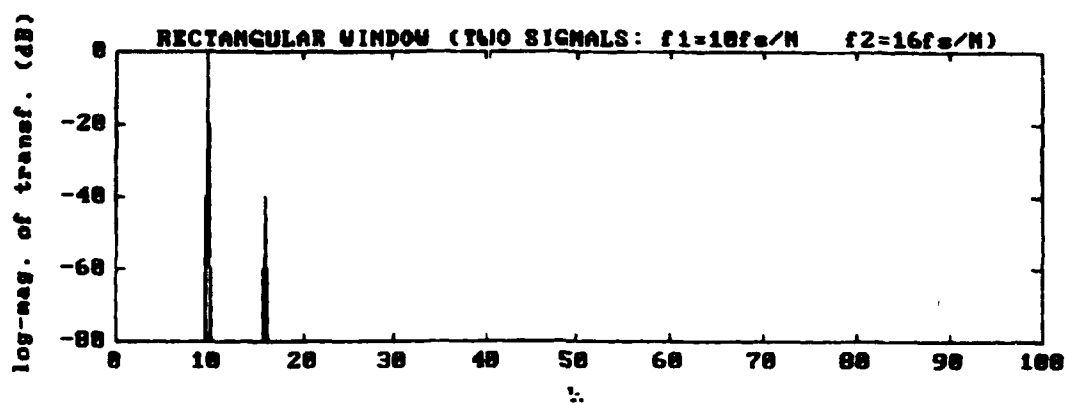


Figure 3.8. Rectangular Window (Two Signals: $f_1 = 10$ bin, $f_2 = 16$ bin)

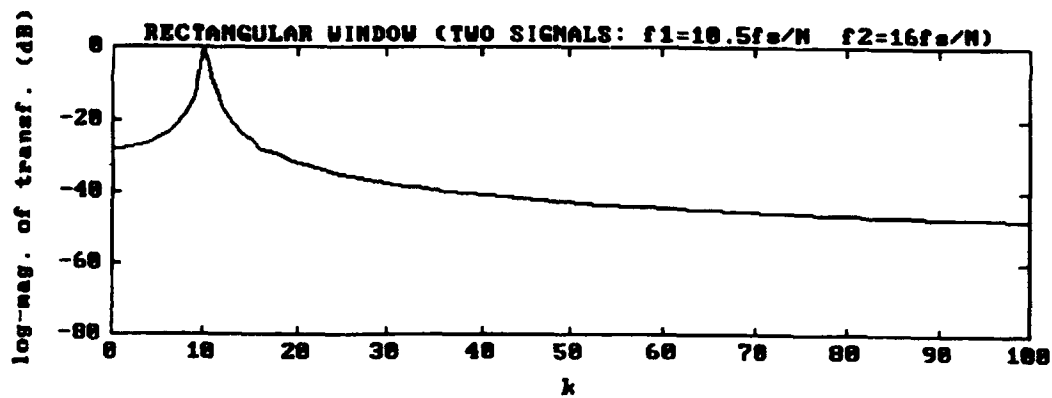


Figure 3.9. Rectangular Window (Two Signals: $f_1 = 10.5$ bin, $f_2 = 16$ bin.)

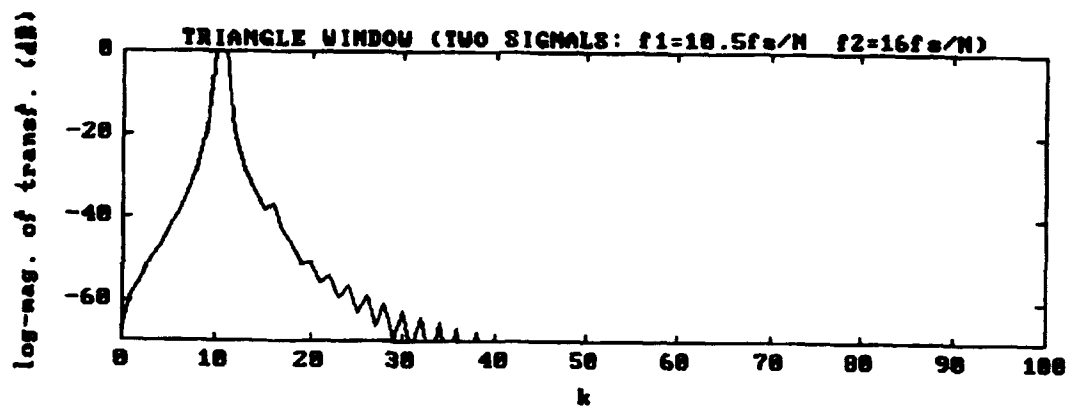


Figure 3.10. Triangular Window (Two Signals: $f_1 = 10.5$ bin, $f_2 = 16$ bin.).

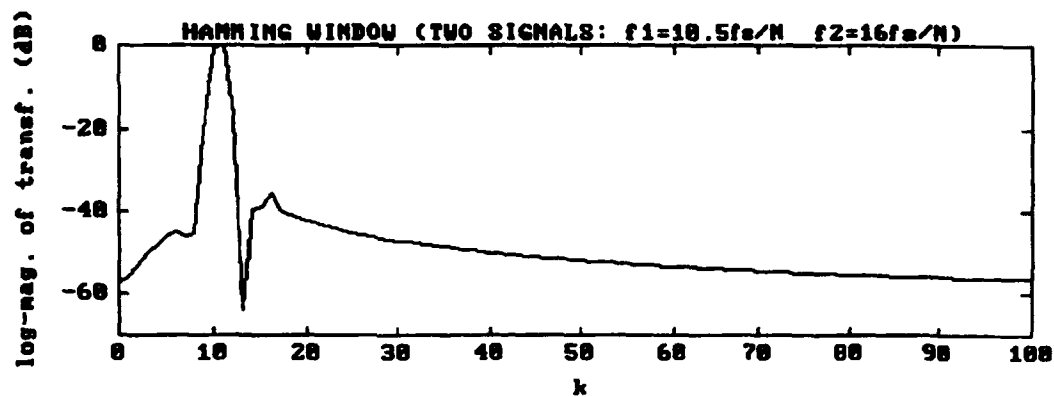


Figure 3.11. Hamming Window (Two Signals: $f_1 = 10.5$ bin, $f_2 = 16$ bin.).

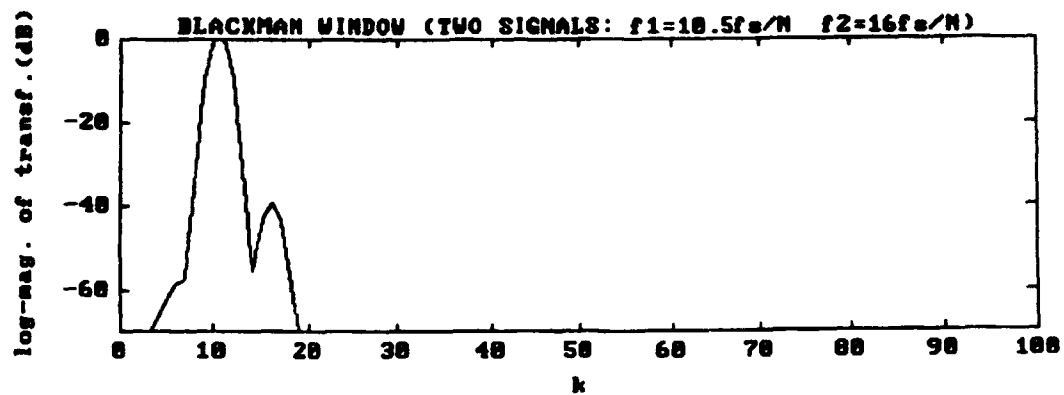


Figure 3.12. Blackman Window (Two Signals: $f_1 = 10.5 \text{ bin}$, $f_2 = 16 \text{ bin}$.).

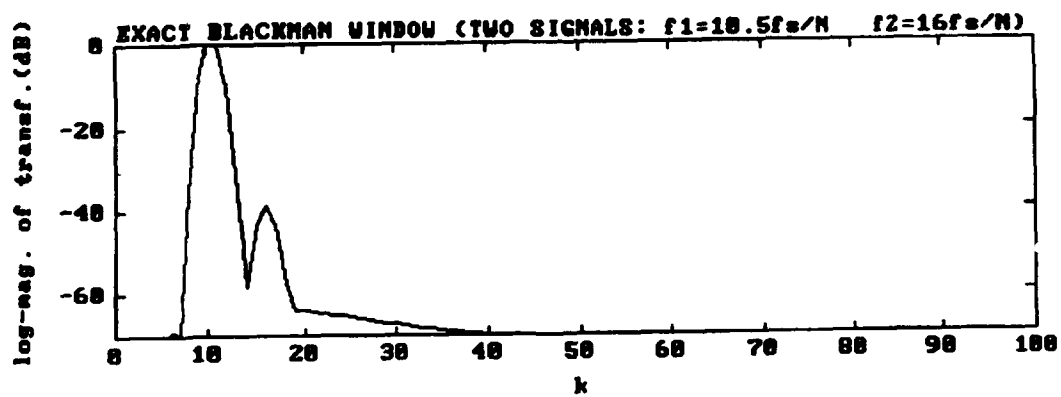


Figure 3.13. Exact Blackman Window (Two Signals: $f_1 = 10.5 \text{ bin}$, $f_2 = 16 \text{ bin}$.).

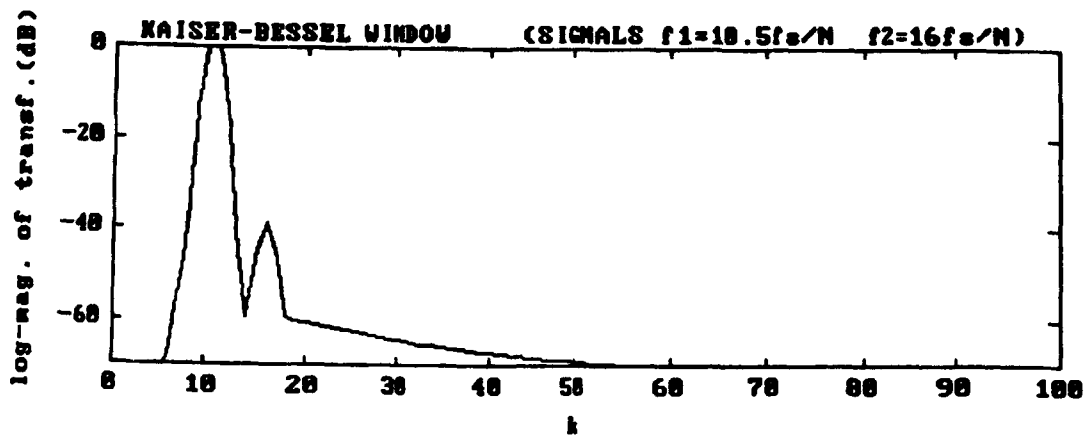


Figure 3.14. Kaiser-Bessel Window, $\alpha = 2$ (Two Signals: $f_1 = 10.5$ bin, $f_2 = 16$ bin.).

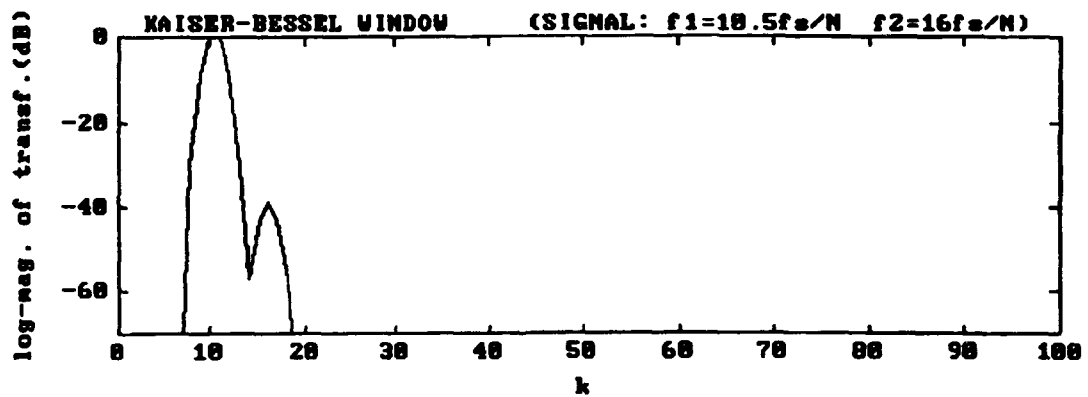


Figure 3.15. Kaiser-Bessel Window, $\alpha = 3$ (Two Signals: $f_1 = 10.5$ bin, $f_2 = 16$ bin.).

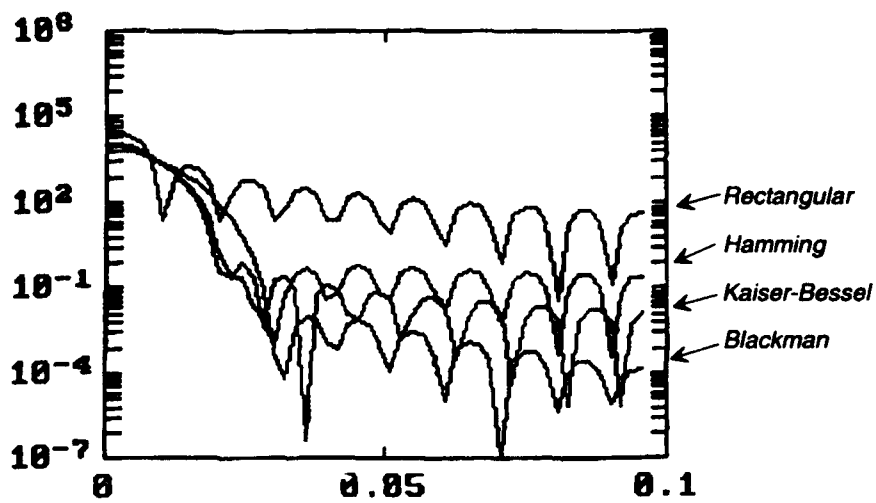
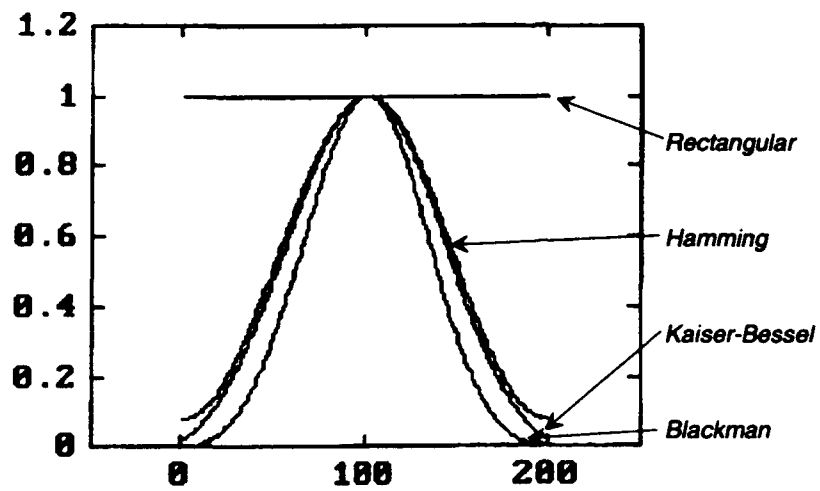
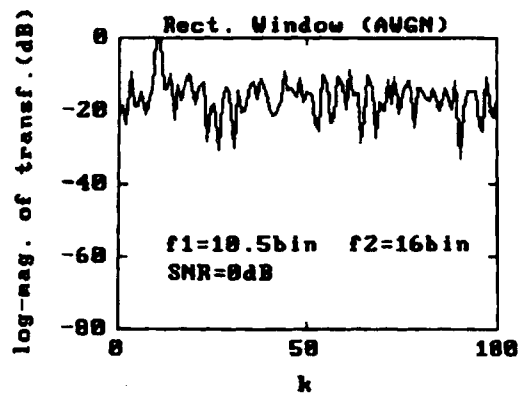
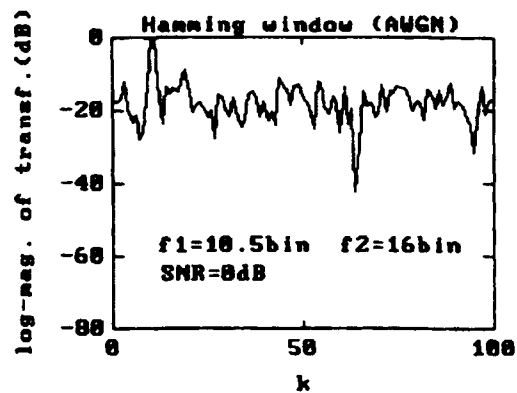


Figure 3.16. Sidelobe Levels of Classical Windows.

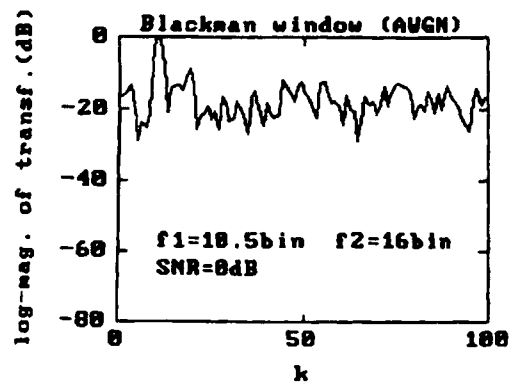
When additive white Gaussian noise (AWGN) corrupts the signals then the larger signal (centered at 10.5 bins) is detected even at low levels of signal to noise ratio (SNR) of 0 dB, as shown in Figure 3.17. The weak signal (at 16 bins) can not be detected even at high levels of SNR (i.e., 30 dB), as shown in Figure 3.18. Therefore, the performance in the presence of noise using classical windows will be simulated using a signal composed of two equal amplitude components, centered at $f_1 = 10.5$ bins and $f_2 = 11.5$ bins, as is demonstrated in Section 4.3.



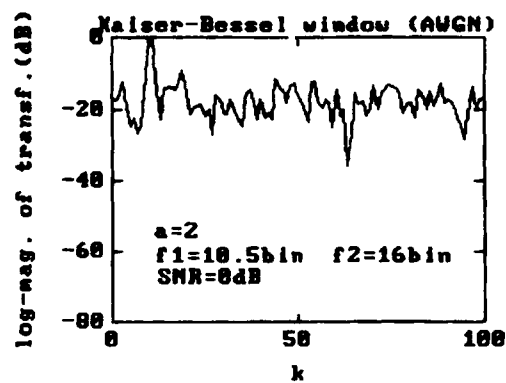
a.



b.

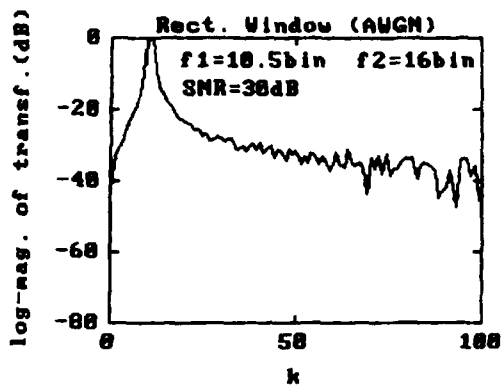


c.

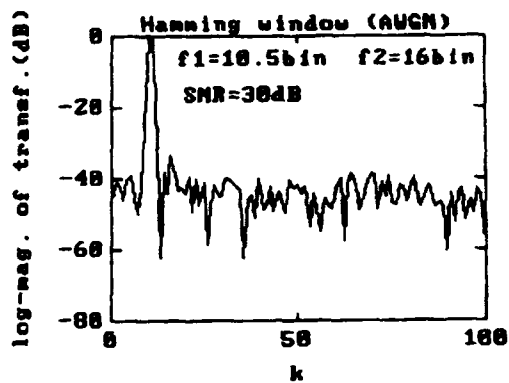


d.

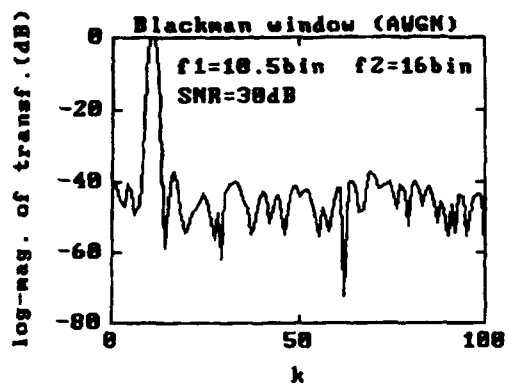
Figure 3.17. Classical Windows Simulation With Low-Level Signal-to-Noise Ratio.



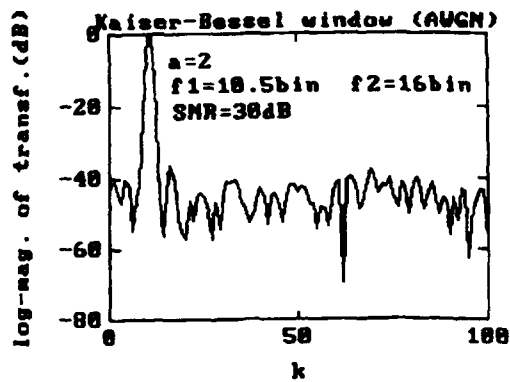
a.



b.



c.



d.

Figure 3.18. Classical Windows Simulation With High-Level Signal-to-Noise Ratio.

IV. NONTRADITIONAL WINDOWS

A. INTRODUCTION

The main objective of this chapter is to study a new data window for use in Fourier-based non-parametric spectral analysis. The weighting function to be studied is complex valued and consists of an analytic linear FM chirp. This is shown in Figure 4.1, where the complex valued function, its real and imaginary part as well as the magnitude is plotted. Due to the fact that this nontraditional window has high resolution capabilities [Ref. 1] and given the ease with which Fourier spectra can be computed (i.e., computationally efficient), this kind of window can become an attractive tool in spectral analysis.

The work to be done here can be summarized as follows:

- ♦ To analyze the results of J. Griffiths [Ref. 1] and to replicate them using MATLAB [Ref. 10];
- ♦ To establish the signal to noise ratio sensitivity of this type of window;
- ♦ To examine the behavior of this window when using damped sinusoidal signals;
- ♦ To develop a mathematical approach to investigate the behavior of this window in the presence of one or several signals.

B. FM CHIRP WINDOW DEFINITION AND EXPERIMENTAL RESULTS

In accordance with J. Griffiths's work, the goal is to define a window $w(n)$ that has high resolution capabilities. The weighting function which meets this objective is the linear FM chirp, defined by

$$w(n) = e^{j\theta(n)}, \quad (85)$$

for $n = 0, 1, \dots, N - 1$, where $\theta(n)$ is the phase term and is defined as

$$\theta(n) = \theta(n - 1) + \Omega(n). \quad (86)$$

In the last expression, the term $\Omega(n)$ is the digital instantaneous frequency, and is expressed as

$$\Omega(n) = \frac{2\pi n}{N}. \quad (87)$$

The phase term is initialized to zero at $n = 0$ and is given by

$$\theta(n) = \frac{2\pi}{N} \frac{n(n+1)}{2}. \quad (88)$$

Once the window is defined, the Fourier-based spectral estimate can be obtained from the magnitude of the Fourier transform of the windowed data sequence $x(n)$ by

$$\hat{P}_{\text{per}}(k) = \left| \sum_{n=0}^{N-1} x(n)w(n)\exp\left(\frac{-j2\pi nk}{N}\right) \right|^2. \quad (89)$$

Note that the periodogram is not normalized by N . In order to simplify the analysis, periodogram averaging is not employed. The simulations to be presented are at sufficiently high SNR that averaging does not significantly change the response.

Several different sets of parameters will be used in the simulations. The data is a 32 point sequence, padded with 96 zeros to allow a 128 point FFT. This 1:4 ratio of data size to transform length is employed throughout the simulations, with the purpose of obtaining "smoother" curves in the frequency domain. The value of the number of sampling points is 32. Using a spacing between samples, of $T_s = 1$ provides a DFT bin width of $1/N$.

The magnitude spectrum for the linear FM chirp window is depicted in Figure 4.2. From this it should be noted that the magnitude of the spectrum shows a deep null at DC (i.e., 0 Hz), and is approximately constant, at 15 dB (or $10\log_{10}(32)$), at other frequencies [Ref. 4]. It is important to observe that the width of the sharp null is less than 1/4th bin (Note that a bin is defined in terms of the 32 point data duration and not the overall transform length, i.e., binwidth = $1/32$).

The phase spectrum for the window under study is shown in Figure 4.3, and it can be observed to have a quadratic behavior. It should also be noted that there is a π discontinuity at the 0 frequency point. The results of the window amplitude and phase simulation in this work agree with those presented by Griffiths.

The next simulation to be performed is for the case of a single complex input sinusoid, in additive white Gaussian noise (SNR = 30 dB). In Section C a noise simulation to determine the signal to noise sensitivity of this kind of window will be performed using different SNR levels. The magnitude spectrum estimate shown in Figure 4.4 is obtained when

$$x(n) = \exp(j2\pi n(\frac{10.5}{32})) \quad (90)$$

is used in Equation (89). The frequency of this complex sinusoid is therefore $f_0 = 0.328125$ Hz. From Figure 4.4 it can be noted that it is the chirp window transform shifted to the frequency of the signal (i.e., $f_0 = 0.328125$ Hz). Since the multiplication of two functions in the time domain corresponds to the convolution of the two corresponding transforms in the frequency domain it should be noted that a sharp null is located exactly at the frequency of the signal.

It is important to note that the frequency of the signal is not DFT bin centered (i.e., $f = 10.5f_s/N$). This means that the simulation is done for the worst resolution case or, in other words, when spectral leakage occurs.

The results of the next simulation are presented in Figure 4.5. It shows the behavior of the transform of the chirp window in the magnitude spectrum when two analytic sinusoids are present. A second complex valued sinusoid is added to the data used for Figure 4.4. The signal frequency is at $f_2 = 0.3125$ Hz, which corresponds to a DFT bin of 10 (i.e., $f_2 = 10f_s/N$), and thus the two signals are one

half bin apart. In Figure 4.5, the magnitude spectrum is observed to be completely different from that produced when a single sinusoid is present. In fact, two nulls are not observed at locations that correspond to the signal frequencies. One explanation as to why two deep nulls are not observed is that a Fourier-based method is employed, and it has linear properties. The shape of the magnitude spectrum illustrated in Figure 4.5 is related to the sum of the response for the case when a single input is present (Figure 4.4), with a similar response that is obtained by shifting to the left by 0.0156 Hz (i.e., 0.328125 Hz-0.3125 Hz). But due to the fact that the periodogram is not a linear process (magnitude squared of the transform) the resultant spectral estimate has to involve the contribution of the implicit crossterms, produced when the magnitude of the Fourier transform sum of the individual weighted data is squared (i.e., $\left| \sum_n (x_{1(n)} + x_{2(n)})w(n)\exp\left(\frac{-j2\pi nk}{N}\right) \right|^2$), where $x_{1(n)}$ and $x_{2(n)}$ are the data sequences representing each one of the analytic signals, respectively.

However, it is important to keep in mind the changes that the chirp window produces in the magnitude spectrum when two closely spaced sinusoids are present in the data, as compared to when only a single sinusoid is present. This can become an advantage over traditional windows, since the chirp window could detect spectral lines that are less than a bin apart.

Figure 4.6 illustrates the magnitude spectrum obtained when using conventional windows. In this case, the data used to produce Figures 4.4 and 4.5

is weighted by a raised cosine (i.e., Hamming window) prior to computing the transform. Figure 4.6a shows the magnitude spectrum for the case of a single complex valued sinusoid located at $f_1=0.328125$ Hz. Figure 4.6b illustrates the magnitude of the transform for the case of two analytic sinusoids that are separated by one half bin (i.e., $f_1 = 0.3125$ Hz $f_2 = 0.328125$ Hz). As expected, only a single peak is observed in both cases, even though Figure 4.6b is the magnitude spectrum for two signals. This is due to the fact that conventional windows can not resolve spectral lines that are separated by less than one bin.

The final example presented by J. Griffiths to illustrate the differences between traditional and FM chirp windows is in the use of a signal containing frequency steps (i.e., frequency shift keying). The signal consists of a sinusoid at 0.2 Hz for the first 16 samples, and 0.4 Hz for the remaining 16 samples. In this case, it is necessary to guarantee a phase continuity of the time waveform at the location of the frequency jump. It was therefore necessary to define an instantaneous frequency $\Omega(n)$ (Equation 87) as the desired discontinuous function and then compute $\theta(n)$ by means of Equation 86.

A marked difference can be observed, as shown in Figure 4.7, when computing the magnitude spectrum for the cases of weighting data with classical and FM chirp windows for a frequency stepped signal. Figures 4.7a and 4.7b illustrate the magnitude spectrum when the weighting function is a traditional window (i.e., a Blackman window 32 points in length) and the data is a sinusoid

containing a frequency which moves from 0.2 Hz to 0.4 Hz at the midpoint of the data record. Figure 4.7a displays a signal with a shift upward from 0.2 Hz to 0.4 Hz, while in Figure 4.7b the frequency shifts from 0.4 Hz to 0.2 Hz (downward) as time progresses. From these figures it can be observed that the traditional magnitude spectra are almost identical for both cases of FSK signals, so it is not possible to determine which way the signal frequency shifts. When the chirp window was used with the same FSK signals, the results depicted in Figure 4.7c are obtained for an upward step and Figure 4.7d when the frequency is stepped downward. It is important to note that in order to be consistent with the results presented by J. Griffiths, an SNR of 30 dB (or better) was employed.

A possible explanation as to why the upward change in frequency causes a result that presents a marked difference from that when the change in frequency is downward is the fact that the chirp introduces a time varying spectral component (instantaneous frequency) which will affect the upward and downward shifts differently. Since the weighting data is an FM chirp with instantaneous frequency defined by $\Omega(n)$, the net instantaneous frequency is simply the sum of the instantaneous frequencies of the data and the window [Ref. 4]. Analysis of Figures 4.7c and Figure 4.7d, shows that an FM modulation, upward or downward, will result in an magnitude spectral estimate which presents multiple nulls in the lower spectral regions, as is shown in region 0.25 Hz to 0.5 Hz in Figures 4.7c and 4.7d. One should also note that the two main peaks in Figures

4.7a and 4.7b are also located in the lower spectral region. If the frequency function of the signal is time reversed such that the high frequency portions appear at the beginning of the record (i.e., step downward), then the location of the maxima and the minima of the spectral estimate are reversed. For instance, we can observe from Figure 4.7c that the maximum value (i.e., 20 dB) of the magnitude spectrum occurs at approximately 0.4 Hz. Whereas in Figure 4.7d the minimum value (i.e., -3 dB) of the spectral estimate occurs at approximately 0.4 Hz.

C. SIGNAL TO NOISE RATIO SENSITIVITY OF FM CHIRP WINDOW

The discussion here relates to the minimum signal to noise ratio at which the chirp window method still yields useful results. For the simulation, we realize that the results are dependent upon the transform length. In the simulation the data length and transform length are 32 and 128 points, respectively. The noise will be additive white Gaussian noise (AWGN).

For the case of a single complex sinusoid, the results of processing the data with the complex window are presented in Figure 4.8, where it can be observed that at a high level of SNR (i.e., 30 dB), a deep null of approximately 30 dB of amplitude is located at the frequency of the input signal (see Figure 4.8a). When simulations are performed at SNR's of 20 dB and 18 dB, good results are still obtained as shown in Figures 4.8b and 4.8c. Therefore, if the SNR is better than

18 dB good results are obtained, which agrees with Griffiths's claim that good performances are achieved for SNR levels between 20 dB and 25 dB [Ref. 1].

When the value of SNR is reduced to 15 dB (Figure 4.8d) the spectra becomes ambiguous, and below that value a null is no longer present at the signal's frequency location. Therefore, the linear FM chirp window is a high resolution weighting function for single sinusoids, but is limited to high SNR levels (i.e., above 15 dB).

To demonstrate the SNR dependency of the chirp window when more than one signal is present the following experiments are performed: Two equal amplitude sinusoids of length 32 which are one bin apart (i.e. $f_1 = 10.5f_s/N = 0.328125$ Hz and $f_2 = 11.5f_s/N = 0.359375$ Hz) are considered. These sinusoids will be weighted by classical windows (i.e., Rectangular and Hamming) and by the chirp window for different levels of SNR. The experiment will then be repeated for sinusoids located one half a bin apart (i.e., $f_1 = 10.75f_s/N = 0.335937$ Hz and $f_2 = 11.25f_s/N = 0.351562$ Hz). Note that in both cases the signals are not bin centered and the sequence is padded with 96 zeros to provide a 128 point FFT.

On observing the lack of two deep nulls at the signal frequencies when the data is weighted by the chirp window, it should be noted that the point Griffiths argues that, when two or more closely spaced sinusoids are present in the input data, the spectral estimate will have a shape that resembles that shown in Figure

4.5. Different levels of SNR have been chosen to determine over which range of SNR values, the magnitude spectrum continues to produce useful results. Data with the same levels of SNR (i.e., 30 dB, 18 dB, 9 dB and 0 dB) will be compared using rectangular, Hamming, and FM chirp windows.

Figure 4.9 shows the results when the input data is weighted by a rectangular window. From this it can be observed that the two higher main lobes are located exactly at the frequencies of the composed signal. At an SNR of 30 dB (Figure 4.9a), detection of the two signals is excellent. At an SNR of 18 dB (Figure 4.9b) and an SNR of 9 dB (Figure 4.9c) good results are also found, whereas at an SNR of 0 dB (Figure 4.9d) the result begins to be ambiguous, even though the signals are still recognizable.

Figure 4.10 shows the results when the weighting function is a Hamming window. As expected, a better sidelobe level is found here than when using a rectangular window, but it should also be noted that the main lobes are now broader. As in the rectangular window, at an SNR of 30 dB (Figure 4.10a) and an SNR of 18 dB (Figure 4.10b) the results of the spectral estimation are good. At an SNR of 9 dB (Figure 4.10c) reasonable results are still obtained, but at an SNR of 0 dB (Figure 4.10d) the observed spectral estimate is ambiguous. Figure 4.11 shows the results when using the complex FM chirp window for the case when the signals are one bin apart. It shows a pattern with multiple deep nulls, and, even though two nulls are observed at approximately the frequency of the

input signals (Figure 4.11a and 4.11b), they cannot be considered detections due to the presence of other nulls at frequencies that differ from the input frequencies. It is interesting to observe that at an SNR of 9 dB (Figure 4.11c), a deep null is present near one of the input frequencies, but this also cannot be considered a detection. However, it should be noted that the shape of the spectrum is almost the same for SNR's of 30 dB, 18 dB and 9 dB (Figures 4.11a to 4.11c). At an SNR of 0 dB the spectral estimate does not convey any information. Another important observation is the fact that the shape of the spectral estimate in figure 4.11, looks totally different from that of Figure 4.5 which is the spectral estimate when two signals are one half bin apart.

The next simulation to be performed has the sinusoids separated by one half bin (i.e., $f_1 = 10.75f_s/N = 0.33597$ Hz and $f_2 = 11.25f_s/N = 0.351562$ Hz). Here also the number of data samples is 32, and the sampling frequency $f_s = 1$ Hz. Figure 4.12 shows the results using a rectangular window. As expected, only one main lobe is present in the spectral estimate due to the fact that traditional windows are not able to resolve spectral lines that are separated by less than one bin. This main lobe can not be resolved for any SNR, for instance of 30 dB (Figure 4.12a), 18 dB (Figure 4.12b) and 9 dB (Figure 4.12c). At an SNR of 0 dB (figure 4.12d) the main lobe still is present but begins to be ambiguous.

Figure 4.13 shows the results obtained when using a Hamming window. As is the case in a rectangular window, only one main lobe is present. Lower

sidelobe levels are obtained, but at the expense of a wider main-lobe width. At SNR's of 30 dB (Figure 4.13a), 18 dB (Figure 4.13b) and 9 dB (Figure 4.13c), a good detection of the main lobe, representing the average spectral location, is achieved. At an SNR of 0 dB (Figure 4.13d) the spectral estimate becomes ambiguous.

Finally, in Figure 4.14, the results obtained using the chirp window are depicted. It should be noted that in all simulation the axis are normalized, so that the maximum value of the magnitude spectrum is 0 dB. Despite the fact that the input signals are located at $f_1 = 10.75f_s/N$ and $f_2 = 11.25f_s/N$, which differs from the locations of the input signals in Griffiths paper (i.e., $f_1 = 10f_s/N$ and $f_2 = 10.5f_s/N$) the shape of the spectral estimate looks similar to that shown in Figure 4.5. At least at 30 dB of SNR (Figure 4.14a) and at 18 dB of SNR (Figure 4.14b) the shape of the spectral estimate looks similar to that shown in figure 4.5. At an SNR of 9 dB, the shape of the spectrum begins to become distorted and at an SNR of 0 dB it is totally different from that in Figure 4.5, hence it is unknown whether more than two signals are present (or any at all).

D. CHIRP WINDOW APPLIED TO DAMPED SINUSOIDS

In this section the effects of the chirp window will be studied when the data is a damped sinusoid. First to be considered is the case of a single "damped" sinusoid of the form

$$x(n) = \exp(j2\pi n(\frac{10.5f_s}{N}))\exp(-T_c n) \quad (91)$$

where n varies from 0 to 31 so that the data length is 32. The sampling frequency $f_s = 1$ Hz and T_c is the time constant of the decaying exponential. This input sequence was weighted by the chirp window for different values of T_c (i.e., $T_c = 1, 1/2, 1/3$, and $1/4$) and the obtained results are depicted in Figure 4.15. An SNR of 30 dB was employed.

Figure 4.15a shows the result when the damped input sequence has a value of $T_c = 1$, and from it we clearly observe that no null is present at the frequency of the signal (i.e. $f_1 = 10.5f_s/N = 0.338125$ Hz). Moreover, the shape of the spectral estimate is similar to that of Figure 4.5. That is, according to Griffiths, the case when more than one input sinusoid is present.

When $T_c = 1/2$ the spectral estimate has the shape shown in Figure 4.15b and from it can be observed that, as in the previous figure, no null is present at the frequency of the input signal. In this case the shape of the magnitude spectrum is similar to that shown in Figure 4.5 (two sinusoids one half bin apart). For values of $T_c = 1/3$ (Figure 4.15c) and $T_c = 1/4$ (Figure 4.15d) no null is

observed at either the signal frequency location, but in these cases the shape of the spectrum is not similar to that of Figure 4.5. Another observation is that at the 0 frequency location for $T_c = 1$ (Figure 4.15a) the magnitude of the spectrum is at approximately 10 dB, whereas when $T_c = 1/4$ the amplitude of the spectrum at the 0 frequency point is approximately 0 dB.

The next simulation performed to determine the behavior of the complex window is when the signal consists of two damped sinusoids. Then the signal is given by

$$x(n) = [\exp(j2\pi n(\frac{10f_s}{N})) + \exp(j2\pi n(\frac{10.5f_s}{N}))]\exp(-T_c n). \quad (92)$$

Note that the complex sinusoids are separated by one half bin.

The results of weighting this input sequence with the complex window are depicted in Figures 4.16a for a value of $T_c = 1$, Figure 4.16b for $T_c = 1/2$, Figure 4.16c for $T_c = 1/3$ and Figure 4.16d for $T_c = 1/4$. From Figure 4.16a we can observe that the shape of the spectral estimate is similar to that shown in Figure 4.5. According to the theory proposed by Griffiths as it relates to the shape that the magnitude spectrum has in the presence of two or more input signals, the simulation is correct. But when the time constant takes values of $1/2$, $1/3$ and $1/4$ the shape of the spectral estimate becomes to be different from that shown in Figure 4.5. It is also important to note that, in this case, the maxima of the

magnitude spectrum remains almost the same, regardless of the value of the time constant.

E. NUMERICAL BEHAVIOR OF CHIRP WINDOW

The spectral estimate obtained from the magnitude of the Fourier transform of the weighted data sequence x_n is given by

$$\hat{P}_x(k) = \left| \sum_{n=0}^{N-1} x_n g_n \exp(-2j\pi kn/N) \right|^2, \quad (93)$$

where x_n is a simple analytic sinusoid (for easy interpretation) of the form

$$x_n = \exp(j2\pi k_0 n/N) \quad (94)$$

(i.e., one complex valued sinusoid with frequency k_0), and

$$g_n = \exp(j2\pi(n^2 + n)/(2N)), \quad (95)$$

is the chirp window equation.

It is known that the transform of the multiplication of two functions in the time domain corresponds to the convolution of the two corresponding transforms in the frequency domain. Therefore,

$$\sum_{n=0}^{N-1} x_n g_n \exp(-2j\pi kn/N) = X(k) * G(k), \quad (96)$$

where

$$X(k) = \delta(k - k_0) \quad (97)$$

is the transform of x_n , and

$$G(k) = \sum_{n=0}^{N-1} \exp(j2\pi(n^2 + n)/2N) \exp(-j2\pi kn/N) \quad (98)$$

is the chirp window transform. Hence,

$$X(k) * G(k) = \delta(k - k_0) * G(k) = G(k - k_0). \quad (99)$$

While finding a close expression for $\sum_n \exp(n^2)$ is difficult, developing a close form expression is too cumbersome. When one signal is present, the spectral shape is the transform of the chirp window will be shifted to the frequency of the signal (i.e., k_0), or

$$\hat{P}_x(k) = |G(k - k_0)|^2. \quad (100)$$

The chirp window has a deep null at the zero frequency point (see Figure 4.2). Due to the convolution the null will be simply shifted to the signal frequency location, making the estimate of the signal possible (see Figure 4.4).

Different results are obtained when more than one signal is present, i.e.,

$$x_n = \exp(j2\pi k_0 n/N) + \exp(j2\pi k_1 n/N). \quad (101)$$

In this case, the Fourier transform of the data sequence is

$$X(k) = \delta(k - k_0) + \delta(k - k_1). \quad (102)$$

The spectral estimate is given by

$$\hat{P}_x(k) = |G(k - k_0) + G(k - k_1)|^2, \quad (103)$$

or

$$P_x(k) = G^2(k - k_0) + G^2(k - k_1) + 2G(k - k_0)G(k - k_1). \quad (104)$$

From the last expression we can observe the presence of crossterms which prohibit the detection of two expected nulls at the signal frequency locations.

Some window parameters are estimated (i.e., mean and standard deviation). The chirp window as in all of our experiments has a length of 32 points and is padded with 96 zeros, permitting a 128 point FFT. Because the magnitude of the FFT is symmetric in frequency, only one-half of the transform length (i.e., from 0 Hz to 0.5 Hz) will be considered, as is shown in Figure 4.17.

To compute the mean and the standard deviation, the first 11 points of the window transform are rejected, with the purpose of obtaining parameter values in the region where the shape of the transform becomes more stable (i.e., from point 12 to point 64). The following are the results of the measurements:

- ♦ Value of window transform at 0 frequency point = 2.3437×10^{-14} (i.e., null)
- ♦ Mean of the window transform = 5.8271
- ♦ Standard deviation of window transform = 0.7275

From the above estimates, we can observe that the value at DC is almost zero, yielding a deep null when the magnitude spectrum of the window is computed. The square of the magnitude of the chirp window transform is bounded by 2.0 and 7.657, if one disregards the null at the zero location (see Figure 4.12). Appendix C depicts an alternative window, which consists of a square chirp window derived from the chirp window presented by Griffiths (Ref. 4).

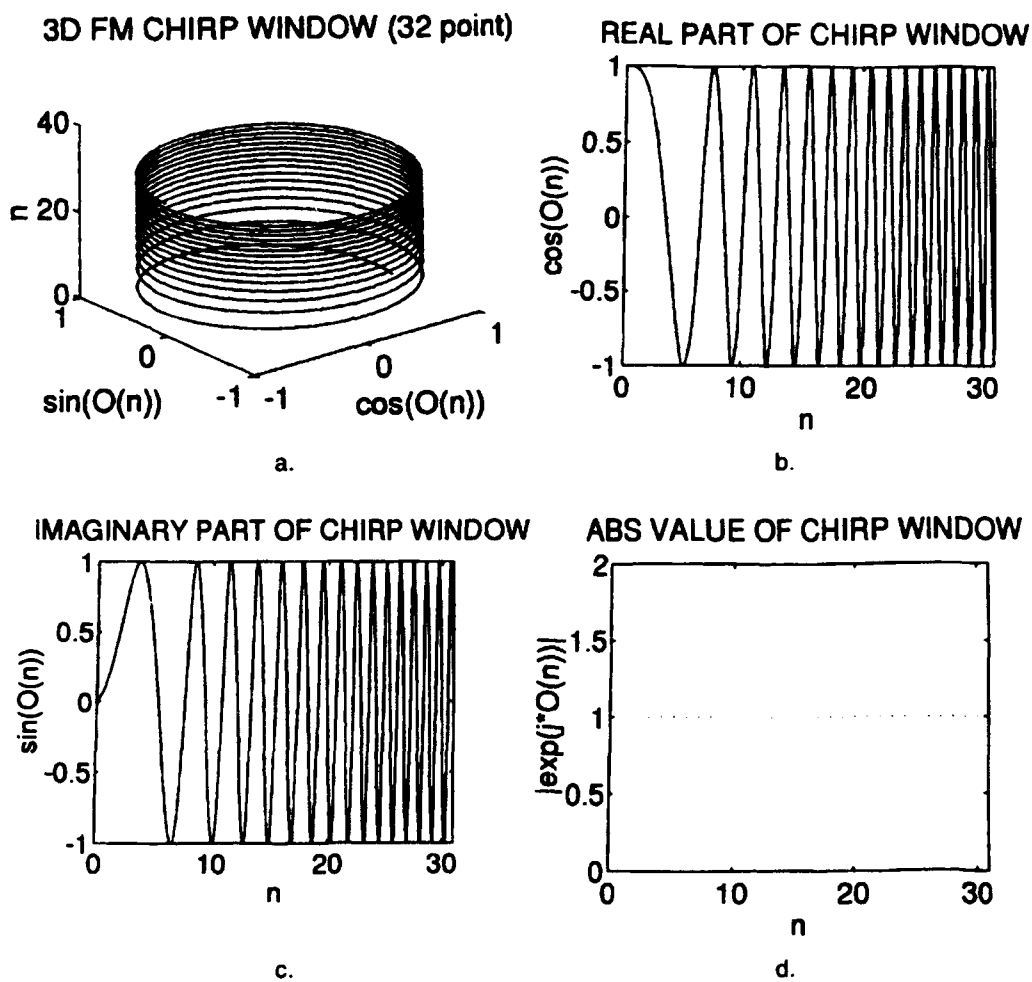


Figure 4.1. Nontraditional Fm Chirp Window.

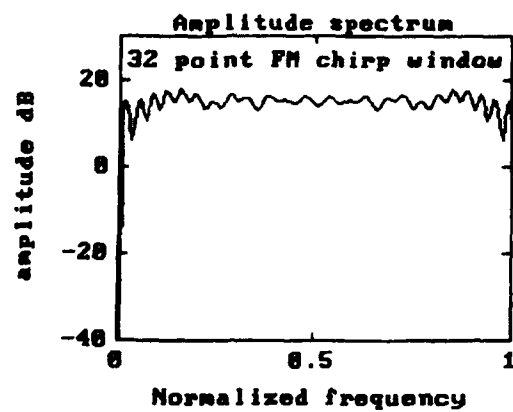


Figure 4.2. Magnitude Spectrum For Linear Fm Chirp Window.

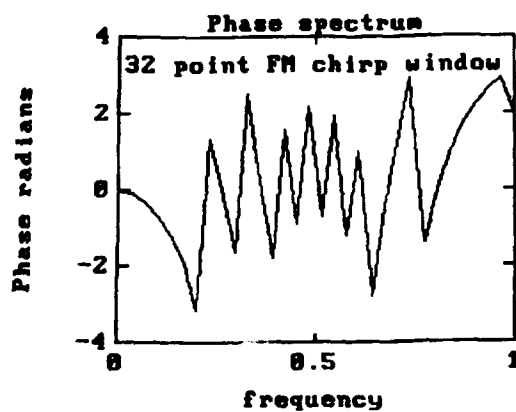


Figure 4.3. Phase Spectrum For Linear Fm Chirp Window.

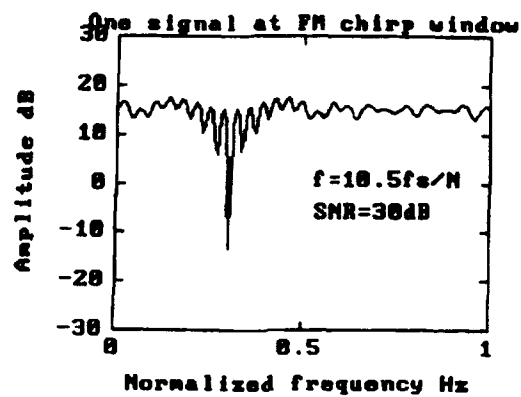


Figure 4.4. Magnitude Spectrum For Single Signal.

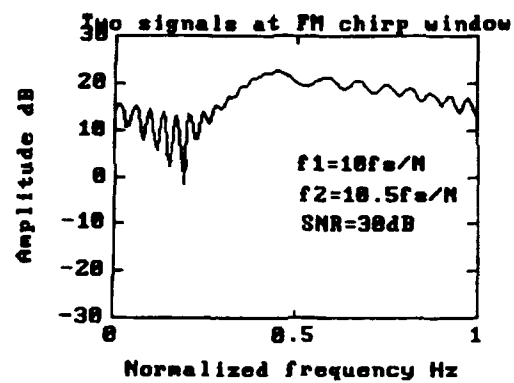
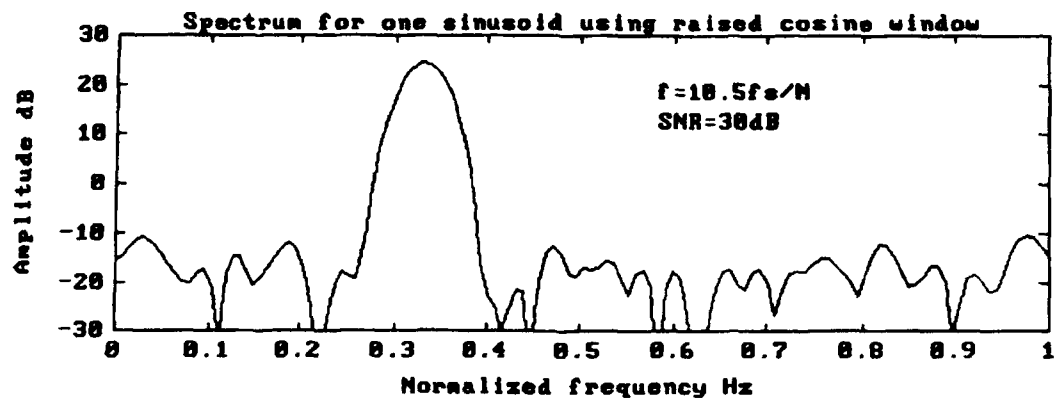
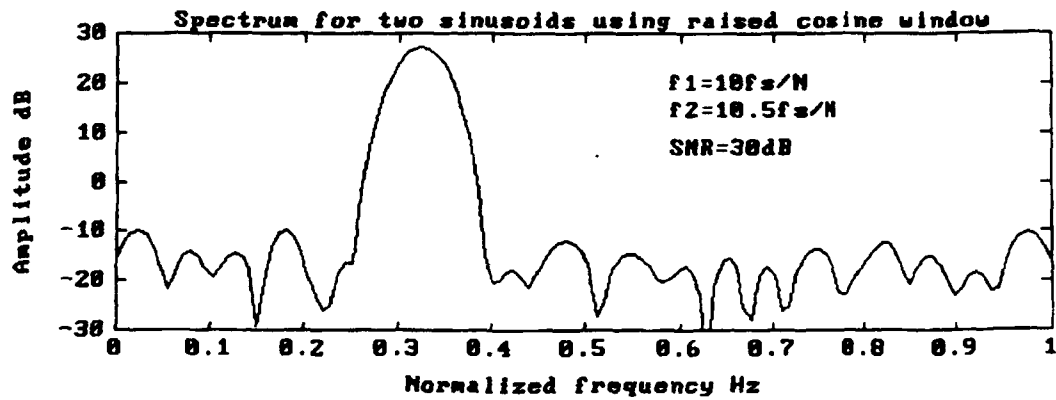


Figure 4.5. Magnitude Spectrum For Two Sinusoids.

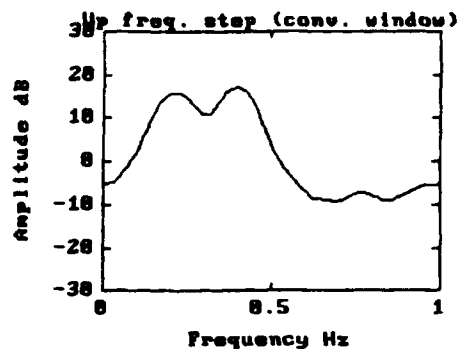


a.

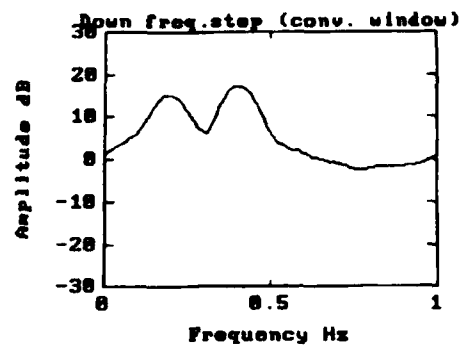


b.

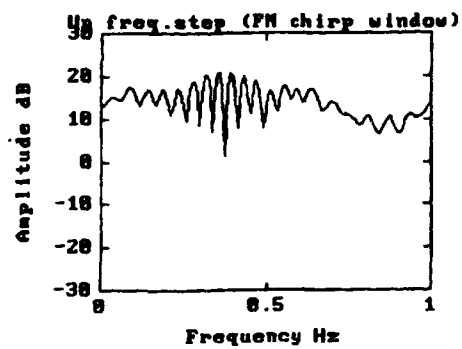
Figure 4.6. Magnitude Spectrum Using Conventional Windows.



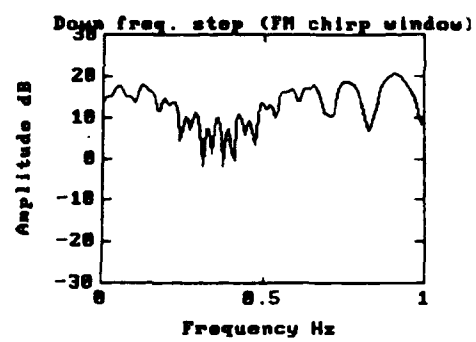
a.



b.

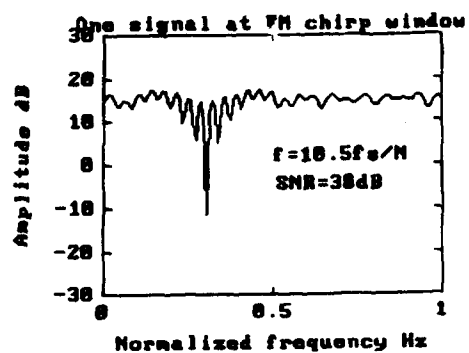


c.

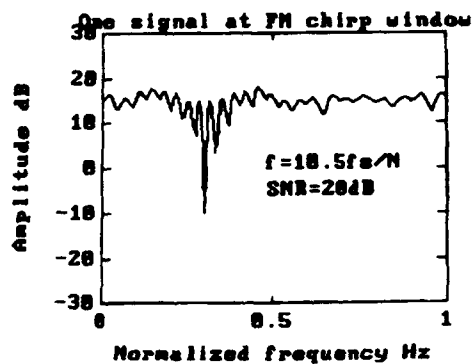


d.

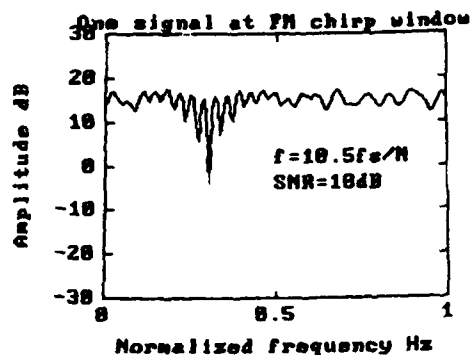
Figure 4.7. Magnitude Spectrum Using A Frequency Stepped Signal.



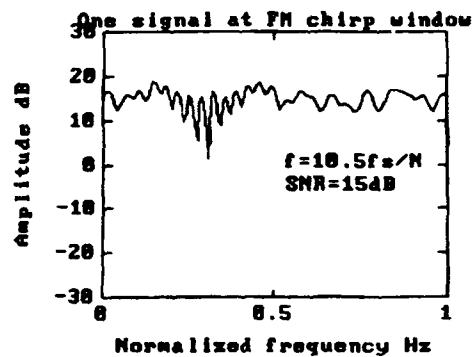
a.



b.

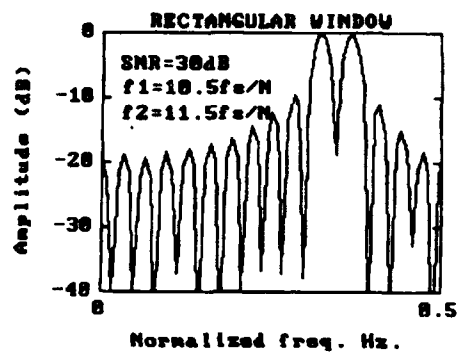


c.

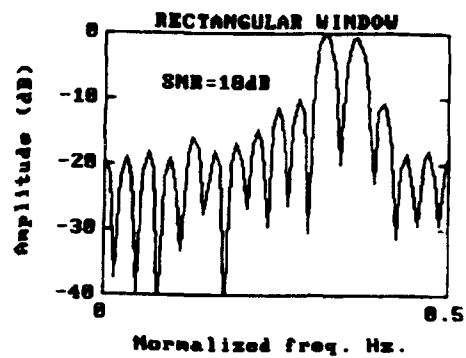


d.

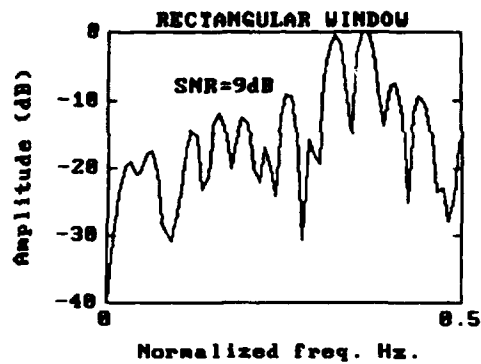
Figure 4.8. Chirp Window With Varying Levels Of Signal To Noise Ratio (Single Sinusoid).



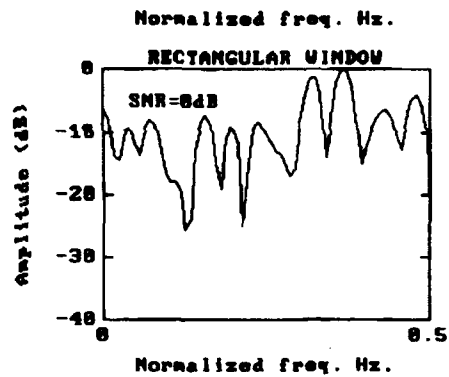
a.



b.

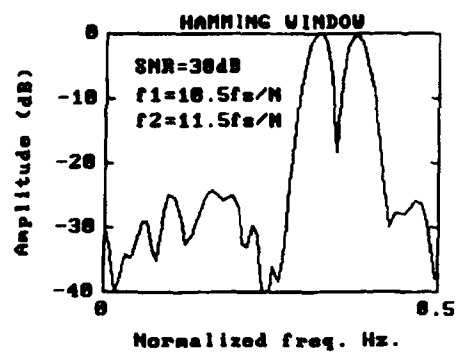


c.

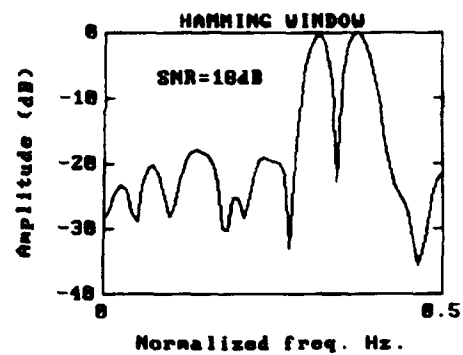


d.

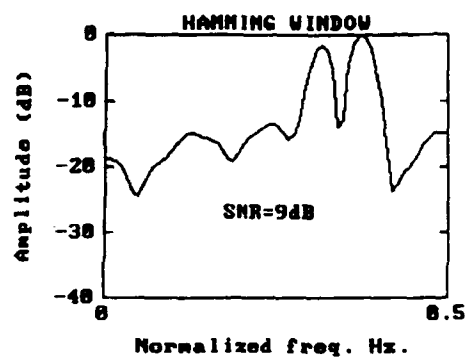
Figure 4.9. Rectangular Window With Varying Levels Of Signal To Noise Ratio (Two Sinusoids One Bin Apart).



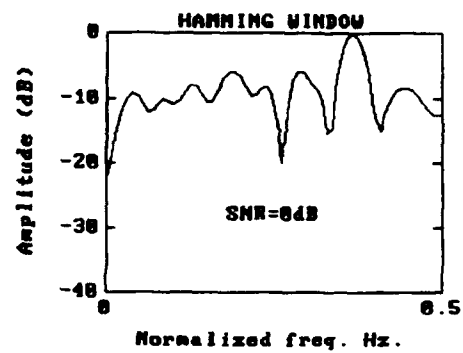
a.



b.

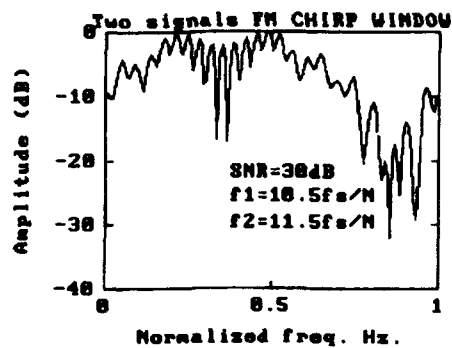


c.

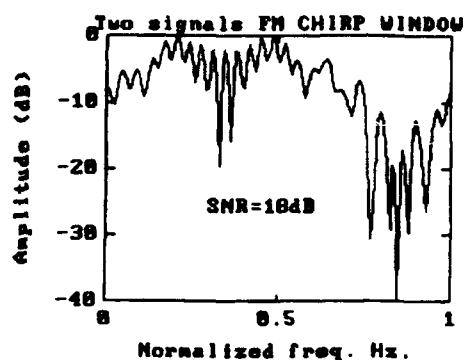


d.

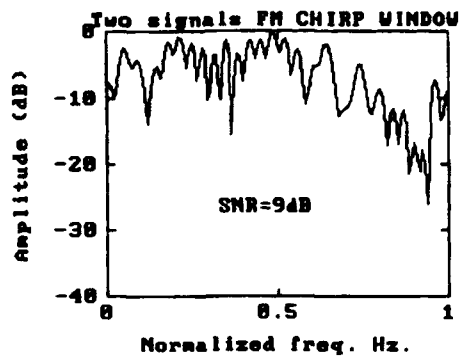
Figure 4.10. Hamming Window With Varying Levels Of Signal To Noise Ratio (Two Sinusoids One Bin Apart).



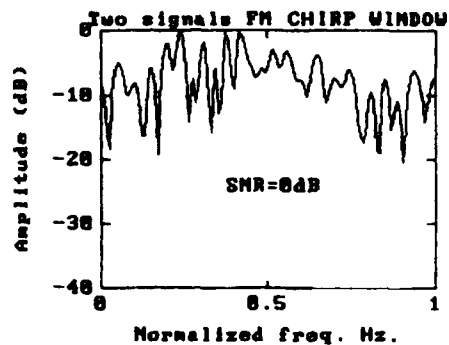
a.



b.

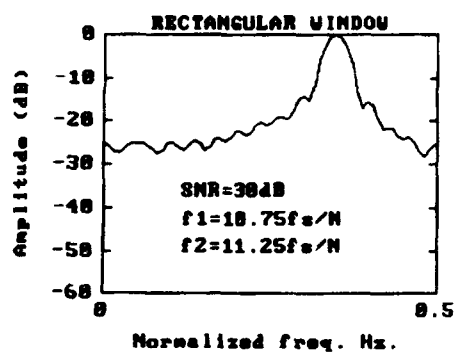


c.

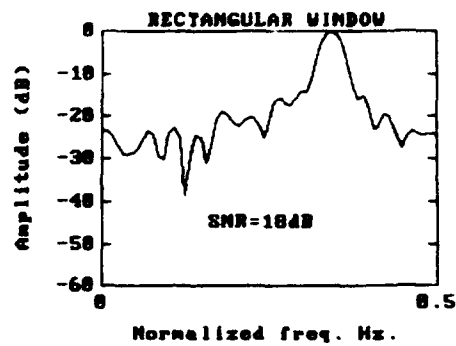


d.

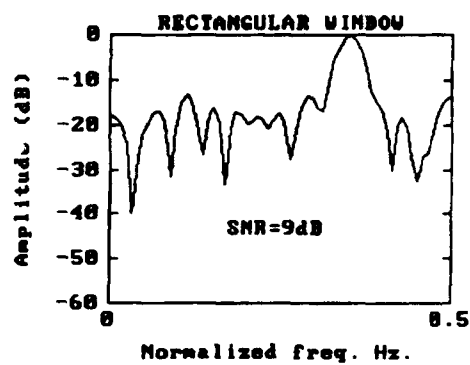
Figure 4.11. Complex Fm Chirp Window With Varying Levels Of Signal To Noise Ratio (Two Sinusoids One Bin Apart).



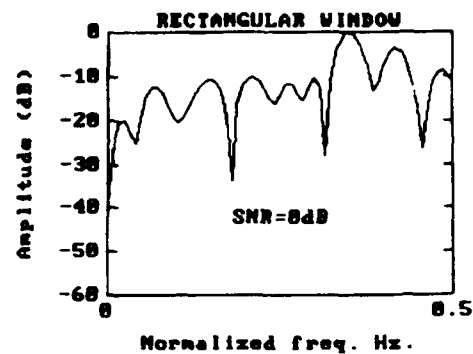
a.



b.

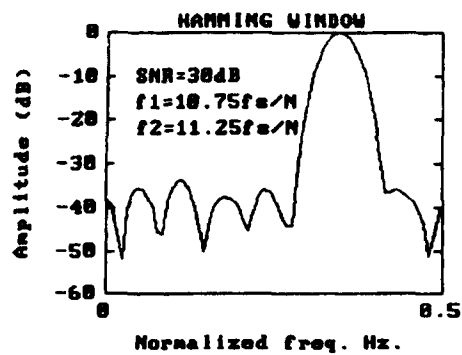


c.

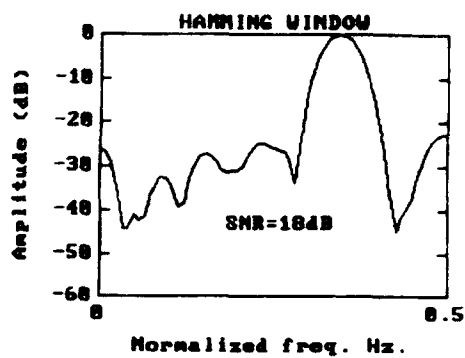


d.

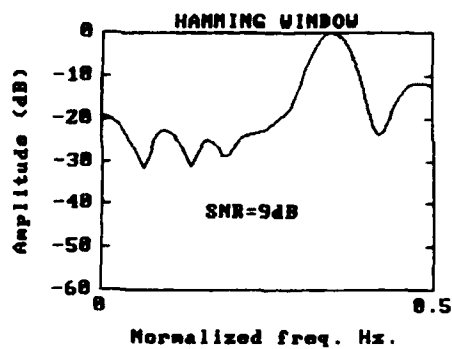
Figure 4.12. Rectangular Window With Varying Levels Of Signal To Noise Ratio (Two Sinusoids One Half Bin Apart).



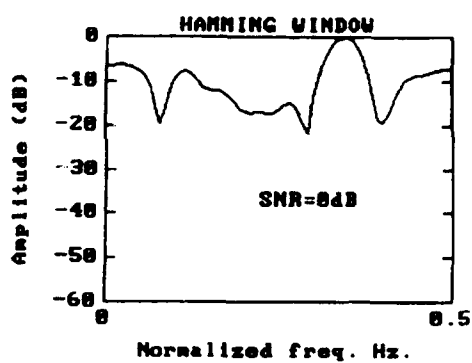
a.



b.



c.



d.

Figure 4.13. Hamming Window With Varying Levels Of Signal To Noise Ratio (Two Sinusoids One Half Bin Apart).

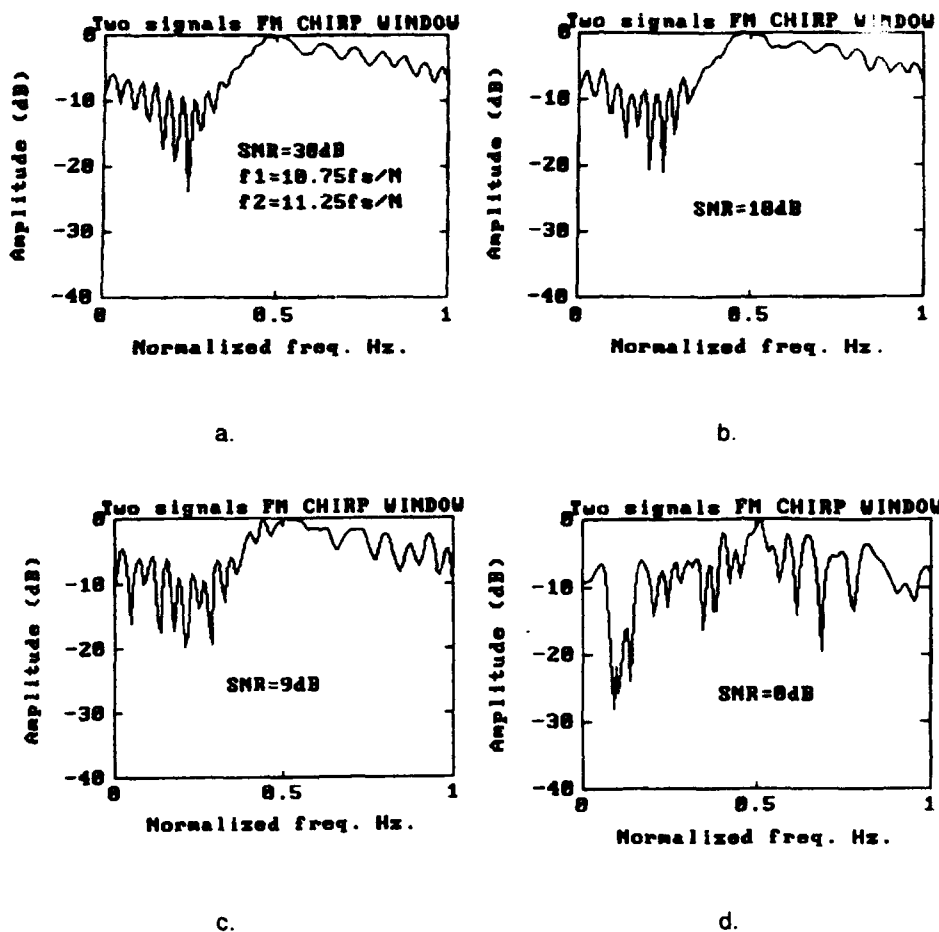


Figure 4.14. Chirp Window With Varying Levels Of Signal To Noise Ratio (Two Sinusoids One Half Bin Apart).

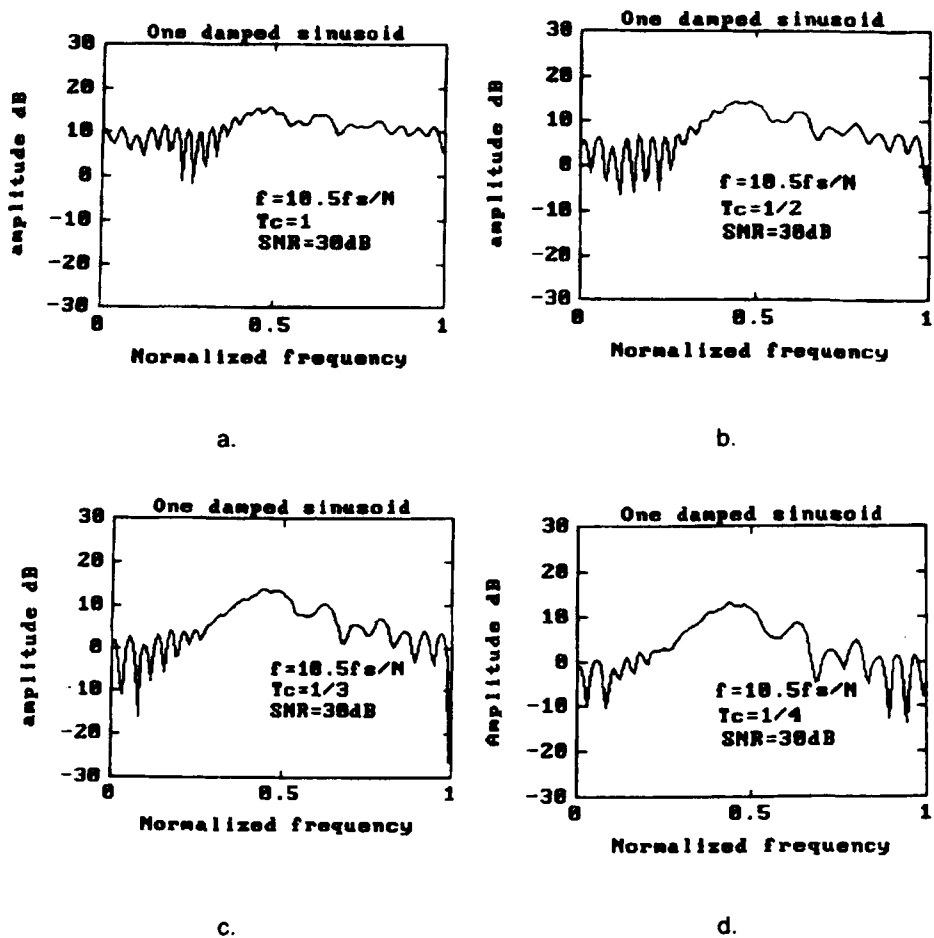
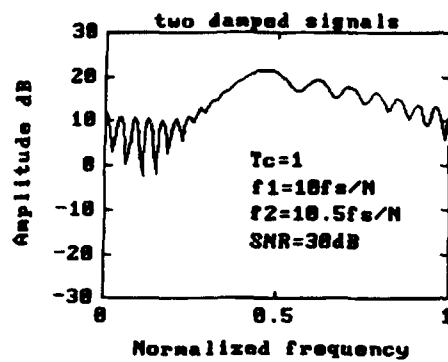
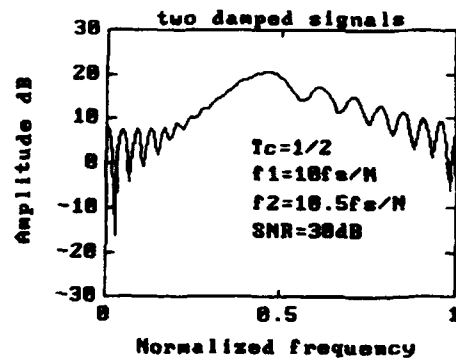


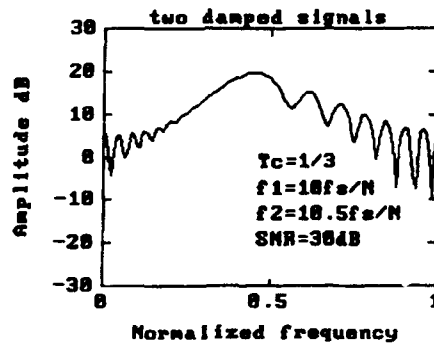
Figure 4.15. Chirp Window With Single Damped Sinusoid (Varying Values Of Time Constant).



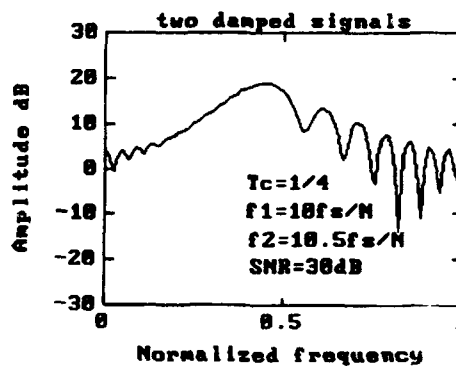
a.



b.



c.



d.

Figure 4.16. Chirp Window With Two Damped Sinusoids (Varying Values Of Time Constant).

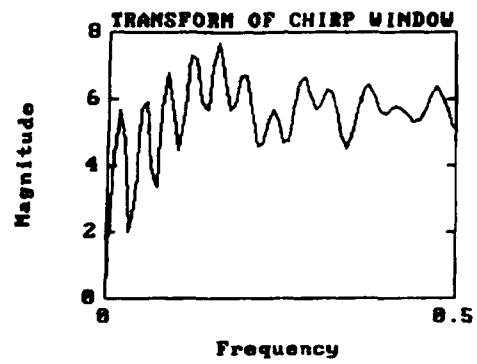


Figure 4.17. Transform Of Chirp Window.

V. CONCLUSIONS AND RECOMMENDATIONS

In this thesis some classical and non-traditional windows have been examined as they apply to the periodogram. The periodogram approach has some advantages and disadvantages:

- ♦ Advantages

1. Computationally efficient, since it uses the fast Fourier transform (FFT).
2. The power spectral density (PSD) estimate is directly proportional to the power of the sinusoidal process.[Ref. 5]

- ♦ Disadvantages

1. Frequency resolution ($\Delta f = \frac{1}{T_0}$) is limited by the record length $T_0 = NT_s$.
2. Suppression of weak signals by strong signal sidelobes.
3. Introduction of distortion in the spectrum due to sidelobe leakage.
4. Periodogram is statistically not consistent (i.e., the variance of the PSD estimator does not tend toward zero as the record length increases). To circumvent this problem the averaged periodogram as defined in Equation 48 can be used, with a proportional loss of resolution.

In describing classical windows' ability to detect a weak spectral line in the presence of a strong nearby line, it was observed that if two spectral lines are located exactly at DFT bin centers, the rectangular window allows each to be

identified without interaction. If any of the spectral lines are not bin centered, spectral leakage occurs, and the sidelobe structure of the larger signal can mask the structure of the smaller signal, thereby prohibiting its detection. One of the most important parameters of classical windows is the sidelobe level.

When analyzing the sidelobe behavior of the classical windows considered in this thesis, and following the method presented by Nuttall (Ref. 3), the window with the best sidelobe behavior is the Kaiser-Bessel window (for $\alpha = 3$). The largest sidelobe is approximately 70 dB below the mainlobe peak. Another important question is the trade-off between sidelobe level and main lobe width of a given window.

A very important limitation of classical windows is their poor capability for detecting spectral lines that are separated in frequency by less than one DFT bin. In fact, as is demonstrated in Figure 4.6b, the magnitude squared Fourier spectrum does not provide an immediate indication of the fact that two closely spaced sinusoids (i.e., one-half bin apart) are present, because only one main lobe beam is obtained. The Fourier-based spectral analysis therefore lacks good resolution. A non-traditional window (the chirp window), which was tested for its resolution capabilities in this thesis.

The simulation results presented in Chapter IV demonstrate that the chirp window can distinguish between single and multiple sinusoidal components when these components are located less than one DFT bin apart.

For a single complex valued sinusoid, simulation results show a deep null located exactly at the signal frequency. This is due to the fact that the magnitude spectrum of the chirp window exhibits a deep null at the 0 frequency point and, if the data consists of a single sinusoid, the spectral shape is simply the transform of the chirp window shifted to the signal frequency. However, it should be noted that this detection is limited to high signal-to-noise ratios (i.e., above 15 dB).

In the case of two equal amplitude complex valued sinusoids, simulation results show that the shape of the spectrum differs from that when a single sinusoid is present. In fact, two nulls are not present at the frequency signal locations, and the pattern observed consists of a non-uniform spectrum which contains nulls at lower frequencies and broad peaks at higher frequencies. One possible explanation as to why two nulls are not observed at the signal frequency locations is that the shape of the magnitude spectrum is related to the sum of the response of the individual weighted signal transforms. The periodogram is not a linear process (i.e., magnitude squared of the Fourier transform). The resultant spectral estimate involves implicit crossterms. The use of the complex valued chirp window creates large differences in the shape of the magnitude spectrum depending upon whether single or multiple frequencies are used. The presence of two or more signals can be inferred from the shape of the magnitude spectrum.

It must be emphasized that the results described above do not apply when the data contains damped sinusoids. When a single damped sinusoid, with a

time constant equal to the data length or one-half the data length, is weighted by a chirp window, the resulting spectral estimate does not have a null at the signal frequency location. The spectrum shape is similar to that found when more than one sinusoid is present. If the sinusoid decays very fast (i.e., the time constant is smaller than one-third of the data length), even less satisfactory results are obtained.

In the case of two damped sinusoids with a time constant equivalent to the data length, the resulting spectral estimate agrees with the results found when using non-damped sinusoids. However, when the time constant has values of one-half and one-third of the data length, the spectral shape yields nulls at lower and higher frequencies. At a time constant value of one-quarter of the data length, nulls are observed only at higher frequencies. The chirp window is not a desirable weighting function when damped sinusoids are present.

Another aspect is the use of the chirp window when the signal contains frequency steps (i.e., FSK). A marked difference in the spectral estimate is noted for the upward change relative to the downward change case. This difference in the spectrum shape is due to the fact that the chirp window introduces a time varying spectral component, or digital instantaneous frequency, which will affect the downward and upward shifts differently. However, this change in the shape spectrum can offer an advantage over traditional windows, since the use of

traditional windows as weighting functions results in a spectral estimate which is almost the same for the downward shift and upward shift cases.

The numerical value of the window transform at the DC location is almost zero. This confirms the presence of a null at the 0 frequency point in the magnitude spectrum. Simulation results show that the alternative non-traditional window presented in Appendix C (which is a square chirp window) behaves much like the chirp window studied in Chapter IV. It should be noted that the square chirp window is limited to high SNR (above 15 dB).

Finally, a continuation of the research into non-traditional windows is recommended, since they have better resolution properties than conventional windowing techniques, such as the raised cosine window.

APPENDIX A. RELATIONSHIP BETWEEN THE TRANSFORM OF A CONTINUOUS SIGNAL AND A SAMPLED SIGNAL.

To demonstrate the relationship between the sample transform $X_s(f)$ and the Fourier transform $X(f)$ of continuous function $x(t)$, define

$$X_s(f) = \frac{1}{T_s} \sum_{n=-\infty}^{\infty} X(f - \frac{n}{T_s}). \quad (A.1)$$

Let $x_\delta(t)$ be a pulse train of delta functions:

$$x_\delta(t) = \sum_{n=-\infty}^{\infty} \delta(t - nT_s). \quad (A.2)$$

Because Equation A.2 is a periodic function, it can be expanded in a Fourier series as

$$x_\delta(t) = \sum_{n=-\infty}^{\infty} x_n \exp(j \frac{2\pi n t}{T_s}), \quad (A.3)$$

where

$$x_n = \frac{1}{T_s} \int_{-T/2}^{T/2} x(t) \exp(-j \frac{2\pi n t}{T_s}) dt. \quad (A.4)$$

If $x(t) = \delta(t)$, and recalling that $\int_{-\infty}^{\infty} x(t) \delta(t - \tau) dt = x(\tau)$, a periodic pulse train of delta functions can be written so that

$$x_n = \frac{1}{T_s} \int_{-T/2}^{T/2} \delta(t) \exp(-j \frac{2\pi n t}{T_s}) dt = \frac{1}{T_s} e^0, \quad (A.5)$$

hence

$$x_n = \frac{1}{T_s}. \quad (\text{A.6})$$

Therefore Equation A.3 can be written as

$$\sum_{n=-\infty}^{\infty} \delta(t - nT_s) = \frac{1}{T_s} \sum_{n=-\infty}^{\infty} \exp(j\frac{2\pi nt}{T_s}). \quad (\text{A.7})$$

If t is replaced by f and T_s by $\frac{1}{T_s}$, Equation A.7 becomes

$$\sum_{n=-\infty}^{\infty} \delta(f - \frac{n}{T_s}) = T_s \sum_{n=-\infty}^{\infty} \exp(j2\pi fnT_s). \quad (\text{A.8})$$

Next, recalling that the Fourier transform of the sampled data is

$$X_s(f) = \sum_{n=-\infty}^{\infty} x(nT_s) \exp(-j2\pi fnT_s), \quad (\text{A.9})$$

and that the continuous function of $x(t)$ can be written as

$$x(t) = \int_{-\infty}^{\infty} X(f') \exp(j2\pi f' t) df', \quad (\text{A.10})$$

replacing Equation A.10 into Equation A.9 yields

$$X_s(f) = \int_{-\infty}^{\infty} X(f') df' \sum_{n=-\infty}^{\infty} \exp(j2\pi n(f - f')T_s). \quad (\text{A.11})$$

Applying Equation A.8 shows that

$$\sum_{n=-\infty}^{\infty} \exp(j2\pi n(f - f')T_s) = \frac{1}{T_s} \sum_{n=-\infty}^{\infty} \delta(f - f' - \frac{n}{T_s}), \quad (\text{A.12})$$

and therefore

$$X_s(f) = \int_{-\infty}^{\infty} x(f') \frac{1}{T_s} \sum_{n=-\infty}^{\infty} \delta(f - f' - \frac{n}{T_s}) df' . \quad (A.13)$$

But by the property of the delta function,

$$\int_{-\infty}^{\infty} x(t) \delta(t - t_0) dt = x(t_0) . \quad (A.14)$$

The final result is

$$X_s(f) = \frac{1}{T_s} \sum_{n=-\infty}^{\infty} X(f - \frac{n}{T_s}) . \quad (A.15)$$

APPENDIX B. PROCESSING GAIN

Processing gain is defined as the ratio of output signal to noise ratio $(\text{SNR})_o$ to input signal to noise ratio $(\text{SNR})_i$, and is given by

$$\text{PG} = \frac{(\text{SNR})_o}{(\text{SNR})_i} \quad (\text{B.1})$$

where SNR is defined as the ratio of signal power to noise power (i.e. S/N).

The derivation of $(\text{SNR})_o = S_o/N_o$. Let the sampled sequence be defined by

$$x(nT_s) = A \exp(j\omega_k nT_s) + q(nT_s), \quad (\text{B.2})$$

where $q(nT_s)$ is a white noise sequence with variance σ_q^2 , and

$$\omega_k = \frac{2\pi k}{NT_s}. \quad (\text{B.3})$$

The component (i.e., signal plus noise) of the Fourier transform is given by

$$X(\omega_k) = \sum_n x(nT_s)w(nT_s)\exp(-j\omega_k nT_s) \quad (\text{B.4})$$

where $w(nT_s)$ is the window sampled sequence.

Using Equation B.2 in Equation B.4 obtains the value of the signal component

$$X(\omega_k)_{\text{signal}} = \sum_n A \exp(j\omega_k nT_s)w(nT_s)\exp(-j2\omega_k nT_s) \quad (\text{B.5})$$

or

$$X(\omega_k)_{\text{signal}} = A \sum_n w(nT_s). \quad (B.6)$$

The power component of the signal is therefore

$$(\text{Power})_{\text{signal}} = S_o = A^2 \left[\sum_n w(nT_s) \right]^2. \quad (B.7)$$

The noise component of the windowed transform is given by

$$X(\omega_k)_{\text{noise}} = \sum_n w(nT_s) q(nT_s) \exp(-j\omega_k nT_s). \quad (B.8)$$

The noise power (the mean square value of this component) is given by

$$\begin{aligned} E[|X(\omega_k)_{\text{noise}}|^2] &= \sum_n \sum_m w(nT_s) w(mT_s) \\ &E[q(nT_s) q^*(mT_s)] \exp(-j\omega_k nT_s) \exp(j\omega_k mT_s) \end{aligned} \quad (B.9)$$

If $m = n$, and the mean of the noise is zero, it follows that

$$E[|X(\omega_k)_{\text{noise}}|^2] = N_o = \sigma_q^2 \sum_n w^2(nT_s), \quad (B.10)$$

and therefore

$$(\text{SNR})_o = \frac{S_o}{N_o} = \frac{A^2 \left[\sum_n w(nT_s) \right]^2}{\sigma_q^2 \sum_n w^2(nT_s)} \quad (B.11)$$

It is known that for an AWGN case, the relationship $(\text{SNR})_{\text{input}}$ is given by

$$(\text{SNR})_i = \frac{A^2}{\sigma_q^2} \quad (B.12)$$

If the results of Equation B.11 and Equation B.12 are applied in Equation B.1, the processing gain is obtained as

$$PG = \frac{(SNR)_o}{(SNR)_i} = \frac{\left[\sum_n w(nT_s) \right]^2}{\sum_n w^2(nT_s)} . \quad (B.13)$$

For the case of a rectangular window, the sum of the window terms is given by

$$\sum_{n=0}^{N-1} w(nT_s) = \sum_{n=0}^{N-1} w^2(nT_s) = N \quad (B.14)$$

then the processing gain for the case of a rectangular window is N , as in

$$(PG)_{\text{rect.window}} = \frac{N^2}{N} = N . \quad (B.15)$$

This gain is obtained when processing an analytic signal (i.e., complex valued sinusoid in AWGN). For any other window, the gain is reduced due to the windows roll-off.

There is a practical approach to computing the processing gain for the case of a rectangular window with real input and a complex input signal. If the input signal is real, then

$$x(t) = A \cos(2\pi ft) . \quad (B.16)$$

Therefore,

$$(SNR)_i = \frac{S_i}{N_i} = \frac{A^2/2}{N_o/2} = \frac{A^2}{N_o} , \quad (B.17)$$

and, because the length of the window is N , it follows that

$$(\text{SNR})_o = \frac{S_o}{N_o} = \frac{A^2/4}{N_o/2N} = \frac{A^2N}{2N_o} \quad (\text{B.18})$$

The processing gain is then given by

$$(\text{PG})_{\text{rect.window}} = \frac{(\text{SNR})_o}{(\text{SNR})_i} = \frac{A^2N/(2N_o)}{A^2/N_o} = \frac{N}{2} \quad (\text{B.19})$$

From Equation B.19, it can be seen that PG for the case of a rectangular window, when the input signal is real, is half that found when the input signal is complex. This is due to the fact that the value of the power output signal (i.e., S_o) is twice the value of S_o when the signal is real. In other words, if the input signal is of the form

$$x(t) = A \exp(j2\pi ft), \quad (\text{B.20})$$

the relationship $(\text{SNR})_i$ remains the same as in Equation B.17, but $(\text{SNR})_o$ is given by

$$(\text{SNR})_o = \frac{S_o}{N_o} = \frac{A^2/2}{N_o/2N} = \frac{A^2N}{N_o} \quad (\text{B.21})$$

Therefore, PG in the case of a complex input signal is

$$(\text{PG})_{\text{rect.window}} = \frac{(\text{SNR})_o}{(\text{SNR})_i} = \frac{A^2N/N_o}{A^2/N_o} = N \quad (\text{B.22})$$

and Equation B.22 agrees with Equation B.15.

APPENDIX C. AN ALTERNATIVE NONTRADITIONAL WINDOW

The alternative chirp window depicted here consists of a hard dipped chirp generated from the chirp window studied in this thesis. The MATLAB program for this window can be found in Appendix D.

This window has a 32 point length and the equation for the chirp window (i.e., $w(n) = \exp(j \theta(n))$) has been modified according to the following equations: The angle Ω is defined by

$$\Omega = \arctan(\text{imag}(w(n))/\text{real}(w(n))) \quad (C.1)$$

then, if

$$\Omega > -\pi/4 \text{ and } \Omega \leq \pi/4 \Rightarrow w(n) = 1 + 0j \quad (C.2)$$

if

$$\Omega > \pi/4 \text{ and } \Omega \leq 3\pi/4 \Rightarrow w(n) = 0 + j, \quad (C.3)$$

if

$$\Omega > 3\pi/4 \text{ and } \Omega \leq \pi \Rightarrow w(n) = -1 + 0j \quad (C.4)$$

if

$$\Omega > -\pi \text{ and } \Omega \leq -3\pi/4 \Rightarrow w(n) = -1 + 0j \quad (C.5)$$

and, if

$$\Omega > -3\pi/4 \text{ and } \Omega \leq -\pi/4 \Rightarrow w(n) = 0 - j \quad (C.6)$$

Figure C.1a, depicts the projection of the window on the real and imaginary plane, while figures C.1b, C.1c and C.1d, show the real, imaginary part and a three dimensional plot of the window, respectively. From this figures it can be observed that the real and imaginary part toggle, this means that when the real part is ± 1 the imaginary part is 0, and vice versa.

Figure C.2a shows the spectrum of the window. It can be observed that the shape is similar to that of the magnitude spectrum for the FM chirp window, with a deep null at the 0 frequency location. This window can therefore be considered as a high resolution procedure for single sinusoids. Figure C.2b shows the magnitude spectrum when a single sinusoid is present. The frequency of the signal is at 0.328125 Hz. (i.e., $f_1 = 10.5fs/N$), and a deep null is observed at the proper signal frequency location. Note that the frequency location is not bin centered. An SNR of 20 dB is employed. It should also be noted that the amplitude of the null seems to be greater than that of the chirp window (compare to Figure 4.4).

Figure C.2c depicts the spectrum when two signals are present. The frequency of the signals are located at 0.3125 Hz (i.e., $f_1 = 10fs/N$) and at 0.328125 Hz (i.e., $f_2 = 10.5fs/N$). This figure shows that the minimum of the

spectrum does not occur exactly at the signal frequency locations, and the spectrum shape is totally different than that resulting from a single signal (Figure C.2b). The magnitude spectrum for this type of window when more than one signal is present has behavior similar to that presented by Griffiths (Figure 4.5), that is, multiple nulls at lower frequencies and smooth spectral shape at higher frequencies, confirming his contention that such a change in the magnitude spectrum can be attributed to the presence of more than one signal.

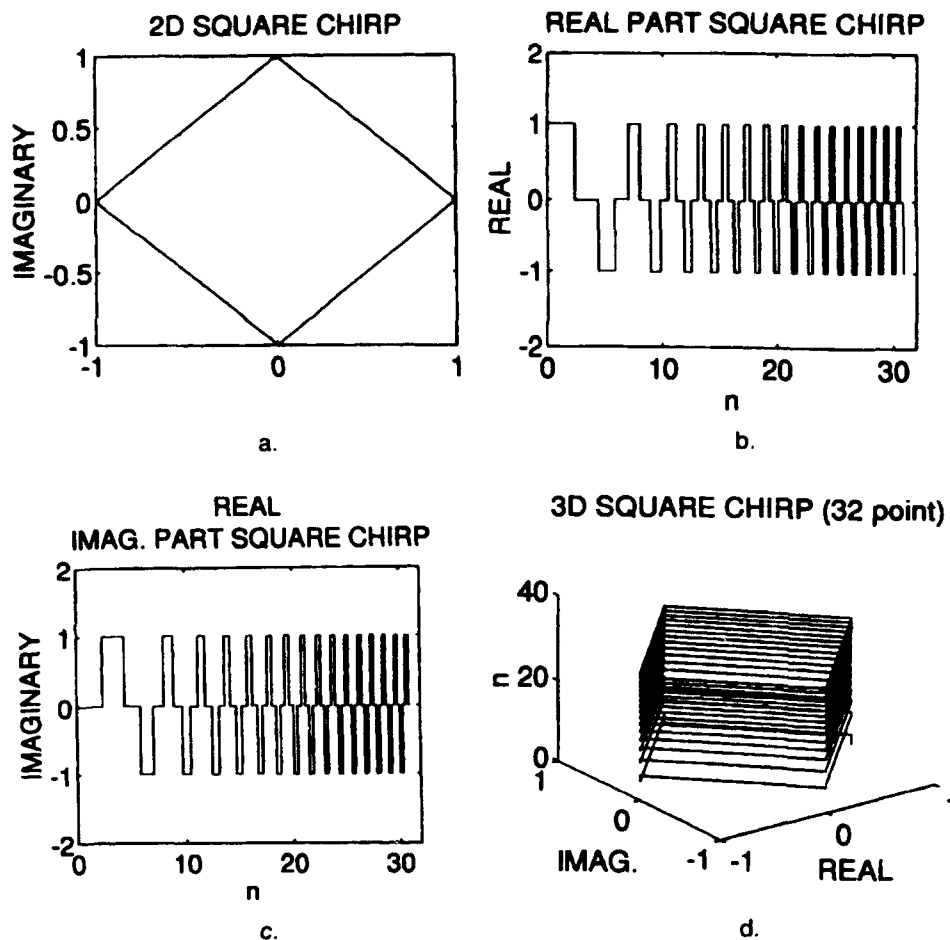
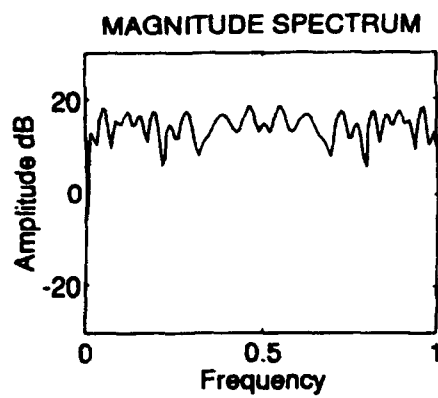
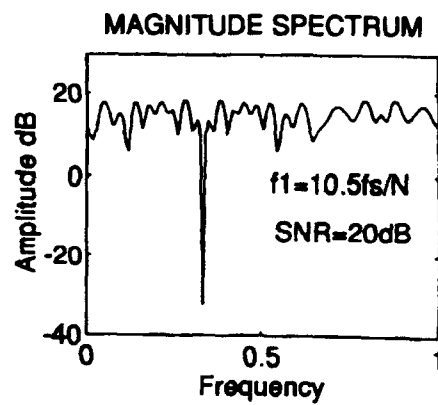


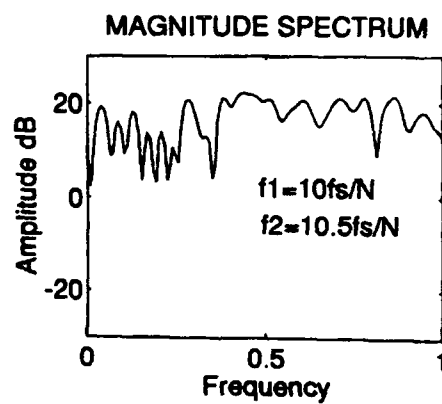
Figure C.1. Square Chirp Window.



a.



b.



c.

Figure C.2. Magnitude Spectrum Of The Square Chirp Window.

APPENDIX D. MATLAB PROGRAMS

%RECTANGULAR WINDOW

```

clg
n=1:51;
x=-25:25;
w=ones(1,length(n));
axis([-30 30 0 1]);
subplot(211),plot(x,w),title('rect.window'),xlabel('n'),ylabel('
    w(n)')
wf=abs(fftshift(fft(w,1024)));
W=20*log10(wf/max(wf));
f=-pi:2*pi/length(W):pi;
axis([-4 4 -80 0]);
subplot(212),plot(f(1:1024),W),xlabel('radian frequency'), ...
ylabel('log-magnitude of transform'), ...
title('1024 point FFT of rectangular window')
grid
pause

```

%TRIANGLE WINDOW

```

clg
n=1:51;
x=-25:25;
w=barlett(51);
axis([-30 30 0 1]);
subplot(211),plot(x,w),title('triangular window'),xlabel('n'),
...
ylabel('w(n)')
wf=abs(fftshift(fft(w,1024)));
W=20*log10(wf/max(wf));
f=-pi:2*pi/length(W):pi;
axis([-4 4 -80 0]);
subplot(212),plot(f(1:1024),W),xlabel('radian frequency'), ...
ylabel('log-magnitude of transform'), ...
title('1024 point FFT of triangular window')
grid
pause
%HAMMING WINDOW

```

```

clg
n=1:51;
x=-25:25;
w=hamming(51);
axis([-30 30 0 1]);
subplot(211),plot(x,w),title('Hamming window'),xlabel('n'),
...
ylabel('w(n)')
wf=abs(fftshift(fft(w,1024)));
W=20*log10(wf/max(wf));
f=-pi:2*pi/length(W):pi;
axis([-4 4 -80 0]);
subplot(212),plot(f(1:1024),W),xlabel('radian frequency'), ...
ylabel('log-magnitude of transform'), ...
title('1024 point FFT of Hamming window')
grid
pause

```

%BLACKMAN WINDOW

```

clg
n=1:51;
x=-25:25;
w=blackman(51);
%w=(7938/18608)-(9240/18608)*cos(2*pi*n/50)+(1430/1
    8608)*cos(4*pi*n/50);
axis([-30 30 0 1]);
subplot(211),plot(x,w),title('Blackman window'),xlabel('n'),
...
ylabel('w(n)')
wf=abs(fftshift(fft(w,1024)));
W=20*log10(wf/max(wf));
f=-pi:2*pi/length(W):pi;
axis([-4 4 -80 0]);
subplot(212),plot(f(1:1024),W),xlabel('radian frequency'), ...
ylabel('log-magnitude of transform'), ...
title('1024 point FFT of blackman window')
grid

```

```

pause

%KAISER-BESSEL WINDOW
clg
n=1:51;
x=-25:25;
w=kaiser(51,2*pi);
%w=kaiser(51,3*pi);
axis([-30 30 0 1]);
subplot(211),plot(x,w),title('Kaiser window
    (a=3)'),xlabel('n'),...
ylabel('w(n)')
wf=abs(fftshift(fft(w,1024)));
W=20*log10(wf/max(wf));
f=-pi:2*pi/length(W):pi;
axis([-4 4 -100 0]);
subplot(212),plot(f(1:1024),W),xlabel('radian frequency'), ...
ylabel('log-magnitude of transform'), ...
title('1024 point FFT of Kaiser window a=3')
grid
pause

%SIDELobe LEVELS OF CLASSICAL WINDOWS
clear
clg
n=200;
dbs=60;
b=0.1102*(dbs-8.7);
w=[boxcar(n)triang(n)hamming(n)blackman(n)kaiser(n,b)];
axis([-50 250 0 1.2]);
subplot(211),plot(w)
gtext('rect.')
gtext('triang.')
gtext('hamming')
gtext('blackman')
gtext('kaiser')
y=fft(w,1024);
[my,ny]=size(y);
f=(0:49)/512;
Pyy=y(1:50,:).*conj(y(1:50,:));
axis;
subplot(212),semilogy(f,Pyy)

gtext('rect.')
gtext('triang.')
gtext('hamming')
gtext('blackman')
gtext('kaiser')
pause

%APPLICATION OF CONVENTIONAL WINDOWS TO DETECT
    A WEAK SIGNAL(amplitude=0.01) IN THE PRESENCE
    %OF A STRONG(amplitude=1) NEARBY
    SIGNAL(amplitude=0.01)
%RECTANGULAR WINDOW (TWO SIGNALS : f1=10fs/N ,
    f2=16fs/N )
clear
clg
n=0:255;
s=(cos(2*pi*10*n/256)+0.01*cos(2*pi*16*n/256));
wf=abs(fft(s));
W=20*log10(wf/max(wf));
axis([0 100 -80 0]);
subplot(211),plot(n,W),xlabel('k'),ylabel('log-mag. of transf.
    (dB)'), ...
title('RECTANGULAR WINDOW (TWO SIGNALS: f1=10fs/N
    f2=16fs/N)')
pause

%RECTANGULAR WINDOW (f1=10.5fs/N , f2=16fs/N)
clear
n=0:255;
s=(cos(2*pi*10.5*n/256)+0.01*cos(2*pi*16*n/256));
% s=(cos(2*pi*10.25*n/256)+cos(2*pi*16*n/256));
wf=abs(fft(s));
W=20*log10(wf/max(wf));
axis([0 100 -80 0]);
subplot(212),plot(n,W),xlabel('k'),ylabel('log-mag. of transf.
    (dB)'), ...
title('RECTANGULAR WINDOW (TWO SIGNALS:
    f1=10.5fs/N f2=16fs/N)')
pause

%TRIANGLE WINDOW (f1=10.5fs/N , f2=16fs/N)

```

```

clear
clg
n=0:255;
s1=(cos(2*pi*10.5*n/256)+0.01*cos(2*pi*16*n/256));
w1=(bartlett(256));
w=w1.*s1;
wf=abs(fft(w));
W=20*log10(wf/max(wf));
axis([0 100 -70 0]);
subplot(211),plot(n,W),xlabel('k'),ylabel('log-mag. of transf. (dB)'), ...
title('TRIANGLE WINDOW (TWO SIGNALS: f1=10.5fs/N f2=16fs/N)')
pause

```

```

%HAMMING WINDOW (f1=10.5fs/N , f2=16fs/N)
clear
n=0:255;
s1=(cos(2*pi*10.5*n/256)+0.01*cos(2*pi*16*n/256));
w1=(hamming(256));
w=w1.*s1;
wf=abs(fft(w));
W=20*log10(wf/max(wf));
axis([0 100 -70 0]);
subplot(212),plot(n,W),xlabel('k'),ylabel('log-mag. of transf. (dB)'), ...
title('HAMMING WINDOW (TWO SIGNALS: f1=10.5fs/N f2=16fs/N)')
pause

```

```

%BLACKMAN WINDOW (f1=10.5fs/N , f2=16fs/N)
clear
clg
n=0:255;
s1=(cos(2*pi*10.5*n/256)+0.01*cos(2*pi*16*n/256));
w1=(blackman(256));
w=w1.*s1;
wf=abs(fft(w));
W=20*log10(wf/max(wf));
axis([0 100 -70 0]);
subplot(211),plot(n,W),xlabel('k'),ylabel('log-mag. of transf. (dB)'), ...

```

```

title('BLACKMAN WINDOW (TWO SIGNALS: f1=10.5fs/N f2=16fs/N)')
pause
%EXACT BLACKMAN WINDOW
w1=(0.42659071-0.49656062*cos(2*pi*n/256)+0.0768486
7*cos(4*pi*n/256));
w=w1.*s1;
wf=abs(fft(w));
W=20*log10(wf/max(wf));
subplot(212),plot(n,W),xlabel('k'),ylabel('log-mag. of transf. (dB)'), ...
title('EXACT BLACKMAN WINDOW (TWO SIGNALS: f1=10.5fs/N f2=16fs/N)')
pause

```

```

%KAISER-BESSEL WINDOW(B=2) (f1=10.5fs/N , f2=16fs/N)
clear
clg
n=0:255;
s1=(cos(2*pi*10.5*n/256)+0.01*cos(2*pi*16*n/256));
w1=(kaiser(256,2*pi));
w=w1.*s1;
wf=abs(fft(w));
W=20*log10(wf/max(wf));
axis([0 100 -70 0]);
subplot(211),plot(n,W),xlabel('k'),ylabel('log-mag. of transf. (dB)'), ...
title('KAISER-BESSEL WINDOW B=2 (SIGNALS f1=10.5fs/N f2=16fs/N)')
pause
%KAISER-BESSEL WINDOW (B=3)
w1=(kaiser(256,3*pi));
w=w1.*s1;
wf=abs(fft(w));
W=20*log10(wf/max(wf));
subplot(212),plot(n,W),xlabel('k'),ylabel('log-mag. of transf. (dB)'), ...
title('KAISER-BESSEL WINDOW B=3 (SIGNAL: f1=10.5fs/N f2=16fs/N)')
pause

```

```
%DETECTION OF WINDOWED SIGNAL IN AWGN
ENVIRONMENT
```

```
%RECTANGULAR WINDOW (f1=10fs/N f2=16fs/N )
```

```
clf
```

```
n=0:255;
```

```
rand('normal');
```

```
r=1/(10^(0/20))*rand(n); %0J0 SNR level
```

```
s2=(cos(2*pi*10.5*n/256)+0.01*cos(2*pi*16*n/256));
```

```
S=s2+r;
```

```
wf1=abs(fft(S));
```

```
W1=20*log10(wf1/max(wf1));
```

```
axis([0 100 -80 0]);
```

```
subplot(221),plot(n,W1),xlabel('k'),ylabel('log-mag. of  
transf.(dB)'),...
```

```
title('Rect. Window (AWGN)')
```

```
gtext('f1=10.5bin f2=16bin');
```

```
gtext('SNR=0dB');
```

```
pause
```

```
%TRIANGLE WINDOW WITH NOISE (f1=10.5fs/N  
f2=16fs/N)
```

```
rand('normal');
```

```
%s=(cos(2*pi*10.5*n/256)+cos(2*pi*16*n/256));
```

```
%s1=s+r;
```

```
wt=(bartlett(256));
```

```
w2=wt.*S;
```

```
wf2=abs(fft(w2));
```

```
W2=20*log10(wf2/max(wf2));
```

```
%subplot(211),plot(n,W2),xlabel('k'),ylabel('log-mag. of  
transf.(dB)'),...
```

```
%title('Triang. window (AWGN)')
```

```
%gtext('f1=10.5bin, f2=16bin');
```

```
%gtext('SNR=0dB');
```

```
%pause
```

```
%HAMMING WINDOW WITH NOISE(f1=10.5fs/N  
f2=16fs/N)
```

```
wh=(hamming(256));
```

```
w3=wh.*S;
```

```
wf3=abs(fft(w3));
```

```
W3=20*log10(wf3/max(wf3));
```

```
subplot(222),plot(n,W3),xlabel('k'),ylabel('log-mag. of  
transf.(dB)'),...
```

```
title('Hamming window (AWGN)')
```

```
gtext('f1=10.5bin f2=16bin');
```

```
gtext('SNR=0dB');
```

```
pause
```

```
%BLACKMAN WINDOW WITH NOISE (f1=10.5fs/N  
f2=16fs/N)
```

```
wb=(blackman(256));
```

```
w4=wb.*S;
```

```
wf4=abs(fft(w4));
```

```
W4=20*log10(wf4/max(wf4));
```

```
subplot(223),plot(n,W4),xlabel('k'),ylabel('log-mag. of  
transf.(dB)'),...
```

```
title('Blackman window (AWGN)')
```

```
gtext('f1=10.5bin f2=16bin');
```

```
gtext('SNR=0dB');
```

```
pause
```

```
%KAISER WINDOW WITH NOISE (a=2)
```

```
wk=(kaiser(256,pi*2));
```

```
w5=wk.*S;
```

```
wf5=abs(fft(w5));
```

```
W5=20*log10(wf5/max(wf5));
```

```
subplot(224),plot(n,W5),xlabel('k'),ylabel('log-mag. of  
transf.(dB)'),...
```

```
title('Kaiser-Bessel window (AWGN)')
```

```
gtext('a=2')
```

```
gtext('f1=10.5bin f2=16bin');
```

```
gtext('SNR=0dB');
```

```
pause
```

```
%NON-CLASSICAL WINDOWS (LINEAR FM CHIRP  
WINDOW)
```

```
%AMPLITUDE SPECTRUM FOR 32 POINT LINEAR FM  
CHIRP WINDOW
```

```
clear
```

```
clf
```

```
n=0:31;
```

```

On=2*pi*n.*(n+1)/(32*2);
w=exp(i*On);
axis;
plot(w)
pause
wf=abs(fft(w,128));
W=20*log10(wf);
f=0:1/127:1;
axis([0 1 -30 20]);
subplot(211),plot(f,W),xlabel('Normalized
    frequency'),ylabel('amplitude dB'),...
title('Amplitude spectrum for 32 point linear FM chirp
    window')
pause

%PHASE SPECTRUM FOR 32 POINT LINEAR FM CHIRP
    WINDOW
P=angle(fft(w));
f1=0:1/31:1;
axis;
subplot(212),plot(f1,P),xlabel('frequency'),ylabel('Phase
    radians'),...
title('Phase spectrum for 32 point linear FM chirp window')
pause

%SPECTRUM FOR ONE COMPLEX SINUSOID AT
    f=0.328125 Hz
clg
rand('normal')
r1=1/(10^(30/20))*rand(n);
x1=exp(i*2*pi*n*0.328125)+r1;
w1=x1.*w;
w1f=abs(fft(w1,128));
axis([0 1 -30 30]);
W1=20*log10(w1f);
subplot(221),plot(f,W1),xlabel('Normalized frequency
    Hz'),ylabel('Amplitude dB'),...
title('One signal at FM chirp window')
gtext('f=0.328125 Hz.')
gtext('SNR=30dB')
pause
r2=1/(10^(20/20))*rand(n);

```

```

x2=exp(i*2*pi*n*0.328125)+r2;
w2=x2.*w;
w2f=abs(fft(w2,128));
W2=20*log10(w2f);
subplot(222),plot(f,W2),xlabel('Normalized frequency
    Hz'),ylabel('Amplitude dB'),...
title('One signal at FM chirp window')
gtext('f=0.328125 Hz.')
gtext('SNR=20dB')
pause
r3=1/(10^(18/20))*rand(n);
x3=exp(i*2*pi*n*0.328125)+r3;
w3=x3.*w;
w3f=abs(fft(w3,128));
W3=20*log10(w3f);
subplot(223),plot(f,W3),xlabel('Normalized frequency
    Hz'),ylabel('Amplitude dB'),...
title('One signal at FM chirp window')
gtext('f=0.328125 Hz.')
gtext('SNR=18dB')
pause
r4=1/(10^(15/20))*rand(n);
x4=exp(i*2*pi*n*0.328125)+r4;
w4=x4.*w;
w4f=abs(fft(w4,128));
W4=20*log10(w4f);
subplot(224),plot(f,W4),xlabel('Normalized frequency
    Hz'),ylabel('Amplitude dB'),...
title('One signal at FM chirp window')
gtext('f=0.328125 Hz.')
gtext('SNR=15dB')
pause

%SPECTRUM FOR TWO SINUSOIDS AT f1=0.328125 Hz,
    f2=0.3125 Hz
clg
rand('normal')
r21=1/(10^(30/20))*rand(n);
x1=(exp(i*2*pi*n*0.328125)+exp(i*2*pi*n*0.3125))+r21;
w1=x1.*w;
w1f=abs(fft(w1,128));
W1=20*log10(w1f);

```

```

axis([0 1 -30 30]);
subplot(221),plot(f,W1),xlabel('Normalized frequency
    Hz'),ylabel('Amplitude dB'),...
title('Two signals at FM chirp window')
gtext('f1=0.328125 Hz')
gtext('f2=0.3125 Hz')
gtext('SNR=30dB')
pause
r22=1/(10^(20/20))*rand(n);
x2=(exp(i*2*pi*n*0.328125)+exp(i*2*pi*n*0.3125))+r22;
w2=x2.*w;
w2f=abs(fft(w2,128));
W2=20*log10(w2f);
subplot(222),plot(f,W2),xlabel('Normalized frequency
    Hz'),ylabel('Amplitude dB'),...
title('Two signals at FM chirp window')
gtext('f1=0.328125 Hz')
gtext('f2=0.3125 Hz')
gtext('SNR=20dB')
pause
r23=1/(10^(15/20))*rand(n);
x3=(exp(i*2*pi*n*0.328125)+exp(i*2*pi*n*0.3125))+r23;
w3=x3.*w;
w3f=abs(fft(w3,128));
W3=20*log10(w3f);
subplot(223),plot(f,W3),xlabel('Normalized frequency
    Hz'),ylabel('Amplitude dB'),...
title('Two signals at FM chirp window')
gtext('f1=0.328125 Hz')
gtext('f2=0.3125 Hz')
gtext('SNR=15dB')
pause
r24=1/(10^(10/20))*rand(n);
x4=(exp(i*2*pi*n*0.328125)+exp(i*2*pi*n*0.3125))+r24;
w4=x4.*w;
w4f=abs(fft(w4,128));
W4=20*log10(w4f);
subplot(224),plot(f,W4),xlabel('Normalized frequency
    Hz'),ylabel('Amplitude dB'),...
title('Two signals at linear chirp window')
gtext('f1=0.328125 Hz')
gtext('f2=0.3125 Hz')

```

```

gtext('SNR=10dB')
pause

%SPECTRUM FOR ONE SINUSOID AT f1=0.328125 Hz
    USING RAISED COSINE WINDOW
clf
rand('normal');
rs=1/(10^(30/20))*rand(n);
x2=exp(i*2*pi*n*0.328125)+rs;
w1=hamming(32);
w3=x2.*w1;
w3f=abs(fft(w3,128));
W3=20*log10(w3f);
axis([0 1 -30 30]);
subplot(211),plot(f,W3),xlabel('Normalized frequency
    Hz'),ylabel('Amplitude dB'),...
title('Spectrum for one sinusoid using raised cosine
    window')
gtext('f=0.328125 Hz')
gtext('SNR=30dB')
pause

%SPECTRUM FOR TWO SINUSOIDS AT f1=0.328125 Hz,
    f2=0.3125 Hz USING RAISED
    COSINE WINDOW
x3=(exp(i*2*pi*n*0.328125)+exp(i*2*pi*n*0.3125))+rs;
w4=x3.*w1;
w4f=abs(fft(w4,128));
W4=20*log10(w4f);
subplot(212),plot(f,W4),xlabel('Normalized frequency
    Hz'),ylabel('Amplitude dB'),...
title('Spectrum for two sinusoids using raised cosine
    window')
gtext('f1=0.328125 Hz')
gtext('f2=0.3125 Hz')
gtext('SNR=30dB')
pause

%SPECTRUM FOR FREQUENCY STEP TIME WAVEFORMS
    USING RAISED COSINE WINDOW
clear

```

```

clg
n=1:32;
rand('normal')
r=1/(10^(30/20))*rand(n);
O(n)=2*pi*n.*(n+1)/(32^2);
F(n)=2*pi*n/32;
O(n)=O(n)+F(n);
w=exp(i*O(n));
wc=blackman(32)';
x1=exp(i*2*pi*(0.15)*0.2);
x2=exp(i*2*pi*(16/31)*0.4);
xu=[x1,x2]+r;
w1=xu.*wc;
w1f=abs(fft(w1,128));
W1=20*log10(w1f);
f=0:1/127:1;
axis([0 1 -30 30]);
subplot(221),plot(f,W1),xlabel('Frequency
    Hz'),ylabel('Amplitude dB'),...
title('Up freq. step (conv. window)')
pause
w2=xu.*w;
w2f=abs(fft(w2,128));
W2=20*log10(w2f);
subplot(223),plot(f,W2),xlabel('Frequency
    Hz'),ylabel('Amplitude dB'),...
title('Up freq. step (FM chirp window)')
pause
xd=[x2,x1]+r;
w3=xd.*wc;
w3f=abs(fft(w3,128));
W3=20*log10(w3f);
subplot(222),plot(f,W3),xlabel('Frequency
    Hz'),ylabel('Amplitude dB'),...
title('Down freq. step (conv. window)')
pause
w4=xd.*w;
w4f=abs(fft(w4,128));
W4=20*log10(w4f);
subplot(224),plot(f,W4),xlabel('Frequency
    Hz'),ylabel('Amplitude dB'),...
title('Down freq. step (FM chirp window)')

```

```

pause

%ANALYSIS OF SNR FOR CLASSIC AND HIGH
    RESOLUTION WINDOWS
%NO NOISE CASE
%RECTANGLE WINDOW (f1=10.75fs/N , f2=11.25fs/N)
clear
clg
n=0:31;
s=(cos(2*pi*10.75*n/32)+cos(2*pi*11.25*n/32));
wf=abs(fft(s,128));
W=20*log10(wf/max(wf));
f=0:1/127:1;
axis([0 0.5 -60 0]);
subplot(221),plot(f,W),xlabel('Normalized freq
    Hz'),ylabel('Amplitude (dB)'),...
title('RECTANGULAR WINDOW')
gtext('NO NOISE')
gtext('f1=0.335937Hz.')
gtext('f2=0.351562Hz.')
pause

%HAMMING WINDOW (f1=10.75fs/N , f2=11.25fs/N)
w1h=(hamming(32))';
w1=w1h.*s;
w1f=abs(fft(w1,128));
W1=20*log10(w1f/max(w1f));
subplot(222),plot(f,W1),xlabel('Normalized freq
    Hz'),ylabel('Amplitude (dB)'),...
title('HAMMING WINDOW')
gtext('NO NOISE')
gtext('f1=0.335937Hz.')
gtext('f2=0.351562Hz.')
pause

%LINEAR FM CHIRP WINDOW ONE COMPLEX SINUSOID
    AT f=0.328125(or 10.75/32)
%NO NOISE CASE
n=0:31;
On=2*pi*n.*(n+1)/(32^2);
wc=exp(i*On);

```

```

x=exp(i*2*pi*n*10.75/32);
w2=x.*wc;
wf2=abs(fft(w2,128));
W2=20*log10(wf2/max(wf2));
f=0:1/127:1;
axis([0 1 -60 0]);
subplot(223),plot(f,W2),xlabel('Normalized freq.
    Hz. '),ylabel('Amplitude (dB)'),...
title('One signal at FM CHIRP WINDOW')
gtext('NO NOISE')
gtext('f1=0.335937Hz.')
pause
% FM CHIRP WINDOW 2 COMPLEX SINUSOIDS AT
    f1=0.335937, f2=0.351562(or 11.25/32)
x1=x+exp(i*2*pi*n*11.25/32);
w3=x1.*wc;
wf3=abs(fft(w3,128));
W3=20*log10(wf3/max(wf3));
subplot(224),plot(f,W3),xlabel('Normalized freq.
    Hz. '),ylabel('Amplitude (dB)'),...
title('Two signals at FM CHIRP WINDOW')
gtext('NO NOISE')
gtext('f1=0.335937Hz.')
gtext('f2=0.351562Hz.')
pause

%SIGNAL TO NOISE RATIO (SNR) ANALYSIS
clg
n=0:31;
rand('normal');
z=30; %level of SNR (dB)
r=1/(10^(z/20))*rand(n);
%RECTANGULAR WINDOW (AWGN)
sr=s+r;
wfr=abs(fft(sr,128));
Wr=20*log10(wfr/max(wfr));
axis([0 0.5 -60 0]);
subplot(221),plot(f,Wr),xlabel('Normalized freq.
    Hz. '),ylabel('Amplitude (dB)'),...
title('RECTANGULAR WINDOW')
gtext('SNR=30dB')
gtext('f1=0.335937Hz.')

```

```

gtext('f2=0.351562Hz.')
pause
z=18;
r=1/(10^(z/20))*rand(n);
sr=s+r;
wfr=abs(fft(sr,128));
Wr=20*log10(wfr/max(wfr));
subplot(222),plot(f,Wr),xlabel('Normalized freq.
    Hz. '),ylabel('Amplitude (dB)'),...
title('RECTANGULAR WINDOW')
gtext('SNR=18dB')
pause
z=9;
r=1/(10^(z/20))*rand(n);
sr=s+r;
wfr=abs(fft(sr,128));
Wr=20*log10(wfr/max(wfr));
subplot(223),plot(f,Wr),xlabel('Normalized freq.
    Hz. '),ylabel('Amplitude (dB)'),...
title('RECTANGULAR WINDOW')
gtext('SNR=9dB')
pause
z=0;
r=1/(10^(z/20))*rand(n);
sr=s+r;
wfr=abs(fft(sr,128));
Wr=20*log10(wfr/max(wfr));
subplot(224),plot(f,Wr),xlabel('Normalized freq.
    Hz. '),ylabel('Amplitude (dB)'),...
title('RECTANGULAR WINDOW')
gtext('SNR=0dB')
pause

%HAMMING WINDOW (AWGN)
clg
z=30;
r=1/(10^(z/20))*rand(n);
sr=s+r;
wh=w1h.*sr;
wfh=abs(fft(wh,128));
Wh=20*log10(wfh/max(wfh));

```

```

subplot(221),plot(f,Wh),xlabel('Normalized freq.
    Hz. '),ylabel('Amplitude (dB)'),...
title('HAMMING WINDOW')
gtext('SNR=30dB')
gtext('f1=0.335937Hz.')
gtext('f2=0.351562Hz.')
pause
z=18;
r=1/(10^(z/20))*rand(n);
sr=s+r;
wh=w1h.*sr;
wfh=abs(fft(wh,128));
Wh=20*log10(wfh/max(wfh));
subplot(222),plot(f,Wh),xlabel('Normalized freq.
    Hz. '),ylabel('Amplitude (dB)'),...
title('HAMMING WINDOW')
gtext('SNR=18dB')
pause
z=9;
r=1/(10^(z/20))*rand(n);
sr=s+r;
wh=w1h.*sr;
wfh=abs(fft(wh,128));
Wh=20*log10(wfh/max(wfh));
subplot(223),plot(f,Wh),xlabel('Normalized freq.
    Hz. '),ylabel('Amplitude (dB)'),...
title('HAMMING WINDOW')
gtext('SNR=9dB')
pause
z=0;
r=1/(10^(z/20))*rand(n);
sr=s+r;
wh=w1h.*sr;
wfh=abs(fft(wh,128));
Wh=20*log10(wfh/max(wfh));
subplot(224),plot(f,Wh),xlabel('Normalized freq.
    Hz. '),ylabel('Amplitude (dB)'),...
title('HAMMING WINDOW')
gtext('SNR=0dB')
pause

%FM CHIRP WINDOW (One signal+AWGN)

```

```

clf
n=0:31;
rand('normal');
z=30; %level SNR
r=1/(10^(z/20))*rand(n);
xr=x+r;
wc1=wc.*xr;
wfc1=abs(fft(wc1,128));
WC1=20*log10(wfc1/max(wfc1));
%subplot(223),plot(f,WC1),xlabel('Normalized freq.
    Hz. '),ylabel('Amplitude (dB)'),...
%title('One signal FM CHIRP WINDOW')
%gtext('f1=0.328125Hz')
%gtext('SNR=-3dB')
%pause
%FM CHIRP WINDOW (Two signals+AWGN)
clf
z=30;
r=1/(10^(z/20))*rand(n);
xr1=x1+r;
wc2=wc.*xr1;
wfc2=abs(fft(wc2,128));
WC2=20*log10(wfc2/max(wfc2));
axis([0 1 -40 0]);
subplot(221),plot(f,WC2),xlabel('Normalized freq.
    Hz. '),ylabel('Amplitude (dB)'),...
title('Two signals FM CHIRP WINDOW')
gtext('SNR=30dB')
gtext('f1=0.335937Hz.')
gtext('f2=0.351562Hz.')
pause
z=18;
r=1/(10^(z/20))*rand(n);
xr1=x1+r;
wc2=wc.*xr1;
wfc2=abs(fft(wc2,128));
WC2=20*log10(wfc2/max(wfc2));
subplot(222),plot(f,WC2),xlabel('Normalized freq.
    Hz. '),ylabel('Amplitude (dB)'),...
title('Two signals FM CHIRP WINDOW')
gtext('SNR=18dB')
%gtext('f1=0.328125Hz')

```

```

%gtext('f2=0.359375Hz')
pause
z=9;
r=1/(10^(z/20))*rand(n);
xr1=x1+r;
wc2=wc.*xr1;
wfc2=abs(fft(wc2,128));
WC2=20*log10(wfc2/max(wfc2));
subplot(223),plot(f,WC2),xlabel('Normalized freq.
    Hz.'),ylabel('Amplitude (dB)'),...
title('Two signals FM CHIRP WINDOW')
gtext('SNR=9dB')
%gtext('f1=0.328125Hz')
%gtext('f2=0.359375Hz')
pause
z=0;
r=1/(10^(z/20))*rand(n);
xr1=x1+r;
wc2=wc.*xr1;
wfc2=abs(fft(wc2,128));
WC2=20*log10(wfc2/max(wfc2));
subplot(224),plot(f,WC2),xlabel('Normalized freq.
    Hz.'),ylabel('Amplitude (dB)'),...
title('Two signals FM CHIRP WINDOW')
gtext('SNR=0dB')
%gtext('f1=0.328125Hz')
%gtext('f2=0.359375Hz')
pause

```

```

%SUM OF TWO SINUSOIDS SHOWING EXP. BEHAVIOR
clear
clg
s=cos(2*pi*(0:1:31)*10/31)+cos(2*pi*(0:1:31)*10.5/31);
axis;
subplot(211),plot(s),xlabel('n'),ylabel('s'),title('Sum of two
    sinusoids')
pause

```

```

%DAMPED SINUSOID
n=0:1:31;
s1=exp(-n/16).*cos(2*pi*n*0.328125);

```

```

subplot(212),plot(s1),xlabel('n'),ylabel('s1'),title('Damped
    Sinusoid')
pause

```

```

%DAMPED SINUSOID SIGNAL WITH HIGH RESOLUTION
WINDOW

```

```

clear
clg
n=0:31;
On=2*pi*n.*(n+1)/(32^2);
w=exp(i*On);
rand('normal')
r=1/(10^(30/20))*rand(n);
x=exp(i*2*pi*n*0.328125).*exp(-n/31)+r;
w1=x.*w;
w1f=abs(fft(w1,128));
W1=20*log10(w1f);
f=0:1/127:1;
axis([0 1 -30 30]);
subplot(221),plot(f,W1),xlabel('Normalized
    frequency'),ylabel('amplitude dB'),...
title('f=0.328125 Time constant=1')
pause

```

```

%TIME CONSTANT = 1/2
x=exp(i*2*pi*n*0.328125).*exp(-2*n/(31))+r;
w2=x.*w;
w2f=abs(fft(w2,128));
W2=20*log10(w2f);
subplot(222),plot(f,W2),xlabel('Normalized
    frequency'),ylabel('amplitude dB'),...
title('f=0.328125 Time constant=1/2')
pause

```

```

%TIME CONSTANT = 1/3
x=exp(i*2*pi*n*0.328125).*exp(-3*n/(31))+r;
w3=x.*w;
w3f=abs(fft(w3,128));
W3=20*log10(w3f);
subplot(223),plot(f,W3),xlabel('Normalized
    frequency'),ylabel('amplitude dB'),...
title('f=0.328125 Time constant=1/3')

```

pause

%TIME CONSTANT = 1/4

x=exp(i*2*pi*n*0.328125)*exp(-4*n/(31))+r;

%x=exp(i*2*pi*n*0.5)*exp(-n/(4*31));

w4=x.*w;

w4f=abs(fft(w4,128));

W4=20*log10(w4f);

subplot(224),plot(f,W4),xlabel('Normalized
frequency'),ylabel('Amplitude dB'),...

title('f=0.328125 Time constant=1/4')

pause

%TWO DAMPED SINUSOID SIGNALS (f1=0.3125Hz
f2=0.328125Hz)

clg

x21=(exp(i*2*pi*n*0.3125)+exp(i*2*pi*n*0.328125))+r;

x1=x21.*exp(-n/31);

w5=x1.*w;

w5f=abs(fft(w5,128));

W5=20*log10(w5f);

subplot(221),plot(f,W5),xlabel('Normalized
frequency'),ylabel('Amplitude dB'),...

title('two damped signals Tc=1')

pause

x2=x21.*exp(-2*n/31);

w6=x2.*w;

w6f=abs(fft(w6,128));

W6=20*log10(w6f);

subplot(222),plot(f,W6),xlabel('Normalized
frequency'),ylabel('Amplitude dB'),...

title('two damped signals Tc=1/2')

pause

x3=x21.*exp(-3*n/31);

w7=x3.*w;

w7f=abs(fft(w7,128));

W7=20*log10(w7f);

subplot(223),plot(f,W7),xlabel('Normalized
frequency'),ylabel('Amplitude dB'),...

title('two damped signals Tc=1/3')

pause

x4=x21.*exp(-4*n/31);

w8=x4.*w;

w8f=abs(fft(w8,128));

W8=20*log10(w8f);

subplot(224),plot(f,W8),xlabel('Normalized
frequency'),ylabel('Amplitude dB'),...

title('two damped signals Tc=1/4')

pause

%MEAN VARIANCE AND DC POINT OF CHIRP WINDOW

clear

clg

n=0:31;

On=2*pi*n.*(n+1)/(32*2);

w=exp(i*On);

wf=abs(fft(w,128));

pause

w1=wf(12:64)

pause

f=0.1/127:1;

axis([0 0.5 0 8]);

subplot(221),plot(f,wf),xlabel('Frequency'),ylabel('Magnitud
e')

title('TRANSFORM OF CHIRP WINDOW')

gtext('Figure 4.17')

pause

w0=wf(1)

m=mean(w1)

sd=std(w1)

x=sum(w1)/53

pause

LIST OF REFERENCES

1. Griffiths, Lloyd J., "A Novel Window for High-Resolution Fourier Transforms," *Nineteenth Asilomar Conference on Circuits, Systems, and Computers*, November, 1985.
2. Harris, Frederick J., "On the Use of Windows for Harmonic Analysis with the Discrete Fourier Transform," *Proceedings of the IEEE*, Vol. 68, No. 1, January, 1978.
3. Nuttall, Albert H., "Some Windows with Very Good Sidelobe Behavior," *IEEE Transactions on Acoustic, Speech, and Signal Processing*, Vol. ASSP-29, No. 1, February, 1981.
4. Fante, Ronald L., *Signal Analysis and Estimation*, New York: John Wiley and Sons, 1988.
5. Kay, Steven M., and Marple, Stanley L., "Spectrum Analysis -- A Modern Perspective," *Proceedings of the IEEE*, Vol. 69, No. 11, November, 1981.
6. Jenkins, D.M., and Watts, D.G., *Spectral Analysis and Its Applications*, San Francisco: Holden-Day, 1968.
7. Rice, J.R., *The Approximation of Functions*, Vol. 1, Reading, MA: Addison-Wesley, 1964, pp. 124-131.
8. Blackman, R.B., and Tukey, G.W., *The Measurement of Power Spectra*, New York: Dover, 1958, pp. 95-100.
9. Kuo, F.F., and Kaiser, J.F., *System Analysis By Digital Computer*, New York: Wiley, 1960, pp. 232-238.
10. MATLAB Program, v.3.5, v.4.0, The Mathworks, Inc., 1992.

INITIAL DISTRIBUTION LIST

- | | |
|--|---|
| 1. Defense Technical Information Center
Cameron Station
Alexandria, VA 22304-6145 | 2 |
| 2. Library, Code 52
Naval Postgraduate School
Monterey, CA 93943-5000 | 2 |
| 3. Chairman, Code EC
Department of Electrical and Computer Engineering
Naval Postgraduate School
Monterey, CA 93943-5000 | 1 |
| 4. Professor Ralph Hippenstiel, Code EC/Hi
Department of Electrical and Computer Engineering
Naval Postgraduate School
Monterey, CA 93943-5000 | 2 |
| 5. Professor Monique P. Fargues, Code EC/Fa
Department of Electrical and Computer Engineering
Naval Postgraduate School
Monterey, CA 93943-5000 | 1 |
| 6. Ecuadorian Air Force Attache
2535 15TH Street, N.W.
Washington, DC 20009 | 6 |
| 7. Major Moreira, Ramiro P.
Av. La Isla #781 y OB. Diaz de la Madrid
Quito, Ecuador
S.A. | 1 |